

12. SITE 680¹

Shipboard Scientific Party²

HOLE 680A

Date occupied: 0700 L, 5 November 1986
Date departed: 2030 L, 5 November 1986
Time on hole: 13 hr 30 min
Position: 11°03.90'S, 78°04.67'W
Water depth (sea level; corrected m, echo-sounding): 252.5
Water depth (rig floor; corrected m, echo-sounding): 263.0
Bottom felt (m, drill pipe): 271.5
Penetration (m): 93.8
Number of cores: 10
Total length of cored section (m): 93.8
Total core recovered (m): 81.23
Core recovery (%): 87
Oldest sediment cored
Depth (mbsf): 93.8
Nature: sand and silty mud
Age: Pleistocene
Measured velocity (km/s): 1.56

HOLE 680B

Date occupied: 2030 L, 5 November 1986
Date departed: 1430 L, 6 November 1986
Time on hole: 18 hr
Position: 11°03.90'S, 78°04.67'W
Water depth (sea level; corrected m, echo-sounding): 252.5
Water depth (rig floor; corrected m, echo-sounding): 263.0
Bottom felt (m, drill pipe): 272.5
Penetration (m): 195.5
Number of cores: 22
Total length of cored section (m): 195.5
Total core recovered (m): 98.45
Core recovery (%): 50
Oldest sediment cored
Depth (mbsf): 195.5
Nature: sand and silt
Age: early Pliocene
Measured velocity (km/s): 1.55

HOLE 680C

Date occupied: 1430 L, 6 November 1986
Date departed: 2200 L, 6 November 1986
Time on Hole: 7 hr 30 min
Position: 11°03.90'S, 78°04.67'W
Water depth (sea level; corrected m, echo-sounding): 252.5
Water depth (rig floor; corrected m, echo-sounding): 263.0
Bottom felt (m, drill pipe): 272.2
Penetration (m): 34.3
Number of cores: 4
Total length of cored section (m): 34.3
Total core recovered (m): 35.4
Core recovery (%): 102
Oldest sediment cored
Depth (mbsf): 34.3
Nature: not studied
Age: Pleistocene (?)
Measured velocity (km/s): 1.54

Principal results: Site 680 is centered on an east-west transect of three sites across the coastal upwelling deposits of the Peruvian outer shelf and upper slope. Coring at Site 680 provided a detailed record of coastal upwelling sediments for investigating vertical shifts in depth of the oxygen-minimum layer through time. In addition, seaward-landward shifts of upwelling centers in response to Pleistocene sea-level fluctuations were also studied.

Three holes were drilled at Site 680. Hole 680A, with a total depth of 93.8 mbsf, recovered 81.2 m of thinly laminated, upper Quaternary, organic-rich, dark olive green, foraminifer-diatomaceous muds and sandy silts. In Hole 680B the same sequence was piston-cored with excellent recovery to a depth of 92 mbsf. The Brunhes/Matuyama boundary was identified at 38 mbsf. Core recovery was

¹ Suess, E., von Huene, R., et al., 1988. *Proc. ODP, Init. Repts.*, 112: College Station, TX (Ocean Drilling Program).

² Erwin Suess (Co-Chief Scientist), Oregon State University, College of Oceanography, Corvallis, OR 97331; Roland von Huene (Co-Chief Scientist), U.S. Geological Survey, Branch of Pacific Marine Geology, 345 Middlefield Rd. M/S 999, Menlo Park, CA 94025; Kay-Christian Emeis (ODP Staff Scientist), Ocean Drilling Program, Texas A&M University, College Station, TX 77843; Jacques Bourgeois, Département de Géotectonique, Université Pierre et Marie Curie, 4 Place Jussieu, 75230 Paris Cedex 05, France; José del C. Cruzado Castañeda, Petroleos del Peru S. A., Paseo de la Republica 3361, San Isidro, Lima, Peru; Patrick De Wever, CNRS, Laboratoire de Stratigraphie, Université Pierre et Marie Curie, 4 Place Jussieu, 75230 Paris Cedex 05, France; Geoffrey Eglinton, University of Bristol, School of Chemistry, Cantock's Close, Bristol BS8 1TS, England; Robert Garrison, University of California, Earth Sciences, Applied Sciences Building, Santa Cruz, CA 95064; Matt Greenberg, Lamont-Doherty Geological Observatory, Columbia University, Palisades, NY 10964; Elard Herrera Paz, Petroleos del Peru, S. A., Paseo de la Republica 3361, San Isidro, Lima, Peru; Phillip Hill, Atlantic Geoscience Centre, Bedford Institute of Oceanography, Box 1006, Dartmouth, Nova Scotia B2Y 4A2, Canada; Masako Ibaraki, Geoscience Institute, Faculty of Science, Shizuoka University, Shizuoka 422, Japan; Miriam Kastner, Scripps Institution of Oceanography, SVH, A-102, La Jolla, CA 92093; Alan E. S. Kemp, Department of Oceanography, The University, Southampton SO9 5NH, England; Keith Kvenvolden, U.S. Geological Survey, Branch of Pacific Marine Geology, 345 Middlefield Rd., M/S 999, Menlo Park, CA 94025; Robert Langridge, Department of Geological Sciences, Queen's University at Kingston, Ontario K7L 3A2, Canada; Nancy Lindsley-Griffin, University of Nebraska, Department of Geology, 214 Bessey Hall, Lincoln, NE 68588-0340; Janice Marsters, Department of Oceanography, Dalhousie University, Halifax, Nova Scotia B3H 4J1, Canada; Erlend Martini, Geologisch-Paläontologisches Institut der Universität Frankfurt, Senckenberg-Anlage 32-34, D-6000, Frankfurt/Main, Federal Republic of Germany; Robert McCabe, Department of Geophysics, Texas A&M University, College Station, TX 77843; Leonidas Ocola, Laboratorio Central, Instituto Geofísico del Peru, Lima, Peru; Johanna Resig, Department of Geology and Geophysics, University of Hawaii, Honolulu, HI 96822; Agapito Wilfredo Sanchez Fernandez, Instituto Geológico Minero y Metalúrgico, Pablo Bermudez 211, Lima, Peru; Hans-Joachim Schrader, College of Oceanography, Oregon State University, Corvallis, OR 97331 (currently at Department of Geology, University of Bergen, N-5000 Bergen, Norway); Todd Thornburg, College of Oceanography, Oregon State University, Corvallis, OR 97331; Gerold Wefer, Universität Bremen, Fachbereich Geowissenschaften, Postfach 330 440, D-2800 Bremen 33, Federal Republic of Germany; Makoto Yamano, Earthquake Research Institute, University of Tokyo, Bunkyo-ku, Tokyo 113, Japan.

poor during XCB drilling in lower Pliocene strata at the bottom of Hole 680B (195.5 m). Clastic feldspar sediments associated with beds of phosphatic conglomerates and sands are characteristic lithologies of the Pliocene unit. Four cores were drilled in Hole 680C with 100% recovery before the hole was abandoned because of failure of a sand line. We froze the samples from this hole for geomicrobiological and organic-geochemical studies.

At Site 680 all stages of dolomite, calcite, and phosphate formation and replacement are common. Dolomite is the predominant authigenic phase and first was found as disseminated rhombs in the diatomaceous mud at 0.79 mbsf. Phosphates occur in all units as thinly laminated beds of friable carbonate-fluor apatite, concentrated in diatom-rich laminae, and as dark, dense peloids typically in sandy and conglomeratic strata. Bedded opal-CT chert, pyrite, and calcite are minor authigenic phases. The sediments, their pore water, and their dissolved-gas chemistries reveal considerable early diagenetic activity, which is uniquely affected by hypersaline pore fluids discovered at Site 680. Salinities, chloride, and other dissolved major ions of these fluids increase to about twice the concentrations of normal seawater at 195.5 mbsf. Replenishment of dissolved sulfate from this source inhibits microbial methane formation and promotes microbial sulfate reduction much beyond the depth normally seen in organic-rich sediments. Thus, these phenomena are responsible for the unexpectedly low biogenic methane contents of these sediments. This brine replenishes magnesium, calcium, and sulfate and also affects dolomitization.

The cores from Site 680 contain all components of a well-developed upwelling facies, provide an expanded record of the late Quaternary period, and reveal low-temperature diagenetic reactions driven by hypersaline subsurface waters.

BACKGROUND AND SCIENTIFIC OBJECTIVES

Site 680 is located in the center of the east-west transect of three sites across the Peruvian upper-slope and outer-shelf areas (Fig. 1). We targeted this site to address paleoceanographic objectives. These objectives relate to the history and geological expression of coastal upwelling and the role of the oxygen-minimum zone (Reimers and Suess, 1983; Smith, 1983). Specifically, objectives are as follows:

1. The vertical change in the oxygen-minimum layer and its role in accumulating and preserving organic matter.
2. The lateral change in upwelling facies along the "average" trail of persistent upwelling plumes that were generated north of the prominent headlands around Islas Mazorcas at a latitude of 11°S.
3. The seaward-landward shift of upwelling centers during changes in sea level.
4. The preservation in these sediments of upwelling water characteristics, such as salinity, temperature, and nutrient composition.

These objectives were also addressed at companion Site 681 and at Sites 684, 686, and 687 of Leg 112. Therefore, this introduction is intended for all sites and will be referred to in individual site chapters. Additional objectives for these shelf sites concern geomicrobiology and early diagenesis. These objectives address issues related specifically to organic-rich sediments, such as what is the depth below seafloor to which microbial activity can be documented, and what drives the mechanisms of phosphate, dolomite, and chert formation? Most geochemists suspect microbial activity in sediments a few meters considerably below the seafloor by the dissolved and gaseous mineralization products in interstitial waters. This view is not shared by all sediment microbiologists, who think that bacterial activity ceases rapidly below the sediment/water interface. The sediments at Site 680 were ideally suited to investigate this problem because of their abundant organic matter and the relatively "pure" and predictable composition of organic matter generated by coastal upwelling productivity. These sediments contain siliceous diato-

maceous debris; organic matter from shelled and organically walled plankton; calcareous benthic foraminifers; and plankton, phosphatic fish debris, and terrigenous clastics.

Analysis of interstitial-fluid and gas chemistries supplemented the evaluation of deep microbial activity and aided in predicting diagenetic phases and their chemical and isotopic composition. Diagenesis severely overprints the primary depositional signal. One must understand early diagenetic processes in this environment to "deconvolve" the sediment record to recognize the original depositional signal.

Using the APC and the XCB, three holes were cored at this site to reach 200 mbsf. This target depth was intended to provide enough samples for high-resolution studies of the Pleistocene-Pliocene uppermost sediment sequence in the area of strongest and persistent recent coastal upwelling.

The seismic data across the site indicate that middle and upper Miocene strata are overlain by Pliocene and Quaternary sections, as was the case at Site 679. The uppermost Quaternary section is much thicker at Site 680 than at Site 679. This section contains a zone of prograding beds 40–50 m thick that pinch out farther downslope. Today, the water depth where we drilled Site 680 into this uppermost sequence is located in the middle of a pronounced oxygen-minimum layer. Therefore, this site occupies a pivotal position along the north-south transect for studying the history of this important oceanographic phenomenon and its role in preserving organic carbon. The oxygen-minimum layer is well developed in the eastern-boundary current regime off Peru, both in intensity and distinctness of its upper and lower limits in the water column. This layer shoals from >400 m in the northern area at 9°S to <100 m in the southern area at 13°. Site 680 is the crossing point of the north-south transect, which was designed to run parallel to the oxygen-minimum layer and the east-west transect across the margin. From this, a three-dimensional framework can be established with which to evaluate the role of the oxygen-minimum zone through time.

OPERATIONS

After retrieving our positioning beacon from Site 679, the ship was under way at 0900 UTC, 5 November 1986, for the transit to Site 680. (Unless indicated, all times are UTC, Universal Time Coordinated, formerly GMT, Greenwich Mean Time.) At 0930 hr we deployed an 80-in.³ water gun, and the *Resolution* set course for the new site. During this run, we crossed Site 679 at 0950 hr to collect additional seismic information. At about 1040 hr, our navigation update showed that the ship had sailed parallel to our projected course, but had offset by about 0.9 nmi to the north (Fig. 2). We confirmed this offset after sailing another 35 min. We set a new course to reach the original line of approach at 1135 hr (Fig. 2). We dropped our beacon on the first pass over the site at 1208 hr when both coordinates and water depth (255 m) told us we had reached our target. The ship continued to collect seismic data until 1217 hr, when we retrieved our gear. The seismic and 3.5-kHz surveys were conducted to see whether acoustic turbulence, "wipe-out" zones, or "pull-down" structures occurred beneath the surface that might indicate free methane gas in these organic-rich sediments of the Peru upwelling zone. We saw no indication of any such features. Instead, our water-gun and 3.5-kHz records showed the expected landward increase in thickness of the upper-slope mud facies—our target for Site 680. An unconformity at about 40 m separated this uppermost sequence from the underlying strata, which had been recovered previously at Site 679.

At Site 680, we first conducted dynamic positioning tests for about 5 hr to fine tune the system and to prepare for the very shallow depths drilled at this and subsequent sites. The Ocean Drilling Program had never drilled in water depths of 200 m or

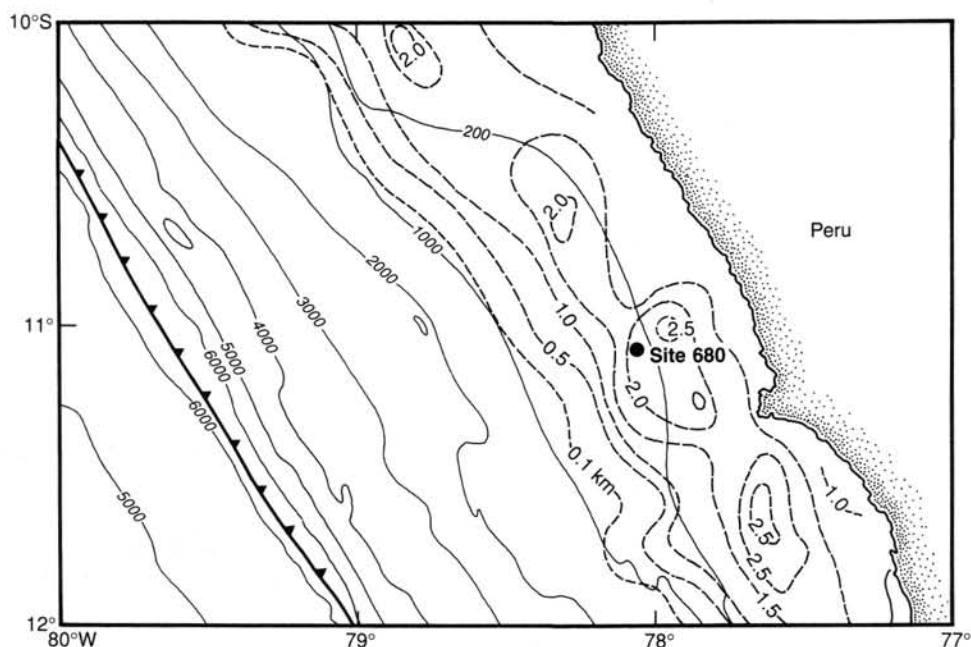


Figure 1. Bathymetry and sediment isopachs along Peru Continental Margin at 11°S; depths are in intervals of 1000 m, beginning at a water depth of 200 m; sediment isopachs are in increments of 0.5 km, beginning at 0.1 km. For an overview of all sites, see Figure 1, Site 679 chapter (this volume).

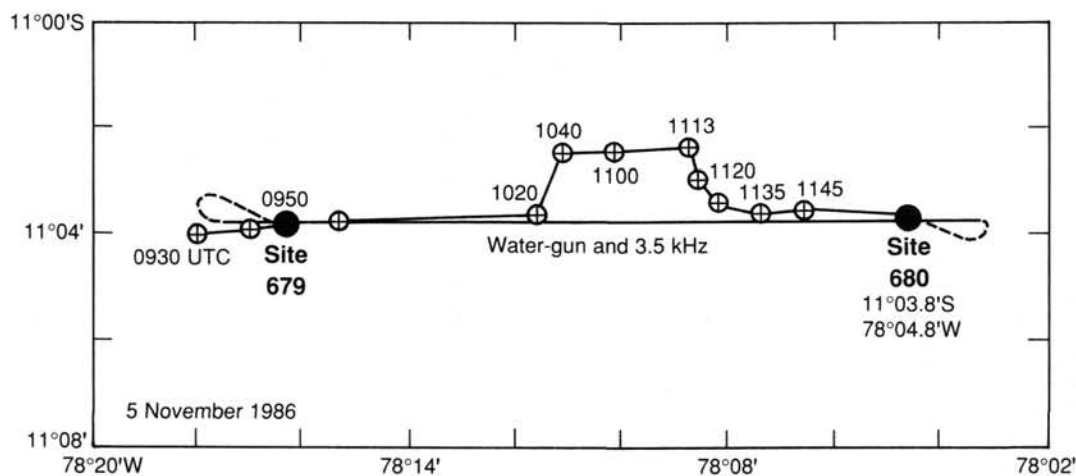


Figure 2. Track chart of *Joides Resolution* approaching Site 680 location.

shallower. The new "shallow water" parameters were entered into our computer, which allowed us to make the necessary adjustments. This system was extremely accurate and functioned perfectly. The maximum deviation during positioning was 2% to 3% of water depth at 261 m.

Hole 680A was spudded at 1200 L. The bottom-hole assembly was run to the mud line during dynamic positioning tests. Five APC cores having 96% recovery were drilled in rapid succession before Core 112-680A-6H (46–56 mbsf) became difficult to recover (the same depth at which our 3.5-kHz survey showed an unconformity). Below that level, coring continued with improved recovery rates to 93.8 mbsf. After Core 112-680A-10H, the *in-situ* pore-water and temperature probe was deployed successfully. While attempting to withdraw Core 112-680A-11H, the barrel box parted at the upper seal sub with only 80,000 lb of overpull, and Hole 680A had to be abandoned.

Hole 680B was spudded with a mud-line APC core after offsetting the ship about 8 m to the north. APC coring continued

successfully to a depth of 92 mbsf. As subsequent lithostratigraphic description showed, we had encountered a hard layer at about 50 mbsf at this site. However, we prevented the core barrel from sticking by controlling the pull-out. After recovering Core 112-680A-7H, the *in-situ* pore-water, pressure, and temperature probe was deployed. Because of increased overpull while retrieving Core 112-680A-9H (40,000 lb), we decided to proceed with XCB coring. Poor recovery rates continued to a total depth of 195.5 mbsf (Table 1).

At 1500 L on 6 November 1986, Core 112-680C-1H was recovered after offsetting the ship by about 8 m laterally. Samples from this hole were designated for special geomicrobiological sampling and other projects requiring whole-round samples. Thus, these core sections were not split nor their lithologies described. *In-situ* heat flow was measured following recovery of Core 112-680C-2H. While retrieving Core 112-680C-4H, the sand line parted; we could not fish for the core barrel because it seemed to be wedged firmly inside the seal bore of the drill col-

Table 1. Coring summary at Site 680.

Core/ section	Date (Nov. 1986)	Time (UTC)	Depth (mbsf)	Length cored (m)	Length recovered (m)	Recovery (%)
<i>Hole 680A</i>						
112-680A-1H	5	1340	0-8.3	8.3	8.30	100.0
2H	5	1350	8.3-17.8	9.5	9.89	104.0
3H	5	1406	17.8-27.3	9.5	9.81	103.0
4H	5	1420	27.3-36.8	9.5	9.93	104.0
5H	5	1440	36.8-46.3	9.5	6.40	67.3
6H	5	1500	46.3-55.8	9.5	1.13	11.9
7H	5	1534	55.8-65.3	9.5	8.04	84.6
8H	5	1610	65.3-74.8	9.5	9.73	102.0
9H	5	1635	74.8-84.3	9.5	8.69	91.5
10H	5	1655	84.3-93.8	9.5	9.31	98.0
<i>Hole 680B</i>						
112-680B-1H	5	2120	0-5.5	5.5	5.55	101.0
2H	5	2130	5.5-15.0	9.5	9.96	105.0
3H	5	2150	15.0-24.5	9.5	9.67	102.0
4H	5	2225	24.5-34.0	9.5	9.87	104.0
5H	5	2250	34.0-43.5	9.5	9.85	103.0
6H	5	2310	43.5-53.0	9.5	9.81	103.0
7H	5	2325	53.0-62.5	9.5	9.63	101.0
8H	6	0125	62.5-72.0	9.5	9.74	102.0
9H	6	0145	72.0-81.5	9.5	9.41	99.0
10H	6	0203	81.5-91.0	9.5	9.37	98.6
11H	6	0225	91.0-92.0	1.0	1.02	102.0
12X	6	0335	92.0-100.5	8.5	0.35	4.1
13X	6	0408	100.5-110.0	9.5	0.00	0.0
14X	6	0520	110.0-119.5	9.5	0.82	8.6
15X	6	0555	119.5-129.0	9.5	0.00	0.0
16X	6	0638	129.0-138.5	9.5	0.00	0.0
17X	6	0720	138.5-148.0	9.5	0.05	0.5
18X	6	0755	148.0-157.5	9.5	0.15	1.6
19X	6	0840	157.5-167.0	9.5	0.39	4.1
20X	6	0915	167.0-176.5	9.5	0.34	3.6
21X	6	0955	176.5-186.0	9.5	1.48	15.6
22X	6	1034	186.0-195.5	9.5	0.99	10.4
<i>Hole 680C</i>						
112-680C-1H	6	1500	0-5.8	5.8	5.80	100.0
2H	6	1522	5.8-15.3	9.5	9.65	101.0
3H	6	1542	15.3-24.8	9.5	9.97	105.0
4H	6	2100	24.8-34.3	9.5	9.62	101.0

lar and could not be retrieved. Because we had completed almost one-half of the geomicrobiological samples, we decided to abandon Site 680 without drilling another hole. We also decided to complete this specific sampling program by drilling another, third hole to 100 mbsf at the next site. The ship was under way for Site 681 by 2200 hr L on 6 November.

LITHOSTRATIGRAPHY

Lithologic Units

The sediments recovered at Site 680 (Fig. 3) are divided into three lithologic units on the basis of visual core descriptions and smear-slide analysis (Table 2). Unit III is further divided into five subunits. Each unit and subunit is described in detail next.

Unit I

Cores 112-680A-1H through 112-680A-7H-1, 57 cm; depth, 0-56.4 mbsf; age, Holocene (Zones NN20 and NN19) to latest Pleistocene.

Cores 112-680B-1H through 112-680B-6H-3; depth, 0-48 mbsf; age, Holocene (NN20 and NN19) to latest Pleistocene.

Unit I consists of foraminifer-diatom mud, ranging from olive, olive gray, and dark olive to dark gray and black. The first meter of Cores 112-680A-1H and 112-680B-1H is composed of soupy mud disturbed by drilling. Drilling disturbance is obvious down to the upper part of Section 112-680A-1H-3.

Unit I is composed primarily of thick, homogeneous olive to dark olive mud and silty mud with thin (<1 cm) pale green to yellow laminations. The sediment is dominated by diatoms (10%-80%), foraminifers (0%-25%), and clay (15%-65%). The light yellow laminae (0.5-1.5 cm) are made up of diatom ooze. Distances between these laminations range from 10-15 cm to 100-400 cm. The yellow layers probably reflect interruption of detrital input, higher productivity, or deposition after winnowing.

Shell-rich beds imbedded in mud matrix (Sections 112-680A-3H-5 and 112-680B-3H-7; Figs. 4 and 5) suggest that the shells were transported from their original environment. In Hole 680A the base of the shell bed is 25 mbsf; in Hole 680B, 8 m to the north, this bed occurs at about 24.5 mbsf. Taking into account that Hole 680B is 1 m deeper than Hole 680A, the shell bed is about 0.50 m lower at Hole 680B than at Hole 680A.

Graded sand and silt layers having sharp basal contacts are prominent in Unit I (Fig. 6). These beds range from 1-4 cm to 30-40 cm thick. One of these sequences is well exposed in Sample 112-680B-11H-1, 85-130 cm, where coarse-grained sand and concentrations of mollusk shells and foraminifers grade up to sandy silt and mud (Fig. 5).

Eight dark-bluish-gray ash layers, varying from 1 to 4 or 5 cm thick, occur in Unit I (Hole 680B). Phosphatic nodules occur throughout Unit I, and dolomite is dispersed as micritic rhombs throughout the entire sediment section.

Unit II

Core 112-680A, no recovery. Cores 112-680B-6H-3 through 112-680B-7H-3, 75 cm; depth, 48-56.5 m; age, Pleistocene.

Diatomaceous silty mud is the dominant lithology of Unit II. Major components are clay (10%-70%), silt-sized quartz and feldspar (40%-50%), and diatom frustules (40%-80%), ranging from olive to olive gray and very dark gray (Fig. 7). Unit II is thinly bedded to laminated with thin, diatom-rich yellow laminae. Distance between individual yellow laminae is from 2-5 cm to 10 cm. The detrital input is probably lower in Unit II than in Unit I, with less dilution of local biogenic sedimentation. These yellow laminae commonly exhibit dolomitization or phosphate replacement, indicating that they serve as preferred paths for fluid circulation (see "Summary and Conclusions," Site 679 chapter, this volume).

Minor lithologies include phosphatic nodules and small chert fragments (Sample 112-680B-6H-4, 135-140 cm).

Unit III

Cores 112-680A-7H-1, 57 cm, through 112-680A-10H; depth, 56.4-93.8 m; age, Pleistocene to early Pliocene.

Cores 112-680B-7H-3, 75 cm, through 112-680B-22X; depth, 56.5-195.5 m; age, Pleistocene to early Pliocene.

Lithologic Unit III is characterized by substantial amounts of clastic material associated with several beds of phosphate conglomerates (Fig. 8) and a high feldspar content (10%-55%). Major components are clay (15-20%), silt-sized quartz and feldspar (30%-60%), and diatoms (0%-35%). Unit III has a lower content of diatoms and clay than Unit II, and its major textural components are silt and sand. The sediments range from gray to dark gray. Unit III is divided into five lithologic subunits (Table 3).

Subunit IIIA

This subunit consists of a coarse-grained phosphate and feldspar gravel having a substantial amount of hard, dark phosphate nodules, including bone fragments. This coarse gravel is underlain by a gray, coarse-grained sand cemented by calcitic dolomite.

Table 2. Lithologic units at Site 680.

Unit	Approx. depth (mbsf)	Lithology	Core-range
I	0-48	Foraminifer-diatomaceous mud and sandy silt, olive to dark gray	112-680A-1H-7H 680B-1H-6H
II	48-56.5	Diatomaceous mud and diatom-ooze (dolomitized)	680A no recovery 680B-6H-7H
III	56.5-195.5	Gray, olive gray, and dark gray sand, phosphatic sand, and mud with phosphatic pebbles	680A-7H-10H 680B-7H-22X

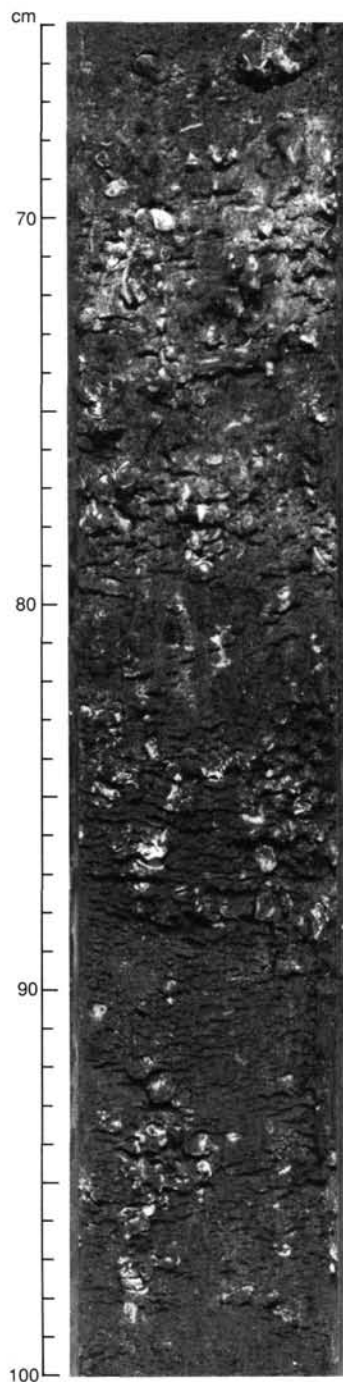


Figure 4. Shell-rich bed in Sample 112-680A-3H-5, 65-100 cm.

dolomite. Thinly laminated to cross-laminated layers occur in Core 112-680B-21X. These structures are similar to those described in Core 679D-19X, where they were identified as hummocky cross-stratification and were interpreted as products of reworking by wind-forced currents. Another similarity with Cores 112-679D-19X, through 112-679D-22X is the cementation of some sand layers by calcitic dolomite.

Diagenesis

Phosphates

Phosphates recovered from Site 680 occur as two major forms, as follows:

1. As thin laminae and small nodules of pale yellow to pale brown, friable, carbonate fluorapatite, which occur in diatom muds (Figs. 7 and 9). We define these as *F-phosphates* (friable phosphates).
2. As dark, hard, dense nodules and peloids that typically occur in sandy or conglomeratic beds (Figs. 8, 10, and 11). These are hereafter called *D-phosphates* (dense phosphates).

The nodules and laminae of F-phosphates are *in situ* and appear to have formed by replacement of the host diatom muds. F-phosphates occur in Units I and II and Subunit IIIC.

D-phosphates occur in all lithologic units except Subunit IIIB and are particularly common in Subunit IIIC. D-phosphates are present in beds up to 30 cm thick within sequences of mud (e.g., Figs. 10 and 11). These beds commonly have sharp, erosional basal contacts, and many show graded bedding. Clasts vary from sand-sized ovoidal peloids to pebble-sized subspherical to irregularly shaped nodules and bone fragments. Most of these beds are relatively well sorted and lack a muddy matrix. Thus, they contrast markedly with the diatom muds with which they are interbedded and indicate episodes of high energy. Thin-section analysis of a D-phosphate nodule from Site 679 showed a compound internal structure suggesting multiple episodes of phosphatization and nodule growth. We believe that D-phosphates may be products of complex, possibly repeated, intervals of erosion and reworking on the seafloor. Thus, beds of D-phosphates probably mark the locations of hiatuses in the sediment column.

Many D-phosphate nodules have a hard, dark, outer coating around a lighter-colored, more friable core, suggesting that at least some D-phosphate nodules evolved from an F-phosphate predecessor, perhaps starting with erosional exhumation of F-phosphate nodules that formed near the seafloor. Lending credence to this suggestion is the co-occurrence in a single conglomeratic bed in Subunit IIIC (112-680A-10H-4, 74-78 cm) of both F- and D-phosphate nodules.

Authigenic Carbonates

Dolomite is the predominant authigenic carbonate phase present at Site 680, but many dolomitic beds are partly calcitic. Therefore, the acid test is inconclusive because at least some of the predominantly dolomitic beds contain calcitic foraminifers and other shells. Some beds, identified as calcite-cemented in the Visual Core Description forms, may actually be dolomites, others are actually calcite. This matter will be resolved by shore-based studies.

Dolomite at Site 680 occurs as (1) disseminated rhombs, (2) small nodules, and (3) thin, hard beds. Sparse dolomite rhombs in diatom muds were first noted at a depth of 0.79 mbsf in Hole 680A (112-680A-1H-1, 79 cm) and at 3.67 mbsf in Hole 680B (112-680B-1H-3, 67 cm). Disseminated dolomite becomes abundant at a depth of 8.25 mbsf (112-680B-2H-4, 125 cm), where some diatom muds contain up to 50% rhombs. The shal-

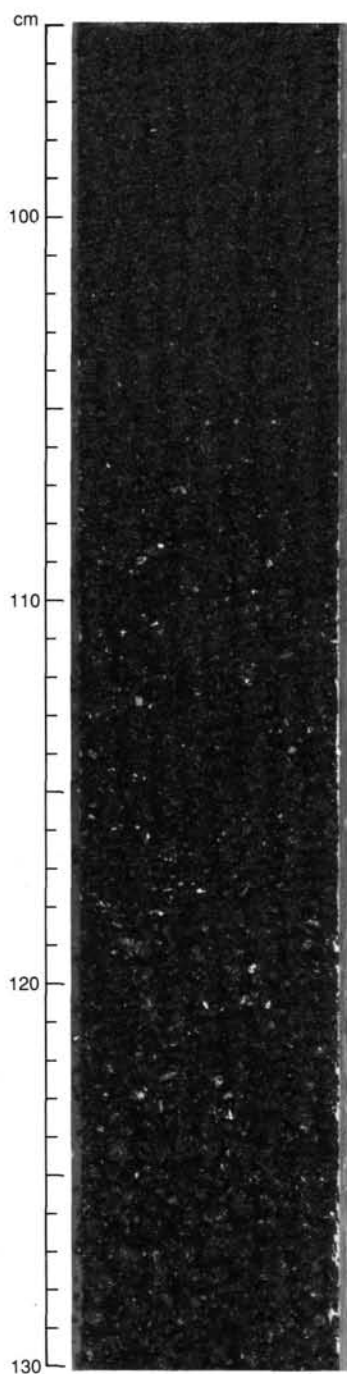


Figure 5. Shell-rich bed in Sample 112-680B-11H-1, 95–130 cm. This bed grades from coarse sand and mollusk shells through foraminifer-rich sand to fine sand and silt.

lowest hard layer of dolomite that we encountered is at 32.8 mbsf (112-680B-4H-6, 78–82 cm). Thus, some dolomitization appears to be an early diagenetic phenomenon at Site 680. One dolomite layer (112-680B-7H-2, 5–7 cm) contains F-phosphate nodules, indicating that phosphatization preceded dolomitization.

Dolomitic layers occur in all units except lithologic Subunits IIIB and IIIE. They appear to be most common in Unit II. At least two varieties of hard, dolomitic beds are present. Thin, pale yellow, dolomite layers appear to replace laminated diatom muds (Fig. 12). Thicker beds (up to 10 cm) are either replace-

ments of diatom muds or are silty to sandy layers cemented by dolomite (Fig. 6; some of these cements may be partly or wholly calcite). Some of the cemented beds contain shell fragments, and many of the uncemented sandy layers with abundant shell fragments contain large amounts of authigenic carbonate, predominantly dolomite (e.g., layers at 112-680A-4H-3, 68–140 cm, a graded shell-bearing sand with up to 50% dolomite rhombs, and 112-680A-4H-5, 45–120 cm, with 15% disseminated rhombs). The original carbonate contents may be an important factor in localizing precipitation of dolomite, which is perhaps acting in conjunction with the increased permeability of the sandy layers.

Unit II contains several dolomitized layers overlain by conglomerates composed of D-phosphate nodules (Figs. 10 and 11). A possible explanation for this relationship is that erosion associated with the deposition of these conglomerates scoured down through soft sediments to the tops of lithified or semilithified layers. In the example illustrated in Figure 11, the top 10 cm of the light gray dolomitic silt is lithified, but the degree of lithification decreases markedly below this depth.

Silica Diagenesis

Small fragments of thinly bedded, dark, opal-CT chert (Figs. 12 and 13) were recovered from two levels in Unit II (112-680A-7H-1, 10–15 cm, 55.9 mbsf; and 112-680B-6H-4, 140–143 cm, 49.4 mbsf). Because fragments occur in intervals of drilling disturbance, little can be said about their exact provenance.

Pyrite

Authigenic pyrite is present in trace amounts in most smear slides examined; it is particularly common in Unit II, where in places it may form up to 5% of the diatom mud.

Clastic Lithologies

Clastic lithologies are common at Site 680 because the site is located on the uppermost continental slope and was probably located in a storm-wave base during periods of glacially lowered sea levels. Most sands are fine- to very fine-grained and silty, except for phosphorite pellets and nodules that formed both *in situ* and as transported, resedimented clasts.

Graded sand and sandy silt beds with sharp, eroded basal contacts are particularly well developed in Cores 112-680B-3H through 112-680B-6H. Many beds are less than 10 to 20 cm in thickness, but a particularly thick unit extends from Sample 112-680B-4H-5, 48–102 cm, and includes fragments of shell debris concentrated near the base. Other shell-bearing sand beds in Holes 680A and 680B range from well graded (Fig. 5) to poorly graded (Figs. 4 and 11). Many of the beds are extensively bioturbated by benthic fauna along their tops. Many of the graded beds exhibit dewatering structures that originate in the coarser intervals near the basal contact and propagate into the overlying muds, presumably indicating rapid deposition and pore-fluid overpressuring in the basal sands during compaction. The graded beds were probably deposited by small density currents—perhaps sediment was catastrophically cast into suspension during storm events, carried beyond the storm-wave base, and deposited on the outer shelf or upper slope. Classical turbidite structures are not developed in these beds, probably because such short transporting distances preclude the mature evolution of density currents and the separation of low- and high-energy components of flow.

Sands, silts, and sandy muds are typically found below nodular phosphorite accumulations, which may represent submarine erosional surfaces. In Hole 680B, about 20 cm of sand and several meters of homogeneous, bioturbated mud that is rich in terrigenous silt underlies a 20-cm-thick zone of phosphatic gravel at Sample 112-680B-7H-3, 78 cm. Sand-rich intervals are also associated with a series of nodular phosphorite beds in Samples

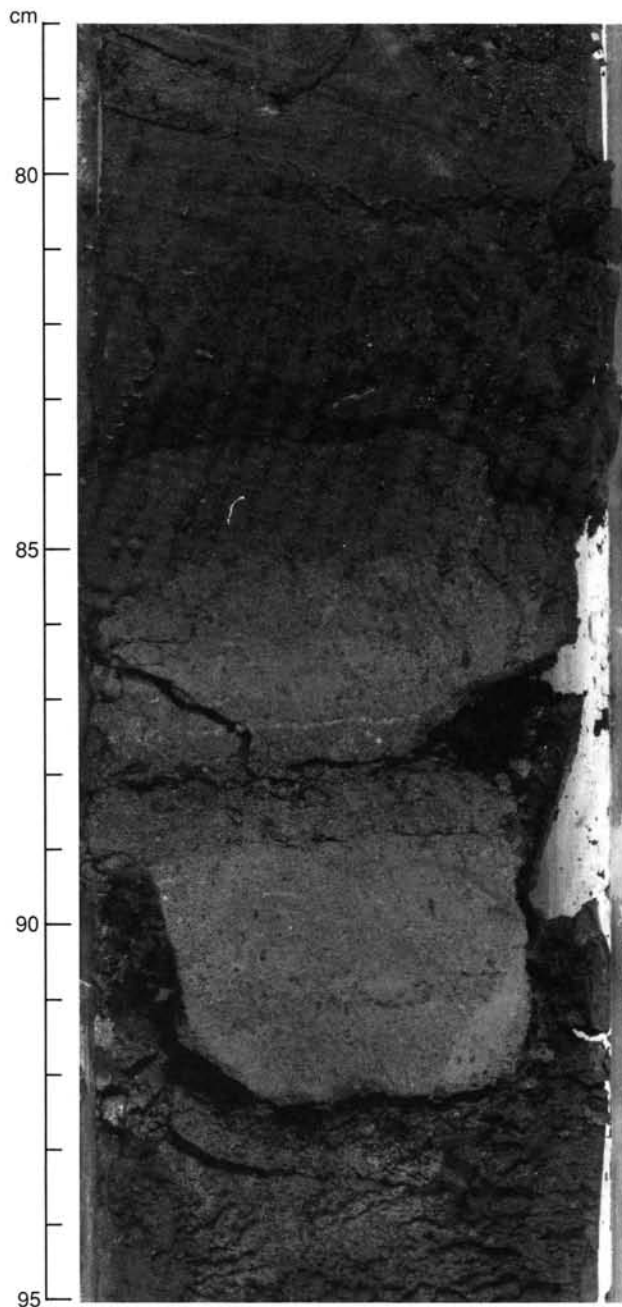


Figure 6. Bed near bottom of photo is a sandstone cemented by dolomite, Unit I (112-680B-5H-5, 78-95 cm). Note the sharp contact below the cemented sandstone (cemented by dolomite).

112-680B-8H-7, 9-10 cm, 112-680B-8H-7, 36-40 cm (Fig. 10), and 112-680B-9H-2, 75-80 cm. Phosphorite formation appears to be associated with strong current reworking of the seafloor; low sedimentation rates or curtailed terrigenous input may also be required.

Resedimented phosphorites are concentrated in an 80-cm-thick graded bed at Sample 112-680B-11H-1, 95 cm (Fig. 5). Phosphorite content decreases from 55% at the base to 20% at the top of the bed, while terrigenous components (quartz, feldspar, and rock fragments) increase from 40% to 60%, base to top, primarily because phosphatic pellets and nodules are concentrated in the coarse sand and gravel fraction. At the top of the same Section 112-680B-11H-1, a clean, matrix-poor sand

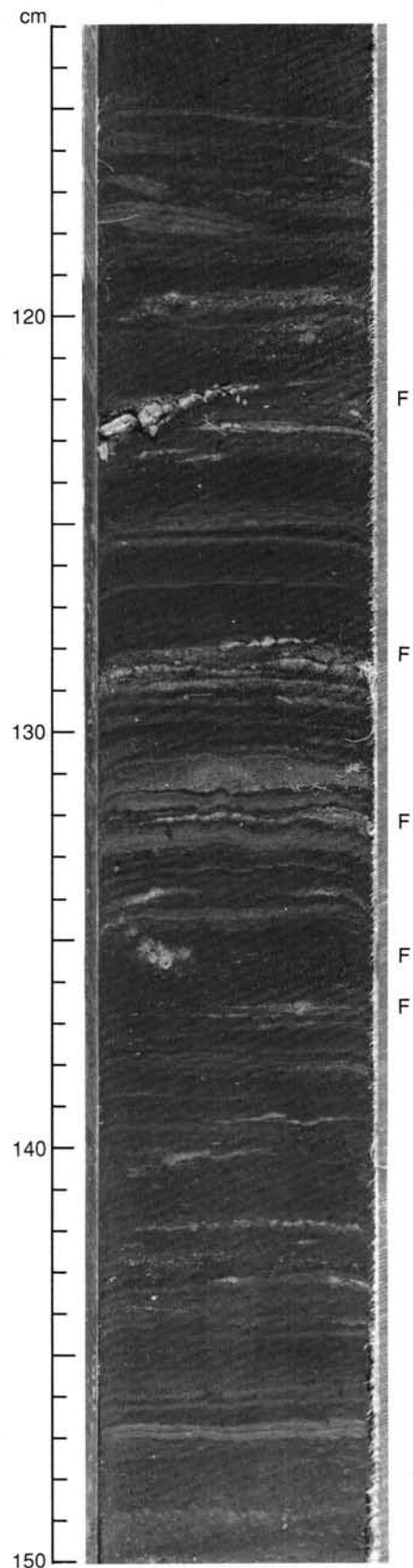


Figure 7. Laminated diatomaceous mud with layers and small nodules of F-phosphate at the levels indicated by the letter F; Unit II (112-680A-6H-6, 113-150 cm).

Table 3. Lithologic subunits of Unit III, Site 680.

Subunit	Approx. depth (mbsf)	Lithology	Core-range
A	56.5-57	Dark gray feldspar sand and phosphatic conglomerate	112-680A-7H 680B-7H
B	57-62	Gray feldspathic mud	680A-7H 680B-7H
C	62-91	Olive gray to dark olive gray feldspathic mud, diatom-bearing, finely laminated	680A-7H→10H 680B-8H→10H
D	91-92	Gray feldspar sand and phosphatic conglomerate	680B-11H
E	92-195.5	Gray to dark gray feldspar silt, siltstone, sand, and sandstone	680B-12H→22X

layer, 56 cm thick, also contains 20% phosphate material. Apparently, phosphorite accumulations in shallow, current-swept environments are sometimes transported to deeper water via density currents along with terrigenous sand.

The migration of carbonate-cementing fluids in the diagenetic environment appears to be controlled to some degree by the enhanced permeability of coarse-grained lithologies. Thus, preferential carbonate cementation may occur at the base of graded beds (112-680B-4H-6, 77-80 cm, 112-680B-5H-5, 84-93 cm, 112-680B-6H-1, 24-33 cm, and 112-680B-6H-4, 24-27 cm) and in the coarsely grained sediments underlying phosphorite accumulations (112-680B-7H-3, 100-110 cm, and 112-680B-10H-1, 43-53 cm). Carbonate-cemented sandstones preserving current laminations and cross-laminations are interbedded with silts and sands at Samples 112-680B-14X, CC (10-16 cm) and 112-680B-12X, CC (20-26 cm). Aside from drilling breccia, small plugs of carbonate-cemented sandstone constitute the sole lithology recovered in Samples 112-680B-17X, CC (0-7 cm), 112-680B-18X, CC (7-14 cm), and 112-680B-19X, CC (0-5 cm, 20-26 cm), while Cores 112-680B-13X, 112-680B-15X, and 112-680B-16X had no recovery. Although Hole 680B was plagued by poor recovery, coarsely grained lithologies appear to be prevalent and may be pervasively cemented between 92 and 167 mbsf.

Structure

Deformation Features

Veins and Dewatering Structures

Mud-filled veins were recognized in Holes 680A and 680B. These were first observed in Core 112-680A-2H-3, occur sporadically in Cores 112-680A-3H through 112-680A-6H, and become common in Cores 112-680A-7H through 112-680A-10H. The veins occur as infill to *en-echelon* tension gashes (Fig. 14) and have a width that rarely exceeds 2 mm, but in some cases reaches more than 0.5 cm. Infilled extensional faults such as those encountered at Site 679 are rare and typically small-scale.

We gained further insight into the development of vein formation in the hinge of a slump fold at Sample 112-680B-10H-2, 86-96 cm (Fig. 15). Veins 3-cm-long originate in the coarse sand below the basal decollement and penetrate folded layers within the slump fold before disappearing. Another set of 3-cm-long sinusoidal veins originates near the top of the slump fold and crosses several beds before disappearing upward (Fig. 15). Small extensional offsets are visible along some of the veins where they cross the basal decollement or beds within the slump fold. These relationships clearly demonstrate that vein formation occurs after slumping.

A more stable tectonic history than that of Site 679 is indicated for Site 680 by the lower intensity of *en-echelon* veining, together with the minimum development of microfaulting and

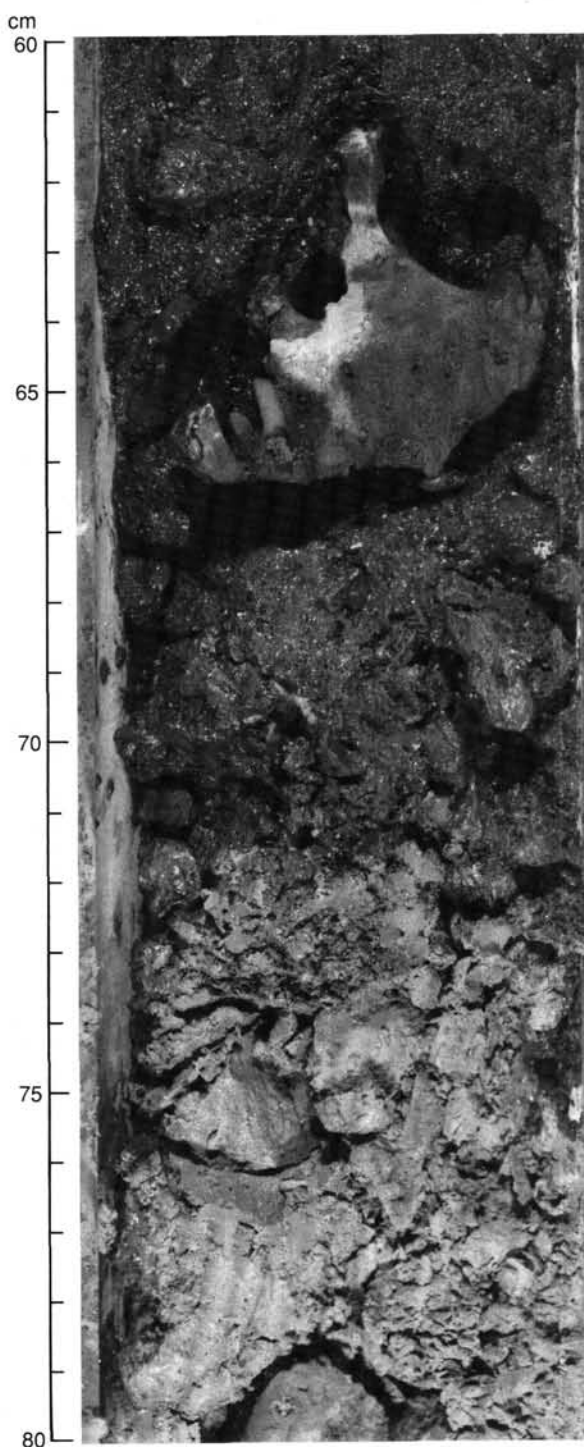


Figure 8. Phosphate conglomerate in Sample 112-680A-7H-1, 60-80 cm.

lack of broader discrete gashes. This is compatible with the position of Site 680 along the shelf edge, as well as its distance from faults observed on the seismic profile.

Slumping and Syn-Sedimentary Deformation

Slump features are rare at Site 680. However, disrupted and convolute bedding, loading, and minor slump folding are common in Cores 112-680B-8H, 112-680A-9H, 112-680A-10H, 112-680B-8H, 112-680B-9H, and 112-680B-10H (Fig. 15). Rather than relative movement between or over strata, these features suggest *in-situ* destabilization of soft sediment, which enhanced

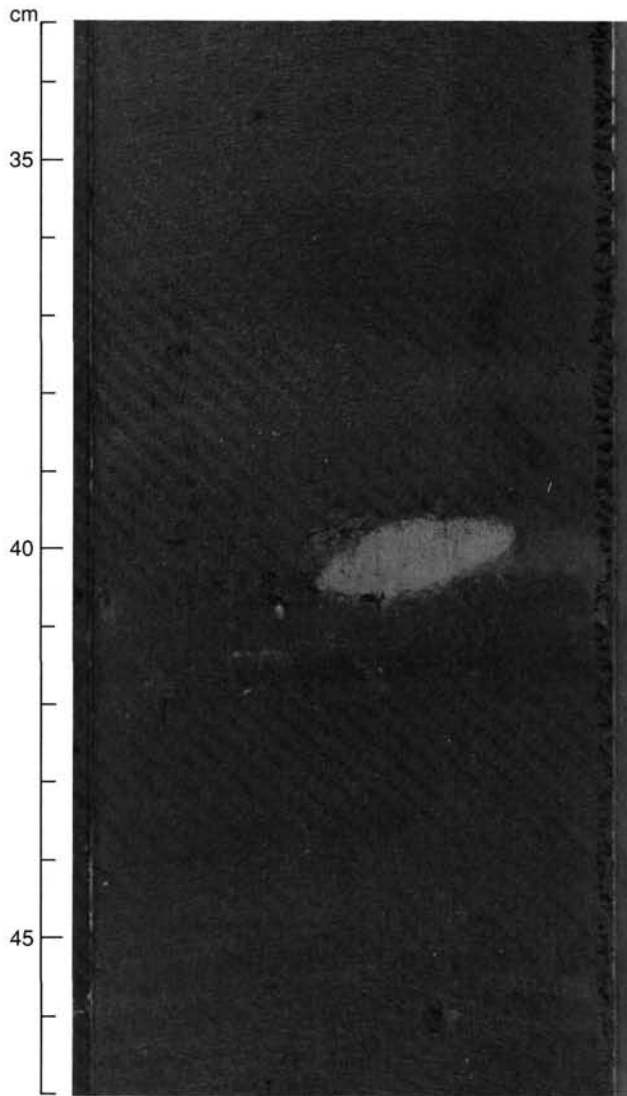


Figure 9. Small F-phosphate nodule in diatomaceous mud, Unit II (112-680A-10H-6, 33-47 cm).

density contrasts and produced localized fluidization. Such structures could be generated by current surges over the sediment during storm events.

Carbonate Measurements

Hole 680A was sampled to determine carbonate concentrations for resolving possible fluctuations of primary input. At least one sample per section was measured, according to the method outlined in "Explanatory Notes" (this volume). As is seen from Figure 16 and Table 4, considerable fluctuations of carbonate content are recorded in sediments of Unit I. The interval of highest variability ranges from Core 112-680A-1H to about Core 112-680A-5H (0-43 mbsf). Lithologic Unit I consists of diatom-foraminifer mud having intercalations enriched by authigenic dolomite and allochthonous shell fragments. These intervals are represented by the spikes of high carbonate concentrations (maximum of 32% in Sample 112-680A-2H-2, 96-98 cm; 10.8 mbsf) in a generally carbonate-lean matrix of diatom mud (on average less than 5% CaCO_3). Because Unit II was not recovered in Hole 680A, no samples were measured for carbonate

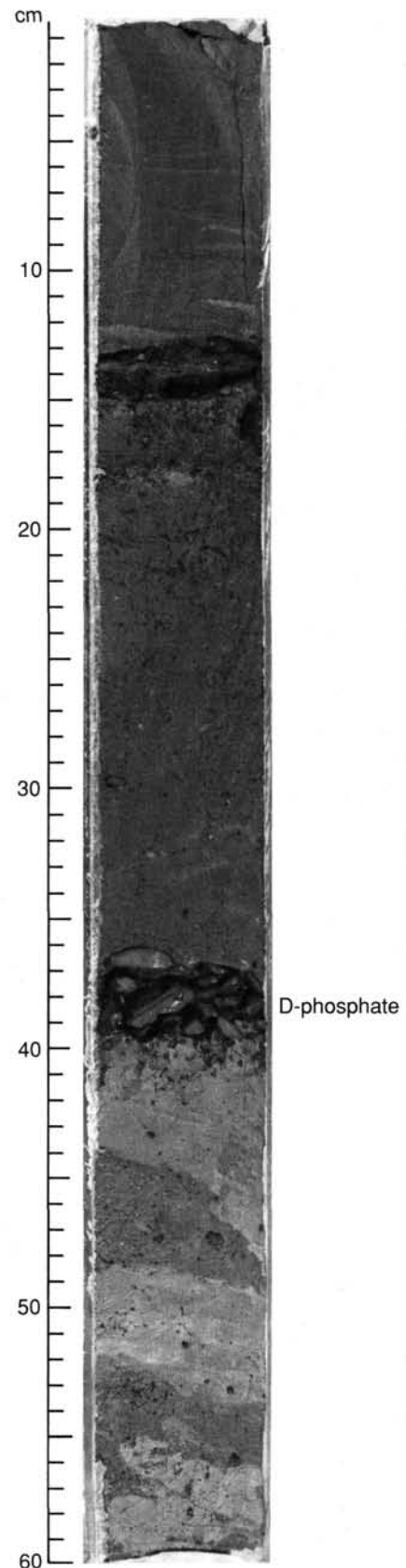


Figure 10. Thin layer of D-phosphate nodules lying above light-colored dolomitic silt and overlain by dark sand and diatomaceous mud, Sub-unit IIIC (112-680B-8H-7, 1-60 cm).

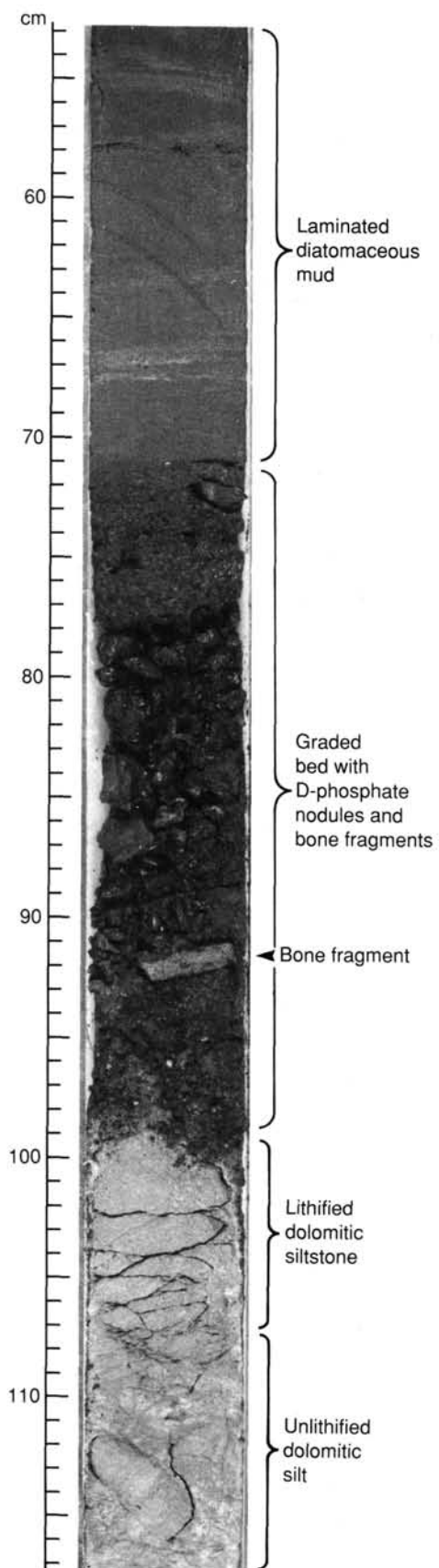


Figure 11. Conglomerate with D-phosphate nodules lying above dolomitized silt bed; see discussions in text; Subunit IIIA (112-680B-7H-3, 53–117 cm).

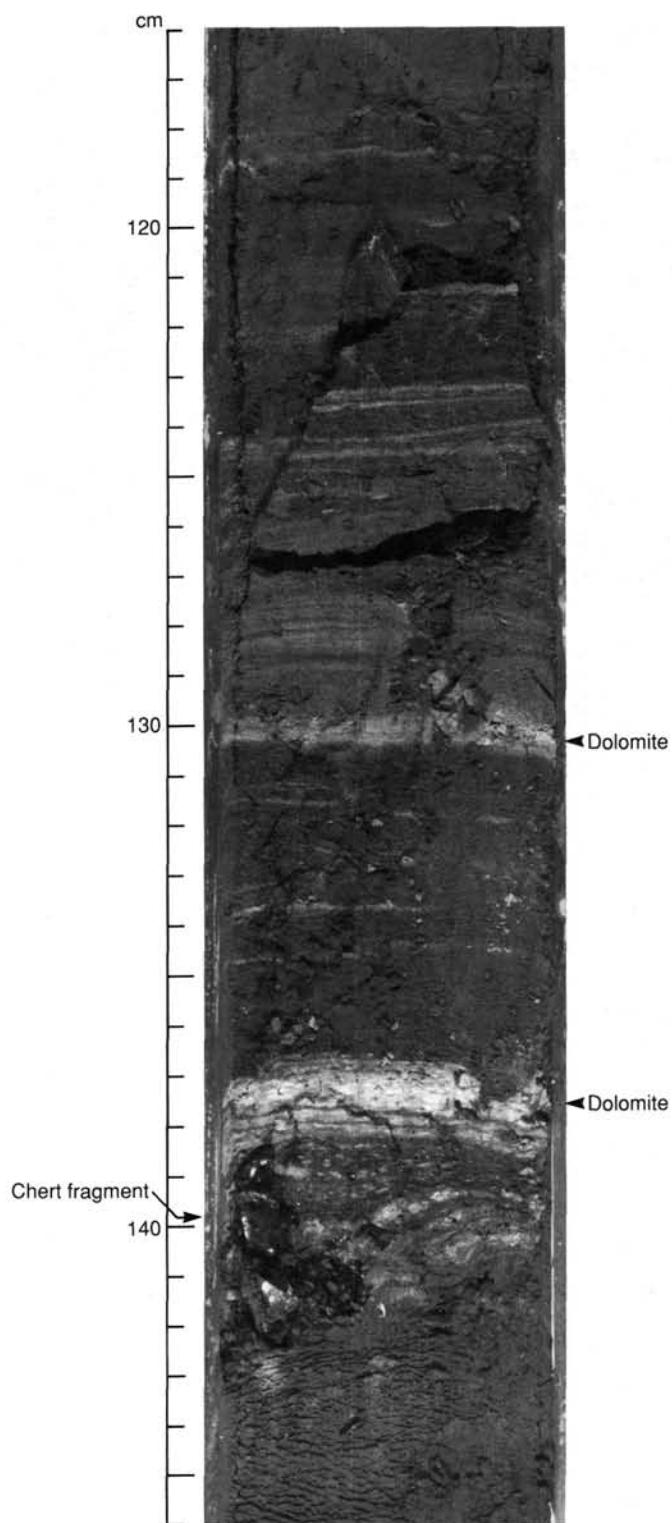


Figure 12. Thin dolomite layers in diatomaceous mud and an opal-CT chert fragment, Unit II (112-680B-6H-4, 116–146 cm).

content. Lithologic Unit III (112-680A-7H to 112-680A-10H, 56.4–93.8 mbsf), a series of lithologies of terrigenous origin, is partly cemented by calcite. Concentrations of CaCO_3 are relatively low throughout (maximum of 6.75% in Sample 112-680A-7H-3, 34–36 cm, at 59.1 mbsf) and do not display any major excursions from a baseline value.

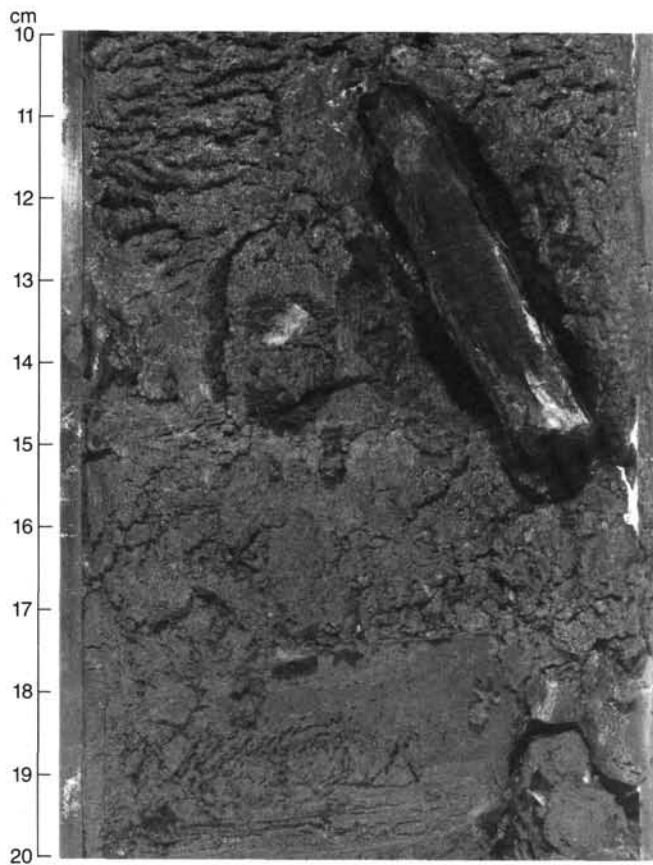


Figure 13. Opal-CT chert fragment, Unit II (112-680B-7H-1, 10–20 cm).

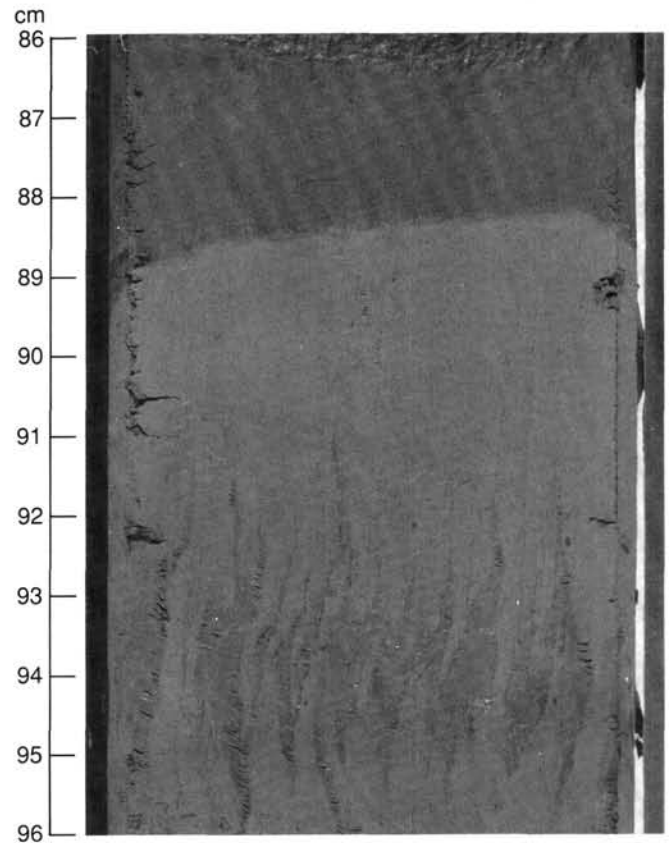


Figure 14. Mud-filled, *en-echelon* tension gashes interpreted as probable dewatering veins (112-680A-9H-4, 86–96 cm).

BIOSTRATIGRAPHY

Three holes were drilled at Site 680 to recover upwelling sediments; the deepest hole terminated at 195.5 mbsf in Pliocene sediments. Siliceous microfossils were abundant in most of the cores recovered, with a predominance of diatoms. Calcareous microfossils occur only in the upper part of the holes drilled. Preliminary information about occurrences, diversity, and abundance of fossil groups can be found in the individual microfossil sections below.

In addition to the usual fossil groups, we noted the occurrence of mollusks in the lowest part of Cores 112-680A-3H and 112-680B-3H, as well as in Section 112-680B-4H, CC. Mollusks include nukulids and pectinids in Section 112-680B-3H, CC.

Correlation between Holes 680A and 680B (Fig. 17) is based on first and last occurrences of both diatom and silicoflagellate species.

Sedimentation rates (Fig. 18) are based primarily on diatom datum levels because the other fossil groups (with the exception of silicoflagellates) were not useful at this site.

Diatoms

We studied all core-catcher samples and some additional significant layers from the split cores; most samples contained well-preserved, abundant diatom assemblages. The character of these assemblages varied between typical upwelling and oceanic. Assemblages dominated by *Chaetoceros*, *Delphineis*, *Thalassionema*, *Thalassiothrix*, and *Nitzschia seriata* were characteristic of upwelling, and assemblages dominated by common *Coscinodiscus nodulifer*, and *Pseudoeunotia doliolus* a.o. were characteristic of oceanic conditions (Schuette and Schrader, 1979, 1981a,

1981b). *Coscinodiscus nodulifer* was abundant in some intervals; dominant diameters varied from large to small.

Displaced shallow-water species did occur occasionally, but never formed a substantial part of the total assemblage. No freshwater species were detected.

Hole 680A

We encountered well-preserved, abundant diatom floras in all core-catcher samples. *Pseudoeunotia doliolus* was found in Sections 112-680A-1H, CC through 112-680A-5H, CC, which places these sections in the Quaternary (0 to <1.8 Ma). *Mesocena quadrangula* occurred in Sections 112-680A-4H, CC through 112-680A-5H, CC, which places these cores in the *Mesocena quadrangula* Zone of Bukry and Foster (1973), 0.79 to 1.8 Ma (Burckle, 1977). *Distephanus pulchra* (silicoflagellate; synonym is *Octactis pulchra*) occurred throughout Sections 112-680A-1H, CC through 112-680A-4H, CC. The occurrence of this species substantiates our assumption that the normal geomagnetic field polarity found in the first four cores represents the Brunhes Magnetic Epoch. *Nitzschia jouseae* was found last in Section 112-680A-8H, CC, and we assigned a tentative age of >2.5 Ma to this sample. Because we did not find *Rossiella tatsunokuchiensis* in the deepest sample, the bottom of this hole should be younger than 2.55 Ma, assuming the LAD of this species is isochronous throughout the Pacific (Koizumi, 1986).

Samples that clearly indicate warm-water, oceanic conditions are from Sections 112-680A-1H, CC, 112-680A-2H, CC, 112-680A-3H, CC, and 112-680A-5H, CC. The more sand-rich samples contained sporadic occurrences of displaced benthic diatoms, which thrive only in a water depth of 0 to 100 m (photic

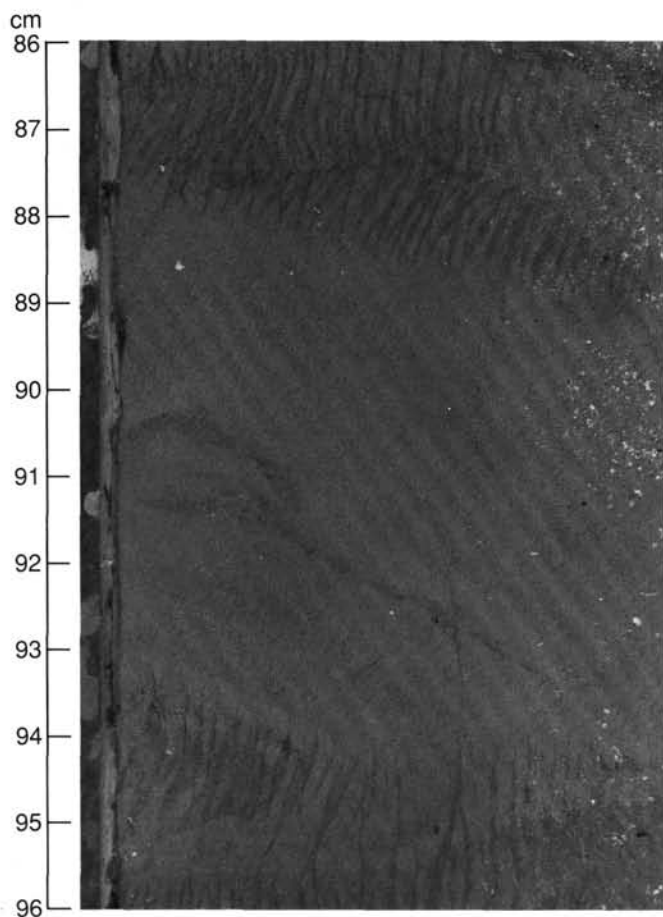


Figure 15. Slump fold with well-developed dewatering veins cross-cutting the basal decollement and folded beds (Sample 112-680B-10H-2, 86-96 cm).

zone). Girdle bands, *Nitzschia "pseudoeunotia,"* and small *Thalassiosira* floods did occur in Section 112-680A-6H, CC and in the light-green to white layers throughout the hole. We could not decide if these layers are caused by intensive, bloomlike production in the photic zone or by winnowing at the bottom.

Hole 680B

All core-catcher samples contained a diversified, well-preserved diatom assemblage, except the following samples: 112-680B-3H, CC, 112-680B-4H, CC, 112-680B-8H, CC, 112-680B-12H, CC, 112-680B-14X, CC, 112-680B-14H, CC, and 112-680B-20X, CC. These samples either had no diatoms or contained only nondiagnostic fragments.

The *Mesocena quadrangula* Zone was recognized in Section 112-680B-5H, CC, which places the interval above this sample into the normal Brunhes Magnetic Epoch and those below this sample into the reversed Matuyama Magnetic Epoch. *Pseudoeunotia doliolus* was found in Section 112-680B-6H, CC, which places this sample in the Pleistocene, younger than 1.8 Ma. *Thalassiosira convexa* occurred in Section 112-680B-7H, CC; a tentative age of >2.3 Ma (LAD of *Thalassiosira convexa* is at 2.3 Ma). Koizumi (1986) was assigned to this sample. *Nitzschia jouseae* was seen last in Section 112-680B-9H, CC (LAD about 2.5 Ma; FAD about 4.5 Ma; Koizumi, 1986). *Rossiella tatsunokuchiensis* occurred last in Section 112-680B-14X, CC (LAD around 2.55 Ma; Koizumi, 1986). *Rossiella tatsunokuchiensis* and *Goniothecium* spp. (large species) co-occurred in Section 112-680B-19X, CC. This interval may be correlated with the lower Pliocene interval at the previous Site 679 (112-679B-9H,

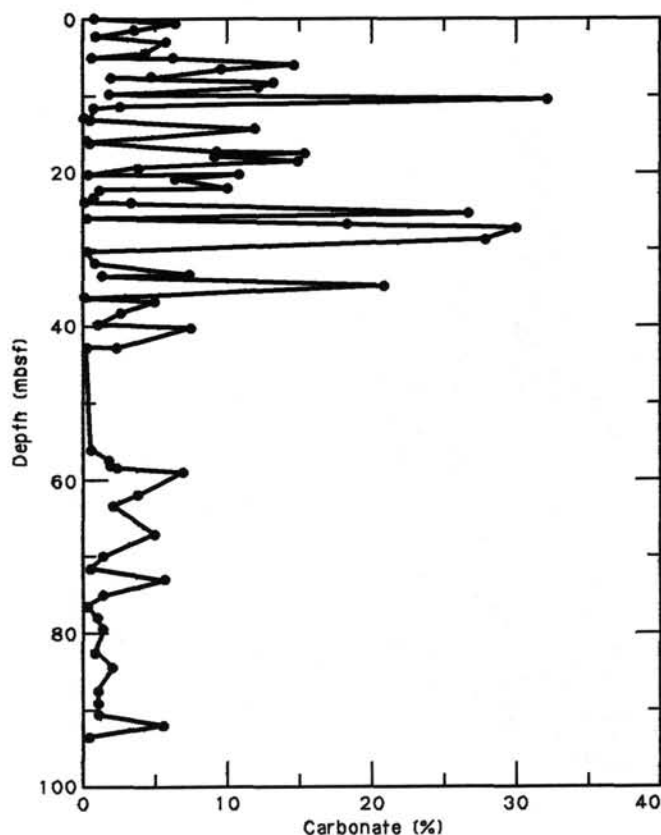


Figure 16. Carbonate contents in Hole 680A.

CC). The deepest section, 112-680B-22X, CC, did not contain *Denticula* or *Rouxia* species and should be younger than the Pliocene/Miocene boundary (< 5.5 Ma).

We found warm-water assemblages in Sections 112-680B-1H, CC and 112-680B-2H, CC. Floods of monospecific assemblages with girdle bands, *Delphineis "capitata,"* *Nitzschia "pseudoeunotia,"* and *Chaetoceros setae* and spores occurred throughout the hole and were concentrated in the distinctly lighter layers. Displaced shallow-water diatoms seemed to be enriched in the more sandy layers (112-680B-14X, CC).

Hole 680C

Three core-catcher samples were available for general study. Of these, only the first two (112-680C-1H, CC and 112-680C-2H, CC) contained siliceous microfossils. Section 112-680C-3H, CC was barren. The siliceous samples contained *Distephanus pulchra* (silicoflagellate) and *Pseudoeunotia doliolus*. The co-occurrence of these two species places these samples in the Brunhes normal Magnetic Epoch. Section 112-680C-1H, CC contained abundant *Cyclotella striata/stylorum*. This species, together with *Delphineis* and *Chaetoceros*, is one member of the upwelling assemblage.

Silicoflagellates

We did not study silicoflagellates in detail, but they do occur in most samples from the three holes. This species is associated with abundant diatoms, some sponge spicules, and rare actiniscids. Representatives of the *Distephanus speculum* and *Dictyocha messanensis* groups are the most common forms in the silicoflagellate assemblages. The only *Mesocena* species found is *Mesocena quadrangula* in Sections 112-680A-4H, CC through 112-680A-6H, CC and Section 112-680B-5H, CC, which are of Pleistocene age.

Table 4. Carbonate concentrations in Hole 680A.

Sample (cm)	Depth (mbsf)	CaCO ₃ (%)
112-680A-1H-1, 25-26	0.25	0.67
1H-1, 89-91	0.89	6.25
1H-2, 25-27	1.75	3.42
1H-2, 104-106	2.54	0.83
1H-3, 25-26	3.25	5.58
1H-4, 25-26	4.75	4.17
1H-4, 77-79	5.27	0.50
1H-4, 88-90	5.38	6.16
1H-5, 25-26	6.25	14.49
1H-5, 81-83	6.81	9.50
1H-6, 25-26	7.75	4.66
1H-6, 37-39	7.87	1.83
2H-1, 25-26	8.55	13.08
2H-1, 86-88	9.16	12.00
2H-2, 25-26	10.05	1.67
2H-2, 96-98	10.76	31.99
2H-3, 25-26	11.55	2.42
2H-3, 51-53	11.81	0.58
2H-4, 25-26	13.05	0.00
2H-4, 56-58	13.36	0.42
2H-5, 25-27	14.55	11.83
2H-6, 25-26	16.05	0.08
2H-6, 68-70	16.39	0.33
2H-7, 25-26	17.55	9.16
2H-7, 44-46	17.74	15.25
3H-1, 25-26	18.05	9.00
3H-1, 93-94	18.73	14.74
3H-2, 25-27	19.55	3.76
3H-2, 121-23	20.46	0.25
3H-3, 25-26	21.05	6.33
3H-3, 116-118	21.96	10.75
3H-3, 145-150	22.25	9.91
3H-4, 25-26	22.55	1.00
3H-4, 119-121	23.49	0.67
3H-5, 25-27	24.05	0.00
3H-5, 31-32	24.12	3.17
3H-6, 25-26	25.55	26.49
3H-6, 81-83	26.11	0.17
3H-7, 25-26	27.05	18.16
4H-1, 25-26	27.55	29.82
4H-2, 25-26	29.05	27.66
4H-3, 25-26	30.55	0.17
4H-4, 25-26	32.05	0.67
4H-5, 25-26	33.55	7.25
4H-5, 40-42	33.70	1.17
4H-6, 25-26	35.05	20.66
4H-7, 25-26	36.55	0.00
5H-1, 18-19	36.98	4.83
5H-2, 18-19	38.48	2.50
5H-3, 18-19	39.98	0.92
5H-3, 57-59	40.37	7.33
5H-4, 17-18	41.47	0.17
5H-5, 17-18	42.96	2.17
7H-1, 35-36	56.15	0.42
7H-2, 33-35	57.63	1.67
7H-2, 80-82	58.10	1.75
7H-2, 124-126	58.54	2.25
7H-3, 34-36	59.14	6.75
7H-5, 34-36	62.13	3.67
7H-6, 27-29	63.56	2.00
8H-2, 35-37	67.15	4.83
8H-4, 33-36	70.13	1.25
8H-5, 34-35	71.66	0.42
8H-6, 34-36	73.15	5.50
9H-1, 34-36	75.14	1.33
9H-2, 34-36	76.64	0.25
9H-3, 34-35	78.14	0.83
9H-4, 34-35	79.64	1.25
9H-6, 34-36	82.64	0.75
10H-1, 25-26	84.55	1.92
10H-3, 25-26	87.55	0.92
10H-4, 25-26	89.05	0.92
10H-5, 25-26	90.55	0.92
10H-6, 20-21	92.05	5.41
10H-7, 20-21	93.50	0.33

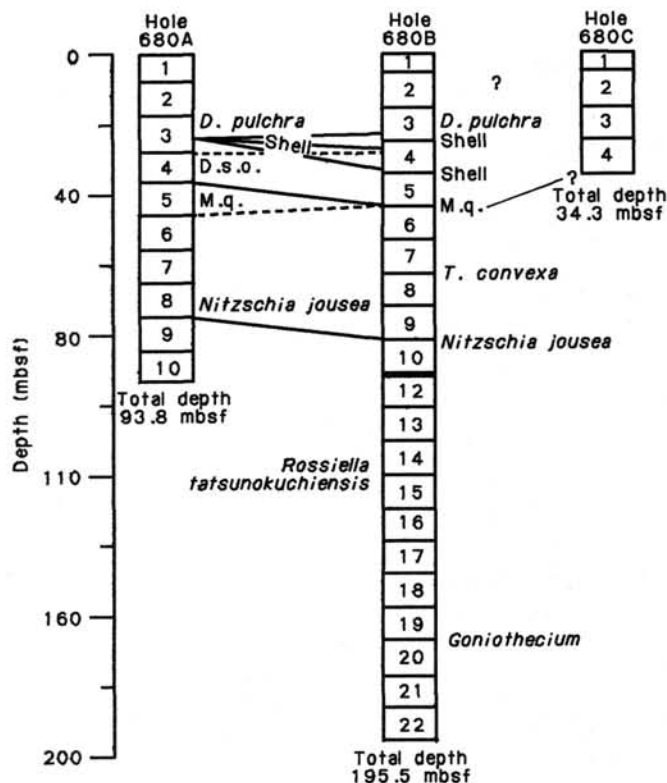


Figure 17. Correlation among holes at Site 680, based on first and last occurrences of silicoflagellates and diatoms. M.q. = *Mesocena quadrangula*; T. = *Thalassiosira*; D. = *Distephanus*; D.s.o. = *Distephanus speculum* var. *octonarius*.

Distephanus bioctonarius bioctonarius was noted in Section 112-680A-3H, CC and in several levels between Samples 112-680B-2H-2, 96-97 cm and 112-680B-4H-2, 90-91 cm, indicating an early Pleistocene age for these samples (for discussion of the *Mesocena quadrangula* Zone, see Locker and Martini, 1986).

Calcareous Nannoplankton

In Hole 680A we found only calcareous nannoplankton in the upper five cores in rather monotonous assemblages at various levels. Assemblages include *Gephyrocapsa oceanica*, *Gephyrocapsa aperta*, *Helicosphaera carteri*, and *Cyclococcolithus leptoporus*, all of Quaternary age (possibly Zone NN20, *Gephyrocapsa oceanica* Zone, for Core 112-680A-1H). In Sample 112-680A-5H-4, 22-23 cm a few specimens of *Pseudoemiliana lacunosa* were found, indicating that this level is not younger than nannoplankton Zone NN19 (*Pseudoemiliana lacunosa* Zone). Cores 112-680A-6H to 112-680A-10H are barren of calcareous nannoplankton.

A similar distribution pattern was found in Hole 680B. Quaternary calcareous nannoplankton is present in the upper five cores. The lowest occurrence of nannoplankton was noted in Section 112-680B-7H, CC, but this may represent downhole contamination. All other cores down to the last core (112-680A-22H) contained no calcareous nannoplankton. *Cyclococcolithus macintyreii* was found in Sample 112-680B-3H-4, 97-98 cm, indicating calcareous nannoplankton Zone NN19a (lower part of *Pseudoemiliana lacunosa* Zone) in this particular level. The higher-level samples are difficult to evaluate because of the low diversity, which may partly represent Zone NN20 (*Gephyrocapsa oceanica* Zone).

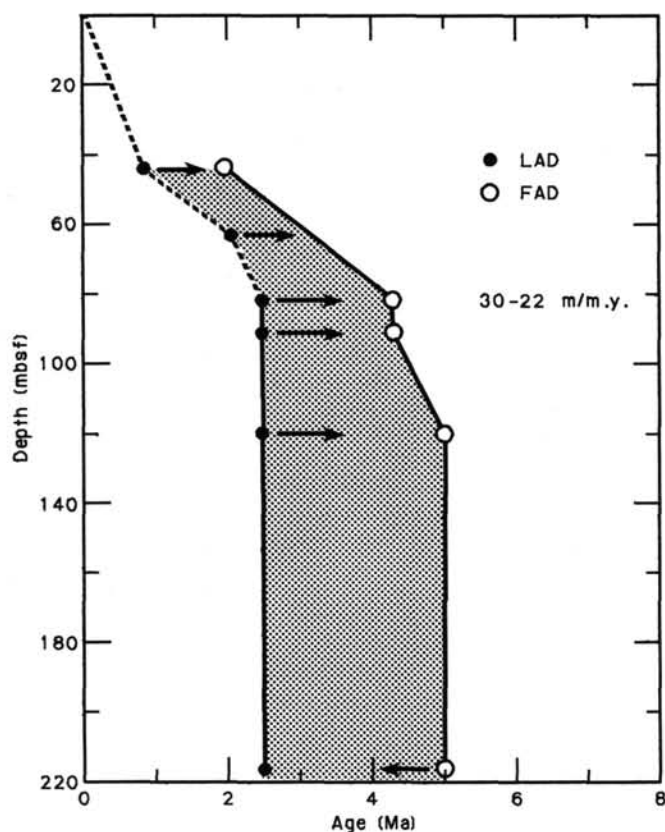


Figure 18. Sedimentation rates (30–22 m/m.y.) at Hole 680B, based on ranges of first (FAD) and last (LAD) occurrences of selected diatom species. A hiatus may be present between Sections 112-680B-10H, CC and 112-680B-11H, CC.

A massive occurrence of calcareous nannoplankton was found in a pale, 4-mm-thick layer in Sample 112-680B-2H-1, 105–106 cm, that represents a bloom of *Helicosphaera carteri* and *Gephyrocapsa oceanica* with preservation of complete cells.

Dolomite rhombs are rather common in several samples from both holes. We noted the negative relationship between these and the abundance of calcareous nannoplankton. With increased dolomite rhombs, nannoplankton assemblages become scarce and finally disappear.

Sections 112-680C-1H, CC through 112-680C-4H, CC were barren of calcareous nannoplankton; Section 112-680C-3H, CC showed abundant dolomite rhombs.

Radiolarians

Hole 680A

All core-catcher samples from this hole were studied for radiolarians. Radiolarians are absent in most samples and, when present, are diluted by diatoms and thus are rare. Preservation is generally good. No age assignments were possible because of scarcity, except for Sections 112-680A-1H, CC through 112-680A-5H, CC.

Liriospyris toxarium, *Octapyle stenozoa*, *Spongurus* sp., *Pterocanium grandiporus*, and *Hexacanthium encanthum* were found in Section 112-680A-1H, CC. *Tholospyris scaphipes*, *Cornutella* sp., *Pterocanium trilobum*, *Octapyle stenozoa*, *Lamprocyrtis haysi*, *Dictyophimus infabricatus* were found in Section 112-680A-2H, CC. *Tholospyris scaphipes*, *Larcospira quadrangula*, *Lithostrobos* (?) *seriatus*, *Theoconus minthorax*, *Cornutella* sp., and *Theocalyptra bicornis* were found in Section 112-680A-3H, CC. *Tholospyris* cf. *scaphipes*, *Liriospyris* (?) *tox-*

arium, *Hexacanthium encanthum*, and *Pterocanium trilobum* were found in Section 112-680A-4H, CC. *Tetrapyle octacantha*, *Cycladophora davisiana*, *Pylospira octopyle*, *Dictyophimus infabricatus*, and *Theocalyptra bicornis* were found in Section 112-680A-5H, CC. These species indicate a Quaternary age.

We could not determine ages for Sections 112-680A-6H, CC through 112-680A-10H, CC.

Hole 680B

We examined core-catcher samples for radiolarians. They are absent in most samples, but do occur in Sections 112-680B-1H, CC, 112-680B-2H, CC, 112-680B-9H, CC, and 112-680B-10H, CC.

Section 112-680B-1H, CC contained a few radiolarians of the following species: *Anthocyrtdium ophirensis*, *Octopyle stenozoa*, *Liriospyris toxarium*, *Echinomma delicatulum*, and *Stylodictya validispina* (existing in the Quaternary).

Section 112-680B-2H, CC yielded the following radiolarians: *Tholospyris scaphipes*, *Tetrapyle octacantha*, *Dictyoceras wircchowii*, *Zygocircus* sp., and *Cycladophora davisiana*. These species indicate a Quaternary age. Although a few radiolarians occur in Sections 112-680B-9H, CC and 112-680B-10H, CC, we encountered no age-diagnostic specimens.

Planktonic Foraminifers

Hole 680A

We examined 10 core-catcher samples for planktonic foraminifers. A few well-preserved planktonic foraminifers occurred in Sections 112-680A-1H, CC and 112-680-5H, CC.

Globigerina bulloides, *G. falconensis*, *G. calida calida*, *Globigerinoides ruber*, *Globigerinita glutinata*, *Globigerinella siphonifera*, *Neogloboquadrina dutertrei*, *N. blowi*, and *Pulleniatina obliquiloculata* were recognized in Section 112-680A-1H, CC. This faunal assemblage is transitional to subtropical (Bé, 1977) and indicates a late Pliocene (N21) to Holocene (N23) age, based on the range of *G. calida calida* and *N. dutertrei*.

We again looked at Section 112-680A-1H, CC and observed these additional species: *Globigerinoides sacculifer*, *G. trilobus*, *G. ruber* (pinkish), *Globigerinita uvula*, *Beela digitata*, *Hastigerina pelagica*, and *Globorotalia menardii*. We assigned a Quaternary age to this sample (N22–N23), based on the presence of *B. digitata*. The occurrence of pinkish *G. ruber* is noteworthy. The LAD assigned to this pink form in the Indo-Pacific is of the order of 120,000 m.y. The occurrence of *Globorotalia menardii* is significant because this species has been quantitatively correlated in cores drilled in the Gulf of Mexico (Kennett and Huddleston, 1972), where the occurrences and absences correlate with the climatic events of the Wisconsin glacial and post-glacial (Thunell, 1984).

Globigerina bulloides, *G. rubescens* (rare), *G. quinqueloba*, *Globigerinita glutinata*, *G. uvula*, *Neogloboquadrina blowi*, *N. dutertrei*, and *N. pachyderma* were recognized in Section 112-680A-5H, CC. This faunal assemblage indicates transitional waters (Bé, 1977), and a late Pliocene (N21) to Holocene (N23) age, based on the range of *N. dutertrei*.

Hole 680B

We examined planktonic foraminifers from 16 core-catcher samples. Well-preserved planktonic foraminifers occur in Sections 112-680B-1H, CC through 112-680B-4H, CC, and 112-680B-7H, CC, although they are few or rare.

Orbulina universona, *Neogloboquadrina humerosa*, and *Pulleniatina obliquiloculata* were recognized in Section 112-680B-1H, CC; this association of species occurs primarily in warm-water environments (Bé, 1977). *Neogloboquadrina humerosa* ranges from Zones N18 to N22, late Miocene to Pleistocene (Srinivasan

and Kennett, 1981). *Pulleniatina obliquiloculata* is present from Zone N19 to the Holocene (Banner and Blow, 1967); we assigned a Pliocene or Pleistocene age to this sample.

Globigerina bulloides, *G. falconensis*, *G. quinqueloba*, *Globigerinita glutinata*, *Globigerinella siphonifera*, *Neogloboquadrina incompta*, and *Pulleniatina obliquiloculata* were recognized in Section 112-680B-2H, CC; this faunal assemblage is transitional to subtropical (Bé, 1977), and is Pliocene to Holocene in age.

Globigerina bulloides, *G. falconensis*, *G. calida calida*, *G. quinqueloba*, *G. rubescens*, *Globigerinoides ruber*, *Orbulina universa*, *Globorotaloides hexagona*, *Globorotalia scitula scitula*, *Neogloboquadrina dutertrei*, *N. humerosa*, and *N. pachyderma* were found in Section 112-680B-3H, CC. *Globigerina bulloides* is common in this sample and accounts for about 50% of the total population; this assemblage is transitional (Bé, 1977). The stratigraphic range of *Neogloboquadrina humerosa* is from Zones N18 to N22, late Miocene to Pleistocene (Srinivasan and Kennett, 1981), whereas *N. dutertrei* ranges from N21 to the Holocene. We assigned a late Pliocene (N21) or Pleistocene (N22) age to this sample.

Globigerina bulloides, *G. rubescens*, *G. quinqueloba*, *Globigerinita glutinata*, *G. iota*, *G. uvula*, *Globorotaloides hexagona*, *Orbulina universa*, and *Globorotalia obesa* were found in Section 112-680B-4H, CC. Transitional species predominate and are of late Pliocene or Pleistocene age.

Rare specimens of *Globigerina bulloides* and *Orbulina universa* were recognized in Section 112-680B-7H, CC.

Benthic Foraminifers

Hole 680A

Benthic foraminifers occur in the upper part of the hole, where they are generally abundant and well preserved. We noted only a few recrystallized specimens in Section 112-680A-6H, CC, among them "*Ellipsoglandulina fragilis*" and *Nonionella*. Sections 112-680A-7H, CC through 112-680A-10H, CC are barren of foraminifers. Proceeding downsection, two benthic-foraminifer assemblages occur and are discussed next.

Bolivina seminuda humilis Assemblage. Foraminifers in this assemblage are abundant and well preserved in Sections 112-680A-1H, CC, 112-680A-3H, CC, 112-680A-4H, CC, and rare with moderate preservation in Section 112-680A-2H, CC (8.1–37.0 mbsf). Some of the components of this assemblage change their frequency downsection. In addition to the nominate species, *Bolivina costata* and *Cassidella glabra* are abundant, and *Nonionella auris* is common in Section 112-680A-1H, CC. *Virgulina* sp. also occurs in this sample. In Section 112-680A-3H, CC the nominate species are accompanied by abundant *Cassidella glabra*, *Suggrunda* sp., and common *Bolivina pacifica* and *Buliminella elegantissima*. In Section 112-680A-4H, CC *Cassidulina auka* and *Epistominella* cf. *subperuviana* are common. The *Bolivina seminuda humilis* assemblage denotes an outer-shelf/upper-bathyal oxygen-minimum environment, with those samples having an abundance of *Nonionella* signifying outer-shelf environment.

Cancris inflatus—*Trifarina carinata* Assemblage. Foraminifers are common and moderately well preserved in this assemblage from Section 112-680A-5H, CC (43.2 mbsf). In addition to the nominate species, *Epistominella* cf. *subperuviana*, *Cassidulina* cf. *pulchella* and *Bolivina* spp. are common. A concentration of the large, robust forms of this assemblage also occur in a shell layer at Sample 112-680A-3H-5, 66–98 cm. This assemblage indicates an upper-bathyal environment or possible shelf-edge setting during a lower sea-level stand, as suggested by the large size of the specimens.

Hole 680B

Benthic foraminifers are abundant and well preserved in Sections 112-680B-1H, CC, 112-680A-2H, CC, 112-680A-3H, CC, and 112-680A-4H, CC. They are common to rare and only moderately preserved in Sections 112-680B-5H, CC, 112-680B-6H, CC, and 112-680B-7H, CC. Sections 112-680B-8H, CC through 112-680B-11H, CC and Sections 112-680B-12X, CC through 112-680B-22X, CC are barren of foraminifers. Benthic foraminifers occur in two assemblages and are discussed next.

Bolivina seminuda humilis Assemblage. Some components of this assemblage change in the biostratigraphic sequence. In addition to the nominate species, *Cassidella glabra* is abundant and *Cassidulina* cf. *pulchella* and *Epistominella subperuviana* are common in Section 112-680B-1H, CC (8.1 mbsf). *Virgulina* also occurs in this sample. Sections 112-680B-2H, CC (18.0 mbsf) and 112-680B-7H, CC (63.8 mbsf) have abundant *Bolivina costata*, *Cassidella glabra*, and common *Nonionella auris* accompanying the nominate species, but in addition, *Buliminella elegantissima* is abundant in Section 112-680B-7H, CC. In Sections 112-680B-5H, CC and 112-680B-6H, CC (43.2 and 47.2 mbsf, respectively) *B. seminuda humilis* is the only abundant species. This assemblage denotes an outer-shelf/upper-bathyal, oxygen-minimum environment, with those samples having an abundance of *Nonionella* signifying an outer-shelf environment.

Cancris inflatus—*Trifarina carinata* Assemblage. This assemblage occurs in Section 112-680B-3H, CC (24.7 mbsf), which is from a shell layer correlative with Sample 112-680A-3H-5, 66–68 cm; it also occurs in Section 112-680B-4H, CC. In addition to the nominate species, *Cassidulina auka* is abundant, and *Epistominella* cf. *subperuviana* is common. This assemblage indicates an upper-bathyal environment or possible occurrence at the shelf's edge during a lower sea-level stand, as suggested by the large size of the specimens.

ORGANIC GEOCHEMISTRY

The organic geochemical program at Site 680 involved measuring hydrocarbon gases, organic carbon, Rock-Eval pyrolysis characteristics on selected samples, and preliminary pigment studies. In addition, we collected sediments for shore-based microbiological studies. The work is an extension of that described in the "Organic Geochemistry" section (Site 679 chapter). Instruments are described in the "Explanatory Notes" (this volume).

Hydrocarbon Gases

Nine 5-cm³ sediment samples from 3 to 101 mbsf were collected at Holes 680A and 680B to analyze hydrocarbon gases using the headspace procedure. The results are shown in Table 5. Methane (C₁) and ethane (C₂) are present in all samples but occur at low concentrations: C₁ is less than 150 μL/L of the wet sediment. Also, three canned-gas samples were obtained from Hole 680B between 3 and 78 mbsf. Results of these analyses are also given in Table 5. We smelled hydrogen sulfide in all cores where hydrocarbon gases were measured, but we did not analyze for this gas in the laboratory. These low amounts of hydrocarbon gases suggest that the uppermost 100 m of sediment at this site is within the sulfate reduction zone where the microbiological generation of C₁ is limited (Claypool and Kaplan, 1974). The situation appears similar to that found at Site 679, where low C₁ concentrations occurred to about 150 mbsf.

Depths to the base of the sulfate reduction zone, which corresponds to the base of the zone where microbial C₁ generation is inhibited, depend on the relative rates of microbiological processes and replenishing the system with sulfate (reviewed by Clay-

Table 5. Methane (C₁) and ethane (C₂) at Site 680.

Hole 680A					Hole 680B				
Core-section interval (cm)	Depth (mbsf)	C ₁ (μL/L)	C ₂ (μL/L)	C ₁ /C ₂	Core-section interval (cm)	Depth (mbsf)	C ₁ (μL/L)	C ₂ (μL/L)	C ₁ /C ₂
112-680A-1H-3, 149-150	4.5	56	8.1	7	112-680B-1H-2, 139-140	2.9	40	22	2
3H-4, 149-150	23.8	132	55	2	3H-4, 0-1	19.5	41	1.7	24
6H-1, 90-91	47.2	55	6.8	8	6H-4, 0-1	48.0	^a 14	^a 2.4	^a 6
9H-4, 149-150	80.8	8	0.8	10	9H-5, 0-1	78.0	84	32	3
					12X-CC	100.0	84	6.4	13

Note: All values were determined by the headspace procedure using the HP gas chromatograph except ^a, which were obtained on the HC gas chromatograph.

Canned-gas samples, Hole 680B

Core-section interval (cm)	Depth (mbsf)	C ₁ (μL/L)	C ₂ (μL/L)	C ₁ /C ₂
112-680B-1H-2, 140-145	3.0	54	1.0	54
3H-3, 140-145	19.5	83	1.8	46
9H-4, 135-140	77.9	66	2.1	31

Note: Values determined on the HC gas chromatograph.

pool and Kvenvolden, 1983). Because both sediment-accumulation rates and the amounts of sedimentary organic matter are both high at Site 680, we expected that sulfate would be deleted rapidly and C₁ would be the dominant gaseous component in these sediments. This expectation was not realized as C₁ never exceeded 150 μL/L of wet sediment. The lack of high C₁ concentrations is probably caused by the replenishment of sulfate that (when sediment accumulation rates are low) can come from the overlying seawater. However, at this site salinity increases with depth to almost twice the seawater values, indicating a deeper source for sulfate ions (see "Inorganic Geochemistry" section, this chapter).

The values for the ratios of C₁/C₂ in the sediments at this site are low, less than about 50 (Table 5). We observed ratios of similar magnitude in the uppermost 150 m of sediment at Site 679 and also in the bottommost sample from Hole 679E (see "Organic Geochemistry" section, Site 679 chapter). We believe the processes leading to the low ratios in the uppermost sediments differ significantly from those which account for the low ratios found at depth. In the uppermost sediments, the small amounts of C₁ that can be generated in the presence of sulfate may be anaerobically oxidized in conjunction with active sulfate reduction (reviewed by Claypool and Kvenvolden, 1983), although the evidence of and the mechanisms for this process are still a matter of debate.

The low amounts of C₁ in these sediments are probably the result of two conflicting processes: selective microbial C₁ production and C₁ consumption. The C₂ hydrocarbon, ethane, is believed to be generated in small amounts in sediments by microbial activity, but little is known about its rate of consumption (Claypool and Kvenvolden, 1983). The results obtained for C₂ by the headspace and canned procedures are not consistent (see Table 5), and additional work is needed to solve the analytical problem. However, C₂ concentrations increase gradually with depth in the uppermost sediments at Site 679 and also at Site 680 (Table 5).

At the bottom of Hole 679E, the low C₁/C₂ ratio of about 20 (see Table 4, "Organic Geochemistry" section, Site 679 chapter) is the result of entirely different nonbiogenic processes, namely the thermogenic production of hydrocarbons from the thermal breakdown of organic matter. These processes eventually lead to the formation of natural gas and petroleum. A thermogenic gas mixture contains not only C₁ but also appreciable quantities of C₂ and higher carbon-number hydrocarbons. We are uncertain

as to the precise source of the hydrocarbons at Site 679, but their abrupt appearance was a cause for concern. The bottomhole temperatures (<20°C) are much lower than those required for the slow thermal generation of significant quantities of hydrocarbons, which begins at about 50°C (Hunt, 1979). Thus, the interpretation of C₁/C₂ ratios must include careful consideration of the environmental and geological setting of the sediments in which these compounds are measured. Site 680 and particularly Site 679 illustrate the point well.

Carbon

Table 6 gives the values of total carbon, carbonate carbon, organic carbon, and total organic carbon (TOC) as obtained from Rock-Eval pyrolysis. Part of the "squeeze cakes" from pore-water studies was used for these measurements. Organic carbon values and TOC agree remarkably well and show that the upper 20 m of sediment is rich in organic matter (average percentage of organic carbon is 7.8%). The deepest sample analyzed (78 mbsf) had an organic-carbon content of about 3%. The results of Rock-Eval pyrolysis are listed in Table 7. All five samples are rich in organic carbon and are immature. This organic matter can be classified as type II from dominantly marine sources. Results are similar to those from the uppermost sediments at Site 679.

Geomicrobiological Studies

Samples from the first three cores in Hole 680C generally followed the procedures outlined in "Organic Geochemistry" section (Site 679 chapter). Because of the break in the wire-line cable for the pore-water sampler, this hole was abandoned before we finished collecting microbiological samples. This collecting of samples was repeated and finished at Site 681.

Pigment Analyses

We examined plant pigments from samples of Core 112-680B-3H. Methods for these analyses are described in the "Explanatory Notes" (this volume). The pigment assay (Table 8) was combined with magnetic data in an attempt to reveal any existing correlations with magnetic-intensity data that showed marked periodic oscillations down the core. Thirty-one samples that were used to determine remanent magnetic intensity for the interval from 16 to 24 mbsf at a spacing of about every 20 cm were freeze-dried, ground, and subsampled for TOC and pigment assay (Table 8).

Table 6. Organic carbon and carbonate carbon, Site 680.

Sample (cm)	Depth (mbsf)	Total carbon (%)	Inorganic carbon (%)	Organic carbon (%)	TOC (%)
112-680C-1H-3, 145-150	4.5	5.62	0.14	5.48	5.47
2H-3, 140-150	10.3	11.05	1.05	10	8.78
3H-2, 145-150	18.3	9.33	1.91	7.42	7.54
112-680B-3H-3, 145-150	19.5	10.59	2.18	8.41	8.52
9H-4, 140-150	78.0	3.05	0.13	2.92	3.01

Note: TOC = total organic carbon from Rock-Eval pyrolysis.

When plotted on a common depth scale, results show little correspondence between magnetization and any of the TOC or the pigment data. Figure 19 shows the relationships among TOC, pigments, and magnetization. The magnetic signal possibly is carried by magnetite (as suggested by the intermediate coercivity of the carrier and demagnetization characteristics seen on vector plots), but this hypothesis has not yet been tested. Magnetite could have a detrital origin, in which case we would anticipate a positive correlation between high magnetic signal and high terrestrial input and, conversely, by a negative correlation with a marine planktonic signal. The signal for the phaeo-pigments shows no correlation, although both signals are low at the 21 mbsf interval (a sand layer) and just below. Benthic bacterial magnetite could be another source of the magnetic signal, but further work is necessary to corroborate any of these hypotheses.

However, this study indicated a positive correlation between TOC and the the completely independent determination of pigments, as would be expected for a sediment sequence having a more or less continuous input of organic matter of upwelling origin. The crude "phaeophytin" and "carotenoid" plots show similar trends, whereas the Carot/Total pigment plot shows a decrease in the ratio of 0.75 at 16.5 mbsf to 0.63 at 22.5 mbsf (Fig. 19). Conceivably, this trend might represent part of a climatic cycle in which carotenoid and phaeophytin-type pigments are either formed in different amounts or degraded at different rates. More detailed studies over the full depth of the hole should clarify this finding.

INORGANIC GEOCHEMISTRY

Introduction and Operation

A total of 10 interstitial-water samples were obtained at Site 680 and analyzed. Of these, only one *in-situ* water sample was recovered in Hole 680A, two *in-situ* plus four whole-round samples in Hole 680B, and three whole-round samples in Hole 680C. The whole-round samples in Cores 112-680B-1H, 112-680B-3H, 112-680B-6H, 112-680C-1H, and 112-680C-3H consisted of 5-cm intervals, the others were 10-cm intervals. For *in-situ* water samples, see special comments in the Site 681 chapter (this volume).

Large increases in salinity, chloride, sulfate, calcium, and magnesium concentrations with depth (Tables 9 and 10) indicate

that a highly concentrated brine exists at greater depths. The chloride concentration profile is a classical diffusion profile between a concentrated solution and the "dilute" seawater. Indeed, in Core 112-680C-1H, the interstitial-water Cl^- concentration is equal to standard seawater (Fig. 20 and Table 9). The SO_4^{2-} , Ca^{2+} , and Mg^{2+} profiles are not simple diffusion profiles. These components are usually not conservative in the diagenetic environment; their concentrations are affected by multiple bio-geochemical reactions.

The Origin of the Brines

Dissolution of subaerial or subsurface evaporite minerals such as halite (NaCl) and gypsum or anhydrite ($\text{CaSO}_4 \cdot 2\text{H}_2\text{O}$ or CaSO_4 , respectively) could explain the observed Cl^- , SO_4^{2-} , and Ca^{2+} concentration profiles. Mg^{2+} concentrations, however, would not increase by the mere dissolution of most evaporite deposits. The observed Mg^{2+} increases in the interstitial waters at Site 680 suggest that a dense brine forms in a Holocene evaporative system on land. It may be flowing to the ocean floor through porous sediment zones at greater depth. Residual brines in sabkha or playa environments are enriched in magnesium. The existence of a fossil brine within the deeper sandy and silty sediments, however, cannot be excluded on the basis of the available data. The temperature-pressure regime at these shallow sites (Sites 680 and 681) excludes the possibility of residual brine accumulation during the formation of gas hydrates. These brines strongly influence the rates and types of early diagenetic reactions, especially in the organic-rich hemipelagic sediments, as encountered in the upwelling facies of the Peru Margin.

Chloride and Salinity

Both Cl^- and salinity increase significantly with depth. Cl^- increases from 556 to 1043 mmol/L at 196 mbsf, and salinity from 34.2 to 64.0 g/kg. The observed increases in salinity are controlled primarily by the anion Cl^- concentrations and alkalies, which we did not analyze on board the ship.

Alkalinity and Sulfate

At 1.3 mbsf high alkalinity values of 16.69 mmol/L and lower-than-seawater sulfate concentrations of 25.26 mmol/L were observed. Organic carbon content in the top three sections (112-680C-1H-1, 112-680B-1H-2, and 112-680C-1H-3) is high, between 5% to 10% (see "Organic Geochemistry" section, this chapter). In such organic-rich sediments, the onset of bacterial sulfate reduction occurs immediately below the sediment/water interface or even in the water column, producing H_2S and HCO_3^- and thus increasing alkalinity. The maximum alkalinity of 19.73 mmol/L is found at 19.5 mbsf, about 28 m shallower than the minimum sulfate concentration. The "apparent" shallower alkalinity maximum probably reflects extensive carbonate diagenesis between 20 to 70 mbsf in the zone of maximum sulfate reduction (lowest sulfate concentrations).

Sulfate reduction is incomplete at this site; the minimum sulfate concentration remains at 5.96 mmol/L at 47.5 mbsf. Below this depth it increases rapidly by diffusion from the subsurface brine. The incomplete sulfate reduction explains the low CH_4

Table 7. Summary of Rock-Eval pyrolysis for Holes 680B and 680C.

Core/section interval (cm)	Depth (mbsf)	Temp. ($^{\circ}\text{C}$)	S ₁	S ₂	S ₃	PI	PC	TOC (%)	HI	OI
112-680C-1H-3, 145-150	4.5	388	4.57	23.69	3.52	0.16	2.35	5.47	433	64
2H-3, 140-150	10.3	389	6.80	40.24	6.88	0.14	3.92	8.78	458	78
3H-2, 145-150	18.3	391	5.64	31.72	5.50	0.15	3.11	7.54	420	72
112-680B-3H-3, 145-150	19.5	397	6.26	38.63	6.61	0.14	3.74	8.52	453	77
9H-4, 140-150	78.0	395	1.52	9.67	1.25	0.14	0.93	3.01	321	41

Note: Rock-Eval parameters are defined in "Organic Geochemistry" section, Site 679 chapter (this volume).

Table 8. Pigment assays for Hole 680B.

Core/ section	Interval (cm)	Depth (mbsf)	Phaeo.	Carot.	Total pigment	Carot./total pigment	Magnetic intensity (mA/m)
112-680B-3H-1	69-71	15.69	9	9	18	0.50	0.89
3H-1	119-121	16.19	24	51	75	0.68	2.81
3H-1	130-131	16.30	31	71	102	0.70	1.34
3H-2	4-6	16.54	28	90	118	0.76	6.03
3H-2	16-18	16.66	33	111	144	0.77	1.27
3H-2	28-30	16.78	34	105	139	0.76	3.00
3H-2	38-40	16.88	30	99	129	0.77	1.22
3H-2	69-71	17.19	27	76	103	0.74	1.58
3H-2	128-130	17.78	24	67	101	0.66	1.66
3H-2	140-142	17.90	21	55	76	0.72	0.50
3H-3	10-12	18.10	15	38	53	0.72	2.98
3H-3	26-28	18.26	25	60	85	0.71	0.83
3H-3	38-40	18.38	34	74	108	0.69	0.80
3H-3	65-67	18.65	30	75	105	0.71	1.90
3H-3	105-107	19.05	24	60	84	0.71	0.94
3H-4	10-12	19.60	33	85	118	0.72	3.73
3H-4	26-28	19.76	30	66	96	0.69	4.25
3H-4	35-37	19.85	30	73	103	0.71	4.41
3H-4	54-56	20.04	25	51	76	0.67	3.76
3H-4	103-105	20.53	26	56	82	0.68	1.72
3H-4	133-135	20.83	21	44	65	0.68	6.94
3H-5	2-4	21.02	7	11	18	0.61	0.94
3H-5	27-29	21.27	8	11	19	0.58	1.17
3H-5	43-45	21.43	33	75	108	0.69	5.50
3H-5	64-66	21.64	43	98	141	0.70	4.61
3H-5	85-87	21.85	39	68	107	0.64	
3H-5	104-106	22.04	39	76	115	0.66	
3H-5	118-120	22.18	53	78	131	0.60	0.29
3H-6	5-7	22.55	52	79	131	0.60	0.58
3H-6	18-20	22.68	54	88	142	0.62	0.85
3H-6	41-42	22.91	41	94	135	0.70	2.06
3H-6	56-58	23.06	34	73	117	0.62	5.09
3H-6	93-95	23.43	22	48	70	0.69	0.47
3H-6	109-111	23.59	25	53	78	0.68	0.86
3H-6	137-139	23.87	15	33	48	0.69	

Note: H = hydraulic piston; Phaeo. = phaeopigments; Carot. = carotenoids.

concentrations observed by the organic geochemists at this site. Only after sulfate is depleted, does fermentation and methane production become the main microbial pathway of organic matter remineralization.

Ammonia

Ammonia concentrations range from 1.71 to 5.19 mmol/L. These concentrations continuously increase with depth. With no data points between 80 to 196 mbsf, we could not compare the depth of maximum NH_4^+ concentration at this site with other sites. Usually, NH_4^+ peaks at a greater depth than alkalinity.

Phosphate

Only a few phosphate values were available because samples with high H_2S concentrations could not be analyzed colorimetrically owing to color interferences. Other methods will be used for future phosphate analyses of these samples. Phosphate concentrations are high immediately in the uppermost few meters, 15 to 17 $\mu\text{mol/L}$, and decrease with depth. As at Site 679 but at a depth between 80 and 197 mbsf (instead of between 1.5 and 80 mbsf at Site 679), PO_4^{3-} concentrations seem to remain constant around 4 $\mu\text{mol/L}$. In the Site 679 chapter ("Inorganic Geochemistry" section, this volume) we suggested that this phosphate value might be controlled by francolite solubility. Unlike Site 679, the higher phosphate values in the top 80 m suggest that the rate of phosphate generation by bacterial degradation of organic matter is faster at the shallower Site 680 than the combined rates of francolite formation plus PO_4^{3-} diffusion into bottom seawater.

Silica

Silica concentrations increase rapidly downhole. At a depth of 1.3 mbsf, 955 $\mu\text{mol/L}$ SiO_2 was observed. This value is close to the solubility of opal-A at bottom temperature (about 13°C) and pressure. Silica values reach a maximum of 1118 $\mu\text{mol/L}$ at 47.5 mbsf, the depth of minimum sulfate concentration, and slowly decrease with depth. The rapid increase in dissolved silica

values near the sediment/water interface may be partially attributed to higher dissolution rates of opal-A below the sediment/seawater interface and at higher ionic strengths.

The decrease in silica concentrations from about 50 mbsf, and especially below 90 to 100 mbsf, coincides with lithological changes from Unit I to Unit II and Unit IIID, respectively (see "Lithostratigraphy" section, this chapter).

Calcium and Magnesium

Immediately below the sediment/water interface, Ca^{2+} and Mg^{2+} concentrations are lower than seawater concentrations. Both continue to decrease with depth down to 20 mbsf. Below this depth, these concentrations increase by diffusion of Ca^{2+} and Mg^{2+} from the subsurface brine, and possibly by the release of Ca^{2+} from the calcite-dolomitization reaction. Thus, in the uppermost 20 m of the section Mg^{2+} and at least some of the Ca^{2+} are continuously replenished by diffusion from seawater as well as from the subsurface brine.

The $\text{Mg}^{2+}/\text{Ca}^{2+}$ (molar ratio) profile indicates that within the first 10 mbsf Ca^{2+} is preferentially consumed relative to Mg^{2+} ; the ratio increases from a seawater value of 5.4 to 6.4. The $\text{Mg}^{2+}/\text{Ca}^{2+}$ ratio remains higher than the seawater ratio to almost 40 mbsf. Such high ratios increase the rate of dolomite formation in every geochemical environment. Even at 196 mbsf, the $\text{Mg}^{2+}/\text{Ca}^{2+}$ ratio is still high enough (3.0) for dolomite formation.

We concluded that the first diagenetic phases formed are Ca^{2+} -rich phases, i.e., francolite and/or calcite. Alkalinity values control the rate and therefore the relative amounts of calcite vs. apatite formed. Consequently, an ideal geochemical environment for dolomite formation is established: while sulfate reduction and alkalinity production continue, the $\text{Mg}^{2+}/\text{Ca}^{2+}$ ratios increase and the initiation of dolomite formation is inevitable. Dolomite formation should continue throughout the entire depth interval drilled.

PALEOMAGNETICS

Introduction

At this site, the upper 33 to 35 m of each core have a strong magnetic signal that was easy to measure with the on-board spinner magnetometer. The deeper sediments were characterized by weak magnetic moments (<0.05 mA/m). We could not measure these samples aboard ship. Shore-based studies, conducted after the cruise, will use a cryogenic magnetometer. We hope that during these land-based studies we can successfully measure the weak remanence.

Results

Figures 24 and 25 show the declination, inclination, and intensity values vs. depth for the samples from Holes 680A and 680B, respectively. The value selected and reported in the figures is the 150-Oe demagnetization value, which was selected on the basis of the vector plots. For samples that occur below the diagenetic front (see below) we used the natural remanent magnetization (NRM) values. Although this causes some selectivity in our set of samples, the samples in the lower cores from Holes 680A and 680B were too weak to demagnetize or measure. Because the direction of the NRM and the 150-Oe demagnetization values for the upper cores from the site are of the same polarity, we suggest that the directions of these samples should also be only slightly affected by demagnetization. Using the NRM value is also justified with these weaker samples because they contain a reversed polarity. Any remagnetization of these samples that would give these sediments a reversed overprint must have occurred before the Brunhes. Next is a summary of results from the two holes.

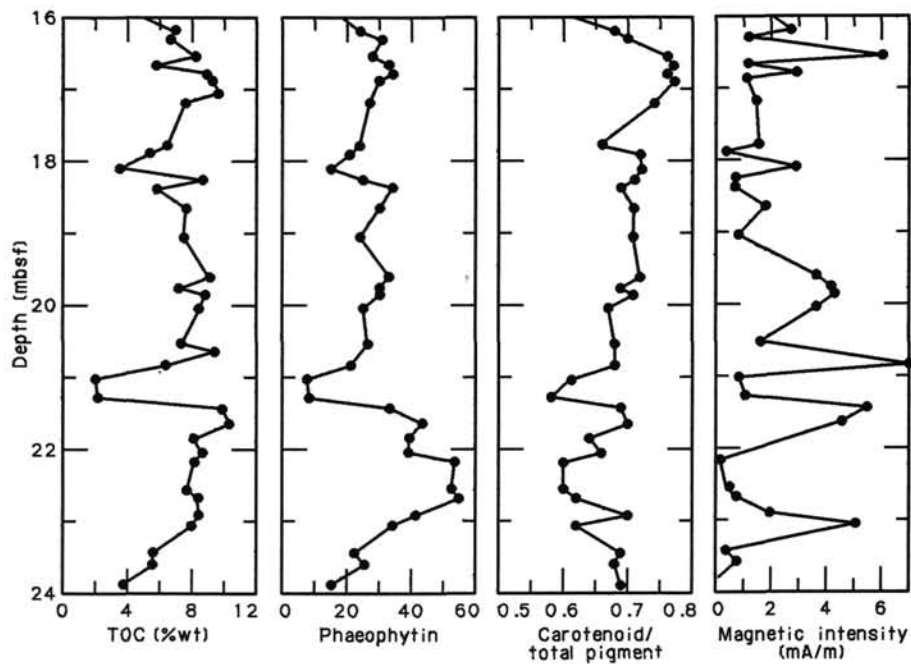


Figure 19. Downhole distribution of TOC, pigments, and magnetic intensity over an interval of 16 to 24 mbsf in Core 112-680B-3H. TOC = total organic carbon (wt%). Magnetic intensity = intensity of remanent magnetization after treatment of 150 Oe of alternating-field demagnetization. The pigment concentrations relate directly to total organic carbon content. The remanent magnetism shows no direct correlation.

Table 9. Concentrations of chloride in Holes 680A, 680B, and 680C.

Sample interval (cm)	Depth (mbsf)	Cl ⁻ (mmol/L)	Cl ⁻ (g/kg)	Percentage of seawater
112-680C-1H-1, 130-135	1.3	556.15	19.268	99.5
112-680B-1H-2, 145-150	3.0	559.95	19.400	100.2
112-680C-1H-3, 145-150	4.5	564.69	19.564	101.0
2H-3, 140-150	10.2	583.68	20.222	104.4
3H-2, 145-150	18.3	595.07	20.617	106.6
112-680B-3H-3, 145-150	19.5	602.66	20.880	107.8
6H-3, 145-150	47.5	643.47	22.294	115.1
<i>In-situ</i> #1	62.5	657.70	22.787	117.7
9H-4, 140-150	77.9	747.86	25.910	133.8
<i>In-situ</i> #2	195.5	1043.02	36.136	186.6
112-680A <i>In-situ</i> #1	93.9(?)	616.89	21.373	110.4

Note: seawater is standard IAPSO: Cl⁻ (mmol/L) = 559 and Cl⁻ (g/kg) = 19.367.

Hole 680A

The samples we collected from this hole are all normal (negative inclination) down to around 35 mbsf. The Brunhes/Matuyama boundary occurs at this depth. Samples recovered from below 35 mbsf show reversed polarity (Fig. 24). Note that the intensity of the samples at 150-Oe demagnetization may show a cyclicity vs. depth (righthand plot in Fig. 24). Below 40 mbsf the intensity of magnetization is low (< 0.5 mA/m). We believe this abrupt change in the magnetic character of these samples is caused by a diagenetic change in the magnetic phases above this zone (labeled the diagenetic front) to phases that do not possess remanence. This change is probably related to the chemical reduction of magnetite and the formation of pyrite or other amorphous iron sulfides during early diagenesis.

From the interstitial-water chemistry (see "Inorganic Geochemistry" section, this chapter), it is obvious that the sediments of Site 680 are in the zone of early diagenesis that is dom-

inated by sulfate reduction. In such a strongly reducing environment, the oxide phases, particularly the oxides of iron, are reduced and reprecipitated as sulfides. Even though strong chemical reduction occurs immediately below the water-sediment interface, the magnetic remanence does not entirely disappear until about 40 mbsf. We attribute this lag to the slow kinetics of magnetite dissolution and concurrent iron reduction. The observations made at Sites 679 and 680 (i.e., that the remanence weakens gradually) agree with such a kinetically controlled process.

Hole 680B

Results from this hole are shown in Figure 25. Because results from Holes 680A and 680B are nearly identical, the description of this hole is similar to that of Hole 680A (described previously).

PHYSICAL PROPERTIES

We used the physical-properties measurements for Site 680 to interpret the characteristics of each lithologic unit in a lens-shaped, organic-rich sediment body produced by upwelling on the continental shelf. Measurements were generally performed on split cores at an interval of one every two sections (3 m) in Hole 680A, and at an interval of one every three sections (5 m) in Hole 680B. All data presented for this site were obtained from good quality APC samples. Material recovered with the XCB in Hole 680B was not suitable for physical-properties testing. Disturbance of the sediment "biscuits" in the XCB cores precluded strength and velocity measurements. The water content of the recovered material had also greatly increased during drilling and splitting with the saw; thus, no XCB samples were measured for index properties.

Index Properties

The index properties measured at Site 680 include water content (presented as a percentage of dry sample weight), porosity, bulk density, and grain density (Table 11). We used the same

Table 10. Interstitial-water analyses at Site 680.

Sample interval (cm)	Depth (mbsf)	pH	Alkalinity (mmol/L)	SO ₄ ²⁻ (mmol/L)	PO ₄ ³⁻ (μmol/L)	NH ₄ ⁺ (mmol/L)	SiO ₂ (μmol/L)	Salinity (g/kg)	Cl ⁻ (mmol/L)	Ca ²⁺ (mmol/L)	Mg ²⁺ (mmol/L)	Mg ²⁺ /Ca ²⁺
112-680C-1H-1, 130-150	1.3	7.8	16.69	25.26	17.44	1.71	955	34.2	556.15	9.54	52.86	5.54
112-680B-1H-2, 145-150	3.0	7.7	16.81	19.40	17.55	2.26	873	34.5	559.95	8.65	53.05	6.13
112-680C-1H-3, 145-150	4.5	7.7	15.69	20.63	15.14	1.68	936	34.5	564.69	8.17	52.41	6.42
2H-3, 140-150	10.2	7.3	16.46	18.13	i	2.17	1068	34.5	583.68	8.67	49.58	5.72
3H-2, 145-150	18.3	7.7	19.05	12.63	i	2.65	990	35.2	595.07	8.54	49.13	5.75
112-680B-3H-3, 145-150	19.5	7.1	19.73	10.95	i	2.54	1083	35.2	602.66	8.36	48.01	5.74
6H-3, 145-150	47.5	7.6	15.62	5.96	i	4.05	1118	38.0	643.47	10.09	52.43	5.20
<i>In-situ</i> #1	62.5	7.7	12.81	10.07	12.10	4.24	992	39.8	657.70	12.41	56.34	4.54
9H-4, 145-150	77.9	7.3	8.95	12.34	5.41	4.93	1081	43.8	747.86	14.70	61.96	4.22
<i>In-situ</i> #2	195.5	7.2	4.54	37.88	3.94	5.19	871	64.0	1043.02	36.14	109.44	3.03

i = color interference.

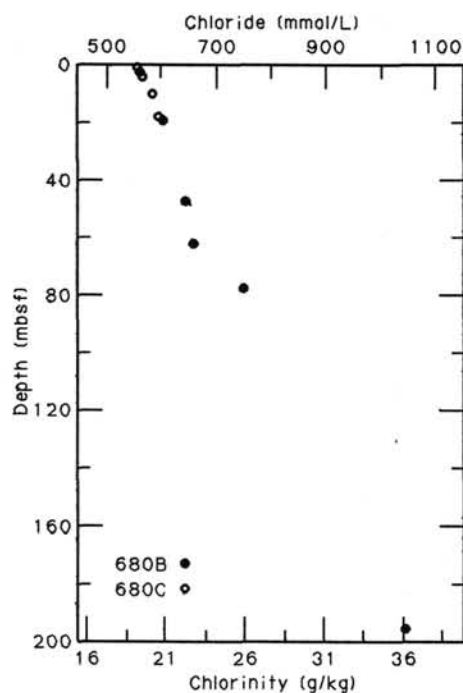


Figure 20. Interstitial chloride concentrations for Holes 680B and 680C.

methods for measuring index properties at Site 680 as those specified in the "Explanatory Notes" (this volume). We assumed that salinity was 35‰ when calculating index properties. However, at this site, the salinity at 92 mbsf was measured at approximately 46‰ (see "Inorganic Geochemistry" section, this chapter). Therefore, we calculated index properties using the appropriate real salinity for the sample depth.

Figure 26 illustrates the downhole trends in water content and porosity with depth and lithologic units for Holes 680A and 680B. Figure 27 shows the trends in bulk density and porosity. Lithologic Unit I is characterized by scattered water content values, which range between 50 and 217%. This variation reflects the diverse lithology of diatomaceous mud and sandy silts within the unit. The high water contents in Unit I are probably from samples taken in diatom-rich facies, with the lower water contents occurring in less-organic silt facies. The porosity in Unit I decreases slightly from a value of 80% near the seafloor to a value of 75% at 47 mbsf. The bulk-density data for Unit I also shows some variation. However, a trend of slight increase can be observed in the data, with values of 1.3 g/cm³ near the seafloor and a value of 1.42 g/cm³ at 47 mbsf. Within this depth range bulk densities vary, reaching as high as 1.88 g/cm³ and as low as 1.23 g/cm³.

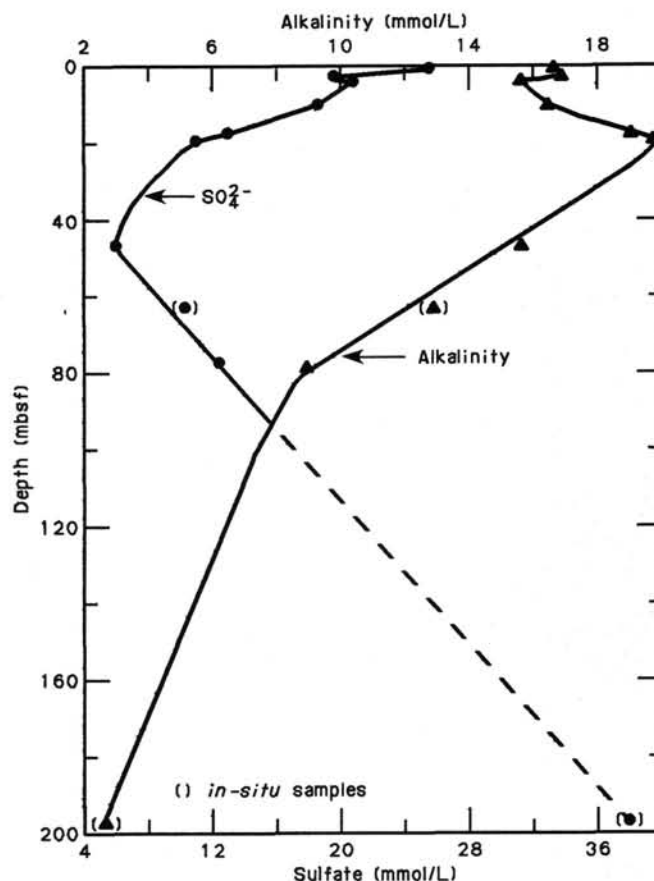


Figure 21. Interstitial sulfate and alkalinity at Site 680.

The boundary between lithologic Units I and II is marked by significant changes in the index properties. Although we recovered no Unit II material in Hole 680A (perhaps because we could not recover approximately 9 m of sediment), we did obtain two index-property samples from Unit II in Hole 680B. There is a sharp increase in water content, to a value of 231% at 52 mbsf, and an increase in porosity, to a value of 85% at 52 mbsf. Bulk density decreases across the boundary, to a value of 1.25 g/cm³ at 52 mbsf, and grain density decreases slightly as well.

The boundary between lithologic Units II and III again is marked by abrupt changes in the index properties. The water content decreases to 49% at 57 mbsf, with the porosity decreasing to 58% at the same depth. The bulk density jumps to 1.82 g/cm³ at 57 mbsf. The change in lithology between Units IIIB and IIIC also is indicated by an increase in water content to

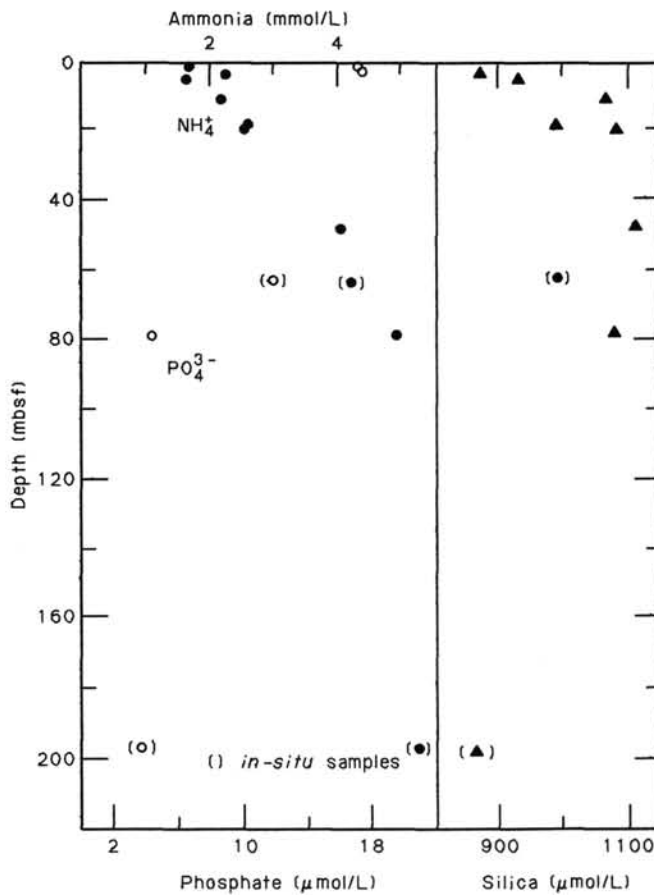


Figure 22. Interstitial ammonia, silica, and phosphate at Site 680.

124% at 68 mbsf. This change appears to occur slightly deeper than at the recorded lithologic boundary. The water content decreases to 59% at 76 mbsf, and again increases slightly but linearly to a value of 106% at 90 mbsf. Bulk density decreases considerably to 1.42 g/cm³ at 68 mbsf. It increases to 1.7 g/cm³ at 76 mbsf, and then decreases slightly to a value of 1.47 g/cm³ at 90 mbsf.

The GRAPE plots (Fig. 28) verify the changes in bulk density that occur from one unit to the next. In particular, the record for Section 112-680B-7H-3 shows the large increase in bulk-density values from approximately 1.3 g/cm³ at 56.7 mbsf to approximately 2.0 g/cm³ at 56.8 mbsf. The values for this section decrease slightly below this peak. Thus, the value of 1.82 g/cm³ measured for the index-property sample obtained at 57 mbsf appears realistic.

Compressional-Wave Velocity

The P-Wave Logger was operated in conjunction with the GRAPE. The P-Wave Logger velocity data were not reduced on board ship. However, inspections of computer printouts indicate velocities close to 1.5 km/s. Velocities also were measured using the Hamilton Frame, in the manner described in the "Explanatory Notes" (this volume).

The Hamilton Frame data is presented in Table 12 and shown in Figure 29. Data from lithologic Unit I are scattered because of the variability of bulk density and water content in this unit. Velocities in Unit I range from near 1.5 km/s to almost 1.6 km/s, with a mean of 1.53 km/s. These low values (near the velocity of water) reflect the high water content of the sediments.

We could not obtain reliable velocity measurements from Unit II using the Hamilton Frame, while values from the P-

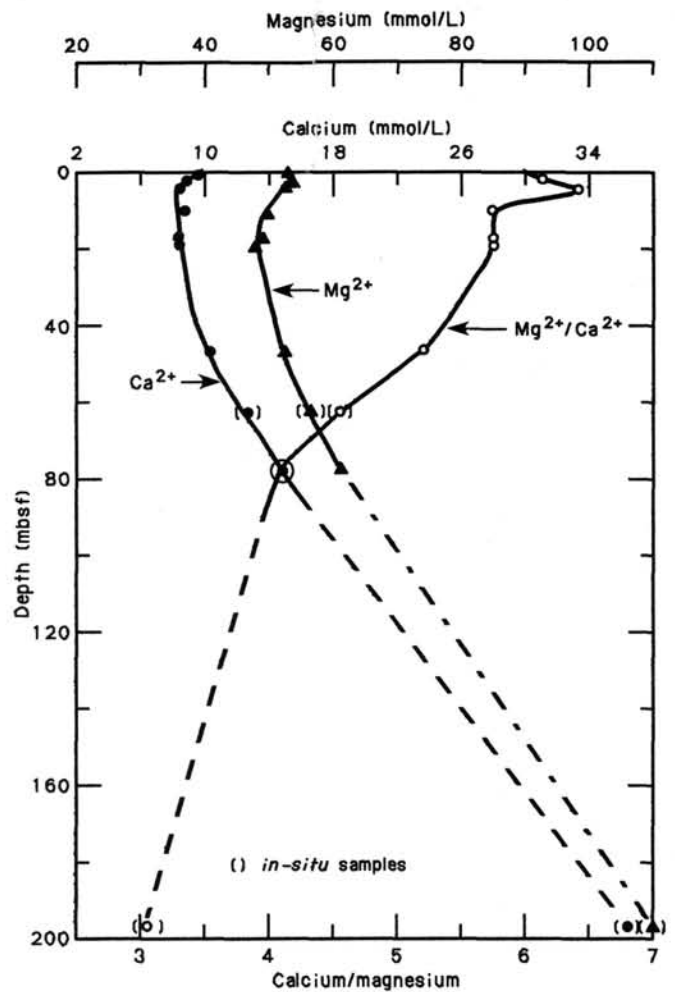


Figure 23. Interstitial calcium and magnesium at Site 680.

Wave Logger have a mean of 1.53 km/s in Unit II. Velocity data from Unit III are less variable than those from Unit I because of the decreased variability in the bulk density and water content. The mean value in Unit III is 1.54 km/s, again reflecting the high water content of the sediments.

Vane Shear Strength

The undrained vane shear strengths at Site 680 were measured using the Wykham Farrance vane apparatus. Values obtained for peak undrained vane shear strength are presented in Table 13 and are shown in Figure 30.

The values obtained for undrained vane shear strength in lithologic Unit I are fairly constant, with values increasing slightly from approximately 80 kPa just below the seafloor to a little greater than 100 kPa near the bottom of Unit I. The boundary between Unit I and Unit II is marked by a sharp increase in undrained vane shear strength to 200 kPa at 52 mbsf in Hole 680B. The strength data for Unit III are scattered but appear to increase slightly with depth below seafloor at the same rate as we observed in Unit II. The two values of vane shear strength above 200 kPa in Unit III, occurring at 61 mbsf and 83 mbsf, have corresponding low water contents.

Thermal Conductivity

Thermal conductivity was measured using the needle-probe method on the samples recovered from Hole 680C. We obtained only four cores from this hole. As Core 112-680C-4H was obvi-

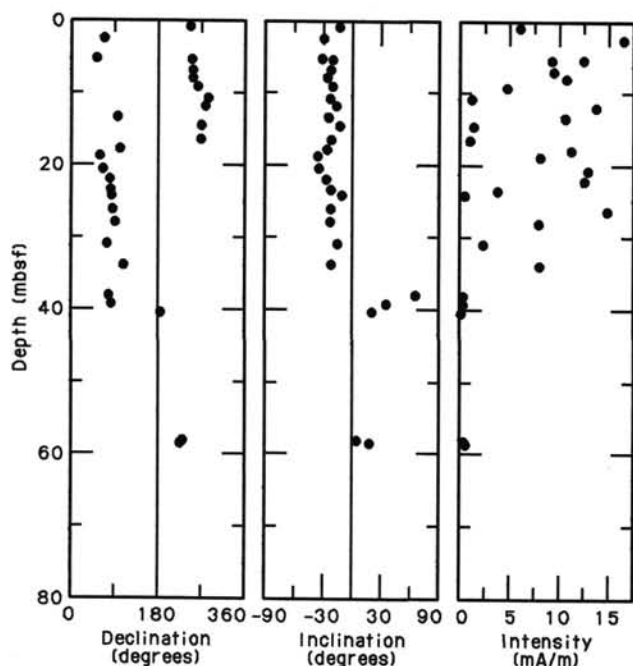


Figure 24. Declination, inclination, and intensity plots vs. depth for Hole 680A. Note that the Brunhes-Matuyama boundary occurs at around 35 mbsf and that the intensity of magnetization fluctuates widely.

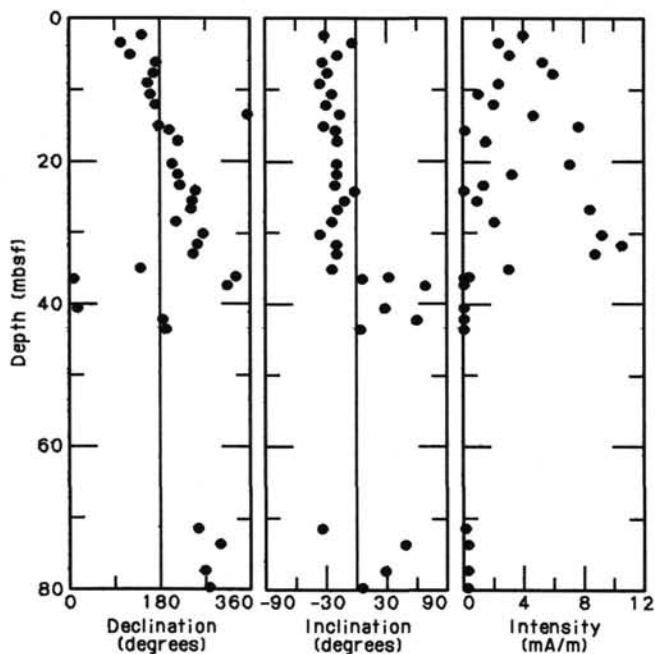


Figure 25. Declination, inclination, and magnetic intensity for Hole 680B. Note that the Brunhes-Matuyama boundary occurs at about 35 mbsf and that the intensity of magnetization shows cyclic fluctuations.

ously disturbed, we measured Cores 112-680C-1H through 112-680C-3H. The values obtained from Core 112-680C-2H were discarded because of low accuracy, probably owing to some disturbance in the core.

Our results are shown in Table 14 and Figure 31. The highly scattered thermal conductivity in Core 112-680C-3H may reflect the variation of water content observed in the samples from

Holes 680A and 680B. The arithmetic mean for the sample from Hole 680C is $0.87 \text{ W/m}\cdot\text{K}$.

Discussion

The physical properties exhibit a close relationship to the lithologic units of Site 680. The boundary between Units I and II is marked by sharp increases in values obtained for water content and shear strength, with a corresponding decrease in bulk density. The Unit II/IIIB boundary is recorded by a sharp decrease in water content and a corresponding increase in bulk density. The boundary between Subunits IIIB and IIIC also is marked by changes in index-property data. The variations of physical properties within individual units appears to be controlled by the facies.

The index-property data, particularly the high water contents, are indicative of the open framework of the diatomaceous muds encountered at this site. The high vane shear strengths are a result of the nature of the framework in these organic-rich sediments. The velocity data curve shows considerable lack of variation. There is little change in velocity resulting from changes in water content when the water contents are so high (greater than 50% of dry sample weight). Indeed, only when the percentage of water was around 50% did the corresponding velocities almost reach 1.6 km/s .

GEOPHYSICS

Seismic Records

Site 680 was positioned so as to sample the seaward flank of an organic-rich sediment body with a lens-shaped cross section produced by today's coastal upwelling off central Peru. A previous site was located on the distal edge of this lens, and a subsequent site was drilled at the center of the lens. Before drilling, this lens was defined on single-channel seismic record (YALOC 74-03-20), a 3.5-kHz record from the 1977 surveys conducted with the *Wecoma*, and from the pre-site survey by the *Moana Wave* in 1985. The seismic record (Fig. 32) shows a reflective sequence that increases in thickness by 0.17 s (approximately 127 m) at a distance of 45 km from the distal to the center position of the transect. At Site 680 this reflective sequence is 0.08-s (approximately 60 m) thick, and the base of lithologic Unit II was placed at 56 m . A small difference between the drilling- and seismic-depth determinations is probably a function of the imprecision of the time measurement on the seismic record. These reflections lap down in a seaward direction, terminating against a continuous reflection at the base of the lens. This geometry suggests seaward growth of the lens through time. Within the lens, smaller lenses or pinchouts can be recognized: they are represented by single reflections suggesting thin ($5\text{--}8 \text{ m}$), local irregularities from currents or incursions of turbidites. However, no such irregularities occur in the reflections beneath the site.

A record made with the 3.5-kHz transducer system on board the *JOIDES Resolution* during our approach and crossing of the site penetrated the seafloor to 35 m shows several continuous reflections (Fig. 33). Most prominent is a regular sequence about 12 m thick beneath the seafloor. Because no marked lithological changes were noted in the first core, these reflections may represent alternating diatom-rich and silty diatom-poor layers, as observed in the lithology of cores from this site. A high-amplitude reflection at a depth of 25 m beneath the site may correspond to a shell-rich bed in a mud matrix noted in the lithology of Sections 112-680A-3H-5 and 112-680A-3H-7. This reflection has considerable lateral extension, especially seaward.

We recorded seismic data during the transit from the previous site. However, these data were not particularly informative when imaged on board ship. A multichannel seismic record from an industry exploration program was taken about 3 km south of

Table 11. Summary of index properties for Site 680.

Core/sect.	Interval (cm)	Depth (mbsf)	Water (% dry wt)	Porosity (%)	Bulk density (g/cm ³)	Grain density (g/cm ³)
<i>Hole 112-680A</i>						
1-2	88	2.38	163.99	79.56	1.31	2.35
1-4	77	5.27	172.09	80.12	1.30	2.26
1-6	21	7.71	217.62	84.28	1.26	2.05
2-2	77	10.57	142.48	79.63	1.39	2.46
2-4	74	13.54	171.85	80.79	1.31	2.35
2-6	77	16.57	93.41	70.97	1.51	2.47
3-2	140	20.70	96.74	71.43	1.49	2.34
3-4	71	23.01	164.70	79.67	1.31	2.33
3-6	106	26.36	37.32	49.95	1.88	2.60
4-1	120	28.50	114.54	74.36	1.43	2.25
4-2	79	29.59	180.69	81.06	1.29	1.95
4-6	106	35.86	72.55	67.70	1.65	2.64
5-2	78	39.08	178.81	80.61	1.29	2.21
5-3	105	40.85	160.27	89.11	1.48	1.89
7-2	71	58.01	47.13	57.70	1.85	2.69
7-4	57	60.87	43.13	54.80	1.86	2.62
7-6	33	63.63	58.49	61.80	1.72	2.74
8-2	91	67.71	123.79	76.86	1.42	2.53
8-4	81	70.61	115.33	76.84	1.47	2.58
8-6	105	73.85	71.02	67.29	1.66	2.67
9-2	70	77.00	77.98	67.36	1.57	2.63
9-4	81	80.11	90.33	70.65	1.53	2.49
9-6	49	82.79	107.77	74.19	1.47	2.42
10-2	60	86.40	76.30	68.34	1.62	2.54
10-4	57	89.37	98.05	72.44	1.50	2.61
10-6	17	91.97	100.16	71.80	1.47	2.45
<i>Hole 112-680B</i>						
1-3	79	3.79	159.17	80.39	1.34	2.37
2-3	70	9.20	265.60	87.19	1.23	2.29
2-6	72	13.72	176.36	80.94	1.30	2.30
3-3	92	18.92	143.27	77.75	1.35	2.30
3-6	71	23.21	150.85	80.18	1.37	2.42
4-3	78	28.28	65.08	63.61	1.65	2.59
4-6	47	32.47	116.85	73.72	1.40	2.40
5-3	65	37.65	189.29	81.57	1.28	2.29
5-6	80	42.30	106.95	72.86	1.44	2.38
6-3	69	47.19	117.51	74.87	1.42	2.53
6-6	63	51.63	231.30	85.22	1.25	2.25
7-3	60	56.60	186.13	81.99	1.29	2.22
7-3	133	57.33	48.79	58.16	1.82	2.75
7-6	72	61.22	59.77	62.88	1.72	2.70
8-1	102	63.52	65.74	64.39	1.66	2.72
8-5	83	69.33	102.30	72.28	1.46	2.53
9-3	78	75.78	58.63	61.29	1.70	2.66
9-6	110	80.60	72.34	67.02	1.64	2.64
10-3	51	85.01	70.18	65.80	1.63	2.69
10-6	49	89.49	105.78	73.11	1.46	2.47

the site and is reported in a line-drawing in Thornburg (1985). This record shows the Salaverry Basin and indicates that the basement beneath the site is 0.8 s (approximately 650 m) deep. The unconformity between the upper and middle Miocene is 0.7 s (approximately 550 m) deep. Such a prominent unconformity could have been subaerially exposed at one time and today may be the recharge surface for the saline fluids (see "Inorganic Geochemistry" section, this chapter).

Heat Flow

Temperature Measurements

Hole 680B

Two APC tools (#5 and #1) were deployed while recovering Cores 112-680B-3H and 112-680B-4H, respectively. No temperature data were obtained from Core 112-680B-3H because tool #5 malfunctioned. A fairly good temperature record was ob-

tained from Core 112-680B-4H using tool #1 (Fig. 34). We estimated that the equilibrium temperature was $13.8 \pm 0.2^\circ\text{C}$ at 34 mbsf.

Below this depth, the APC tools could not be used as the sediment was too stiff. We ran the T-probe following Cores 112-680B-7H and 112-680B-22X. No data were recovered on the first run because the battery was dead. We did not analyze the temperature record obtained on the second run because it was extremely unstable and anomalously high.

Hole 680C

The two APC tools also were used during recovery of Cores 112-680C-3H and 112-680C-4H. The temperature record from tool #1 in Core 112-680C-3H had periodic and spikey noises, as shown in Figure 35. However, the decay of frictional heating could fit the theoretical curve if one excludes the data acquired just after penetration. The calculated equilibrium temperature is $13.3 \pm 0.1^\circ\text{C}$ at 24.8 mbsf. Tool #5 again failed to record tem-

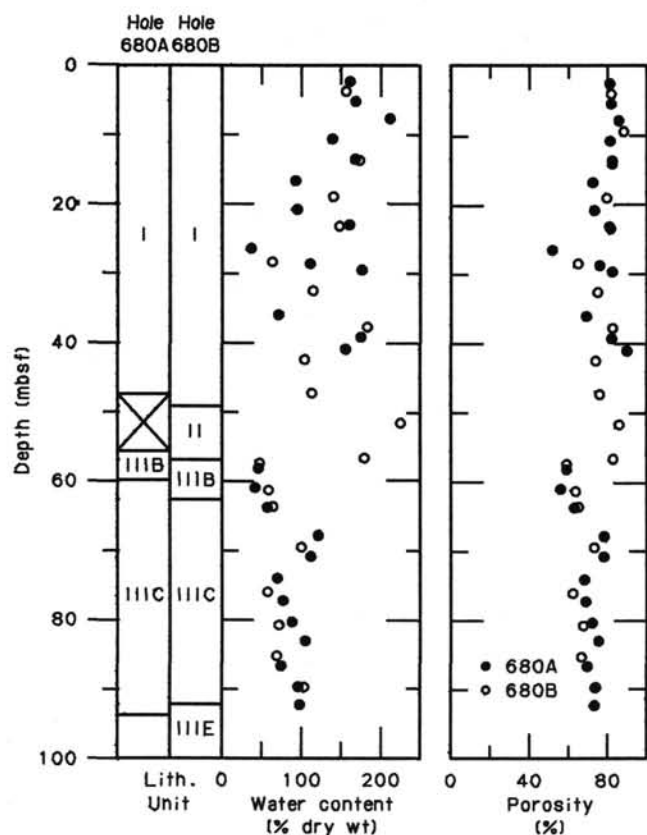


Figure 26. Profiles of water content and porosity for Site 680. Lithology is shown schematically.

perature data. No further measurements were performed because we abandoned Hole 680C following drilling problems with Core 112-680C-4H.

Estimating Heat Flow

We obtained one temperature value each for Holes 680B and 680C. Combining these temperature data gave a geothermal gradient of $54 \times 10^{-3} \text{ } ^\circ\text{C/m}$. This value was calculated by using the sub-bottom depth from each hole and is thus less reliable than if the two values had been obtained from one hole. The small temperature difference of these two measurements compared to the error in the estimated equilibrium temperatures results in a greater temperature-gradient error.

We measured thermal conductivity only on Cores 112-680C-1H and 112-680C-3H (see "Physical Properties" section, this chapter). We assumed that the mean thermal conductivity of Core 112-680C-3H ($0.88 \text{ W/m}\cdot\text{K}$) could be applied to the depth range where the temperature gradient was obtained. This assumption was supported by the observation that the water content does not vary systematically with depth from 20 to 40 mbsf (see "Physical Properties" section, this chapter) because the thermal conductivity of marine sediments is controlled mainly by the water content (e.g., Ratcliffe, 1960). Correction for temperature and pressure effects gave an *in-situ* thermal conductivity of $0.86 \text{ W/m}\cdot\text{K}$. Therefore, we estimated that the heat flow was 46 mW/m^2 . This value is close to those measured at the southern shelf sites (Sites 686 and 687), even though the error is large.

SUMMARY AND CONCLUSIONS

Site 680 is centered on an east-west transect of three sites across a lens-shaped sedimentary body of coastal upwelling deposits of the Peruvian outer shelf and upper slope. Seismic rec-

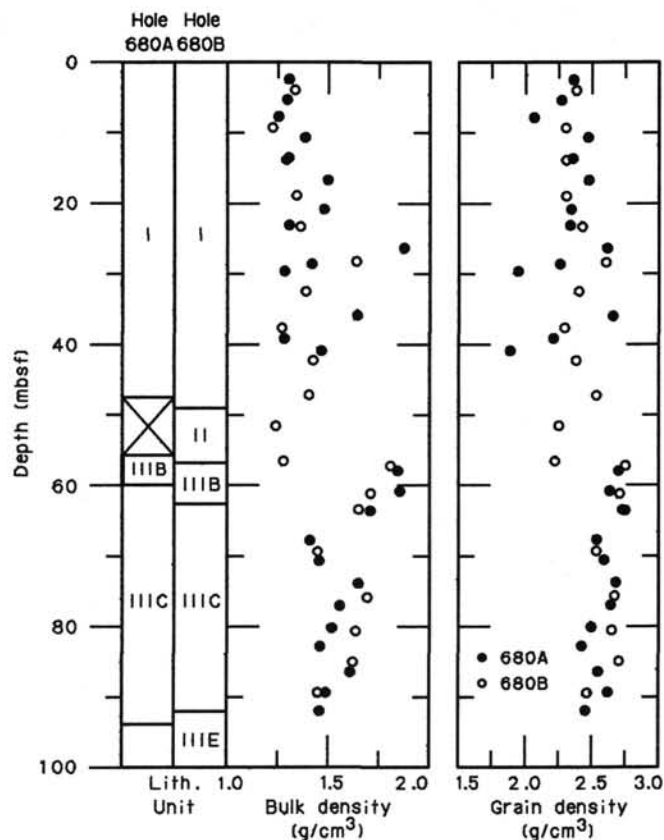


Figure 27. Bulk- and grain-density profiles for Site 680. Lithology is shown schematically.

ords show a reflective sequence that decreases in thickness from the central position (Site 680) to the distal position (Site 679) of the transect. The reflections in the lens prograde seaward and terminate against a continuous reflector on the top of the underlying strata. These reflections display the character of a downlap-filled seismic facies. Thus, at Site 680 we cored in the upper sequence (56.6 m thick) of an expanded record (compared with Site 679) of Holocene-late Pleistocene coastal upwelling. This record contains the sedimentary and geochemical signals of vertical and lateral shifts of the oxygen-minimum layer, organic-carbon preservation, and flux rates of biogenic constituents through time in response to fluctuations in sea level. In the lower section, below the continuous reflector, a Pleistocene to lower Pliocene sequence with more terrigenous affinities was sampled. This sequence was previously encountered at Site 679 and was deposited in a near-shore environment well outside the influence of coastal upwelling.

Three holes were drilled at Site 680. At Hole 680A, 81.2 m of core was recovered from the 93.8-m-thick sediment. A thinly laminated, dark olive green foraminifer-diatom mud of lithologic Unit I (0–48 m) is Holocene and late Pleistocene in age. The organic-carbon content is high, ranging from 6–10 wt%, whereas the calcium carbonate content fluctuates between extremes of <1% and >25%, depending on the distribution of foraminifer sand and dolomite layers. Near the base of this unit (36 mbsf), we identified the Brunhes/Matuyama boundary. Lithologic Unit II (48–56.4 m) consists of thinly laminated, diatomaceous silty mud with authigenic dolomites and phosphates concentrated in diatom-rich laminae or sandy layers. Unit II is in sharp contact with Unit III at 56.4 mbsf, coinciding with the contact between the prograding mud-lens reflectors and the underlying continuous reflector seen in the seismic data. Unit III

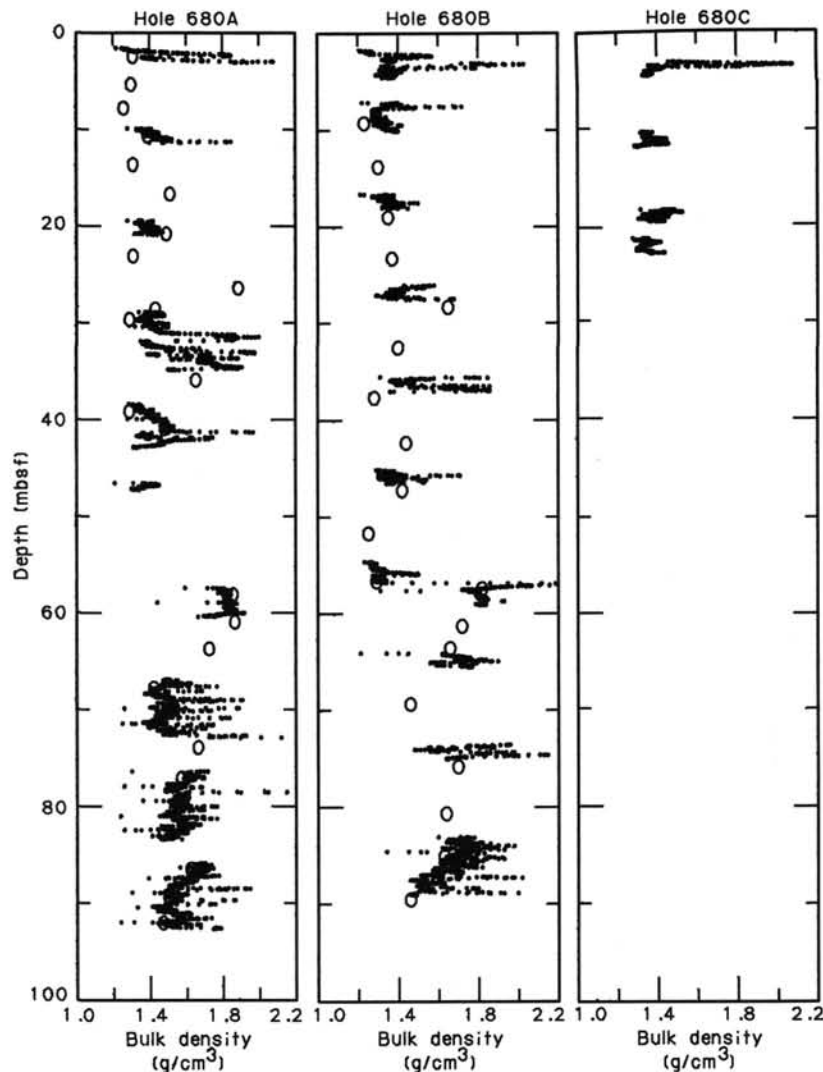


Figure 28. GRAPE bulk-density profiles for Site 680. Data from discrete samples are also shown (open circles).

contains substantial amounts of clastic material associated with several beds of phosphatic conglomerates. All units contain well-preserved and abundant diatom floras but appear to be repeatedly interrupted by hiatuses. At Hole 680B the same late Quaternary sequence was piston-cored with excellent recovery to a depth of 92 mbsf (bottom of Subunit IIID). Core recovery was poor during subsequent XCB drilling through sediments of early Pliocene age to the bottom of Hole 680B at 195.5 mbsf. Feldspar clastic sediments associated with beds of phosphatic conglomerates and sands are characteristic lithologies of this Pliocene unit. Four cores (34.3 mbsf) were drilled in Hole 680C with 100% recovery before the hole was abandoned because of a sand-line failure. We preserved whole-round samples from this hole for geomicrobiological, organic geochemical, and geotechnical studies.

At Site 680 all stages of dolomite, calcite, and phosphate formation and replacement are common. Dolomite is the predominant authigenic phase and was first found as shallow as 0.79 mbsf as disseminated rhombs. Phosphates occur in all units as thinly laminated beds of friable carbonate-fluorapatite, concentrated in diatom-rich laminae, and as dark, dense peloids and nodules, commonly found in sandy and conglomeratic strata. Bedded opal-CT chert, pyrite, and calcite are minor authigenic

phases at Site 680. This sediment sequence and its pore-water and dissolved-gas chemistries reveal considerable early diagenetic activity that is affected by highly saline pore fluids discovered at this site. Salinities, chloride, and other dissolved major ion contents in pore waters increased to about twice the concentrations of normal seawater at 195.5 mbsf, suggesting incursion of superhaline fluid. Abundant fluid-escape structures that penetrate the otherwise impermeable clay provide additional evidence of fluid movement. Replenishment of dissolved sulfate from this brine may inhibit microbial methanogenesis and promote sulfate reduction much beyond the depth normally seen in organic-rich sediments. This process thus is responsible for the low concentrations of biogenic methane and, in a general way, must also affect the composition and activity of microbial communities in the sediment. Ongoing sulfate reduction and iron sulfide formation with depth at the expense of iron oxides such as magnetite is reflected in a gradual weakening of the magnetic remanence. Below 45 mbsf the magnetic signal became too weak to be measured with shipboard instruments. The lag between this diagenetic front and the loss of remanence may result from slow reduction rates of magnetite.

Despite the preliminary nature of shipboard studies, our data indicate that the cores from Site 680 (1) contain all components

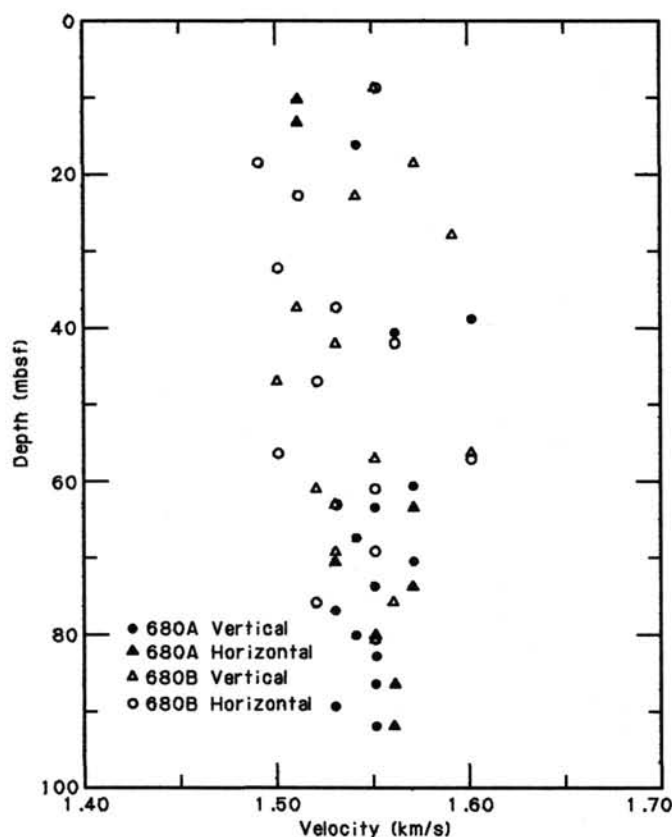


Figure 29. Hamilton Frame velocity data for Site 680.

Table 12. Compressional-wave velocity, Site 680.

Depth (mbsf)	Vertical velocity (km/s)	Horizontal velocity (km/s)
<i>Hole 112-680A</i>		
4.27		1.47
10.57		1.51
13.54		1.51
16.57	1.54	1.54
39.08	1.60	
40.85	1.56	
60.87	1.57	1.57
63.63	1.55	1.57
67.71	1.54	1.54
70.61	1.57	1.53
73.85	1.55	1.57
77.00	1.53	1.53
80.11	1.54	1.55
82.79	1.55	1.55
86.40	1.55	1.56
89.37	1.53	1.53
91.97	1.55	1.56
<i>Hole 112-680B</i>		
9.20	1.55	1.55
18.92	1.57	
23.21	1.54	1.51
28.28	1.59	1.57
32.47	1.47	1.50
37.65	1.51	1.53
42.30	1.53	1.56
47.19	1.50	1.52
56.60	1.60	1.50
57.33	1.55	1.60
61.22	1.52	1.55
63.22	1.53	1.53
69.33	1.53	1.55
75.78	1.56	1.52
80.80	1.55	1.55

of a well-developed upwelling facies, (2) cover the late Quaternary period with an expanded record, and (3) reveal unique low-temperature diagenetic reactions sustained by an incursion of brine. Models of diagenesis in Peruvian upwelling sediments must account for the effects of interchange between such hypersaline solutions and primary constituents of upwelling sediment.

REFERENCES

- Banner, F. T., and Blow, W. H., 1967. The origin, evolution and taxonomy of the foraminiferal genus *Pulleniatina* Cushman, 1927. *Micropaleontology*, 13:133-162.
- Bé, A. W. H., 1977. An ecological, zoogeographic and taxonomic review of Recent planktonic foraminifera. In Ramsay, A. T. S. (Ed.), *Oceanic Micropaleontology*, 1:1-100.
- Bukry, D., and Foster, J. H., 1973. Silicoflagellate and diatom stratigraphy, Leg 16, Deep Sea Drilling Project. In van Andel, T. H., Heath, G. R., et al., *Init. Repts. DSDP*, 16: Washington (U.S. Govt. Printing Office), 815-871.
- Burckle, L. H., 1977. Pliocene and Pleistocene diatom datum levels from the equatorial Pacific. *Quat. Geol.*, 7:330-340.
- Claypool, G. E., and Kaplan, I. R., 1974. The origin and distribution of methane in marine sediments. In Kaplan, I. R. (Ed.), *Natural Gases in Marine Sediments*: New York (Plenum), 94-129.
- Claypool, G. E., and Kvenvolden, K. A., 1983. Methane and other hydrocarbon gases in marine sediment. *Annu. Rev. Earth Planet. Sci.* 1983, 11:299-327.
- Hunt, J. M., 1979. *Petroleum Geochemistry and Geology*: San Francisco (W. H. Freeman).
- Kennett, J. P., 1972. Late Pleistocene paleoclimatology, foraminiferal biostratigraphy, and tephrochronology, Western Gulf of Mexico. *Quat. Res.*, 2:38-69.
- Koizumi, I., 1986. Pliocene and Pleistocene diatom datum levels related with paleoceanography in the northwest Pacific. *Mar. Micropaleontology*, 10:309-325.
- Locker, S., and Martini, E., 1986. Silicoflagellates and some sponge spicules from the southwest Pacific, Deep Sea Drilling Project, Leg 90. In Kennett, J. P., von der Borch, C. C., et al., *Init. Repts. DSDP*, 90: Washington (U.S. Govt. Printing Office), 887-924.
- Ratcliffe, E. H., 1960. The thermal conductivities of ocean sediments. *J. Geophys. Res.*, 65:1535-1541.
- Reimers, C. E., and Suess, E., 1983. Late Quaternary fluctuations in the cycling of organic matter off central Peru: A proto-kerogen record. In Suess, E., and Thiede, J. (Eds.), *Coastal Upwelling: Its Sediment Record*, Part I: New York (Plenum Press), 497-526.
- Schuette, G., and Schrader, H., 1979. Diatom taphocoenosis in the coastal swelling off western South America. *Nova Hed. Beih.*, 64: 359-378.
- Schuette, G., and Schrader, H., 1981a. Diatoms in surface sediments: A reflection of coastal upwelling. In Richards, F. A. (Ed.), *Coastal Upwelling*, 372-380.
- Schuette, G., and Schrader, H., 1981b. Marine diatoms. In Emiliani, C. (Ed.), *The Sea, Vol. 7, The Oceanic Lithosphere*: New York (John Wiley and Sons), 1179-1232.
- Smith, R. L., 1983. Circulation pattern in upwelling regimes. In Suess, E., and Thiede, J. (Eds.), *Coastal Upwelling: Its Sediment Record*, Part I: New York (Plenum Press), 13-35.
- Srinivasan, M. S., and Kennett, J. P., 1981. Neogene planktonic foraminiferal biostratigraphy and evolution: equatorial to sub-Antarctic, South Pacific. *Mar. Micropaleontology*, 6:499-533.
- Thornburg, T. M., 1985. Seismic stratigraphy of Peru forearc basins. In Hussong, D. M., et al. (Eds.), *Atlas of the Ocean Margin Drilling Program, Peru Continental Margin, Region VI*: Woods Hole (Marine Science International).
- Thunell, R. C., 1984. Pleistocene planktonic foraminiferal biostratigraphy and paleoclimatology of the Gulf of Mexico. In Healy-Williams, N. (Ed.), *Principles of Pleistocene stratigraphy applied to the Gulf of Mexico*: Boston (Intl. Human Res. Dev. Corp.), 25-64.

Table 13. Vane shear strength, Site 680.

Depth (mbsf)	Undrained peak vane shear strength (kPa)
<i>Hole 112-680A</i>	
10.55	82.80
13.52	81.05
16.55	86.29
19.85	90.96
23.06	92.13
26.33	92.13
29.57	95.04
35.86	52.48
39.15	107.28
40.94	116.61
58.05	142.85
60.86	200.58
63.61	108.45
67.67	116.61
70.59	145.77
73.83	118.95
77.06	108.45
80.09	145.77
82.77	219.24
86.37	106.12
89.45	141.10
91.94	142.27
<i>Hole 112-680B</i>	
3.84	83.96
9.24	74.63
13.77	85.13
18.90	75.80
23.26	93.29
28.32	73.47
32.52	87.46
37.69	111.95
42.28	100.29
47.23	100.29
51.62	201.74
56.59	104.95
57.31	76.97
61.21	151.60
63.57	92.13
69.37	106.12
75.83	100.29
80.68	106.12
85.06	102.62
89.54	158.60

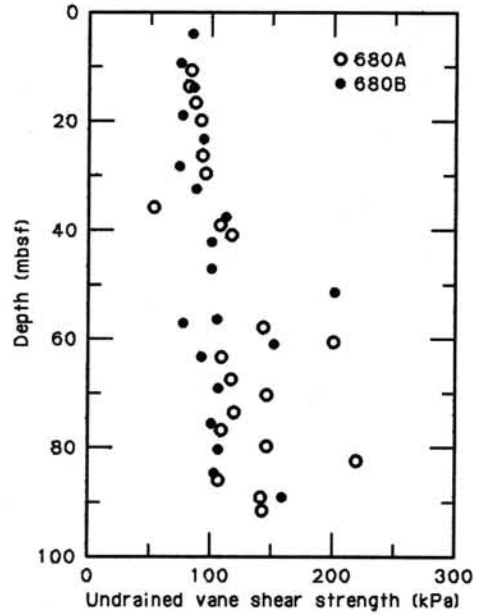


Figure 30. Profile of undrained vane shear strength for Site 680.

Table 14. Thermal conductivity, Hole 680C.

Core/section	Interval (cm)	Depth (mbsf)	Thermal conductivity (W/m·K)
112-680C-1-3	70	3.7	0.898
1-3	128	4.3	0.910
3-3	15	18.5	0.994
3-3	60	18.9	0.864
3-3	109	19.4	0.904
3-5	15	22.5	0.896
3-5	75	22.1	0.945
3-5	135	22.7	1.002

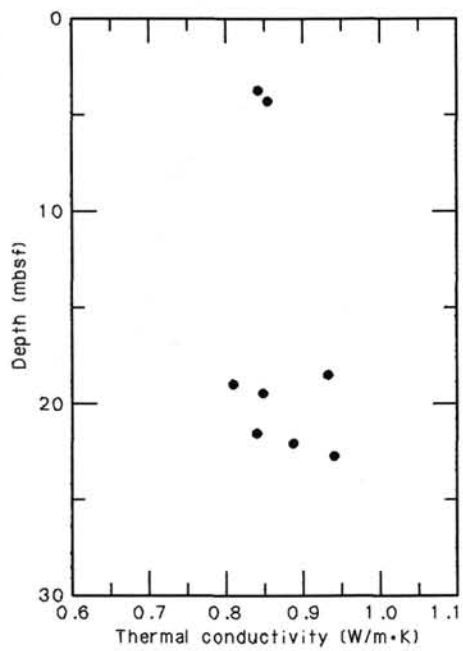


Figure 31. Thermal conductivity at depth below seafloor for Hole 680C.

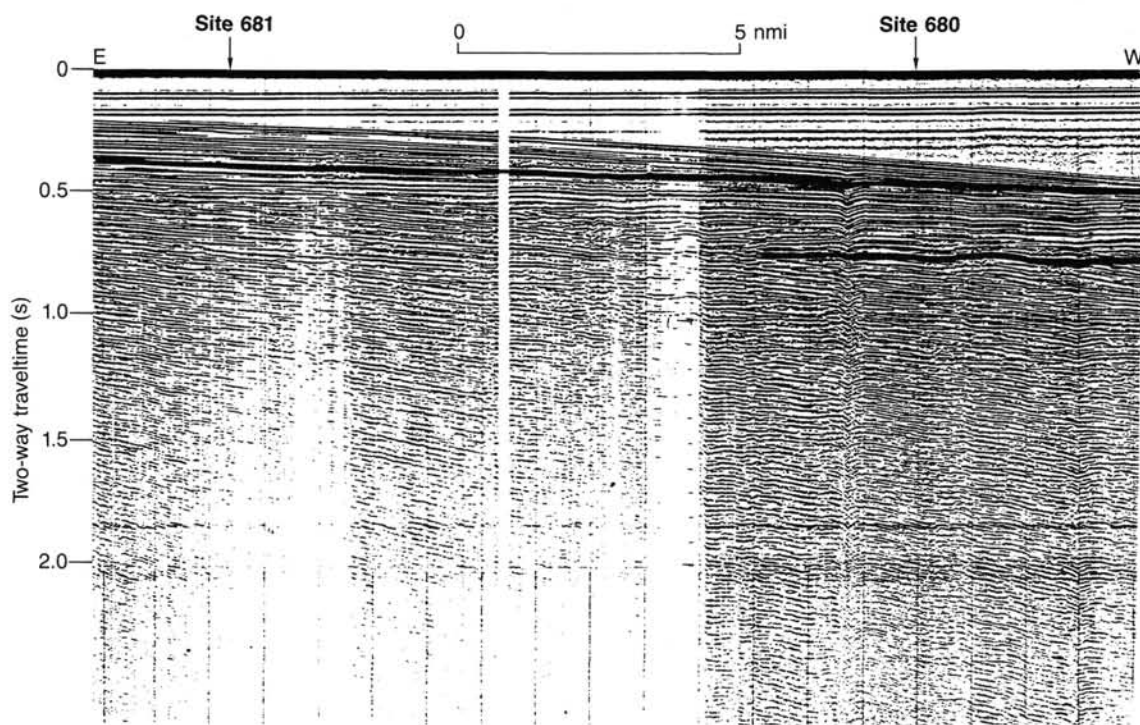


Figure 32. Single-channel seismic record for Leg 112 (YALOC 20-03-74), showing locations of Sites 680 and 681.

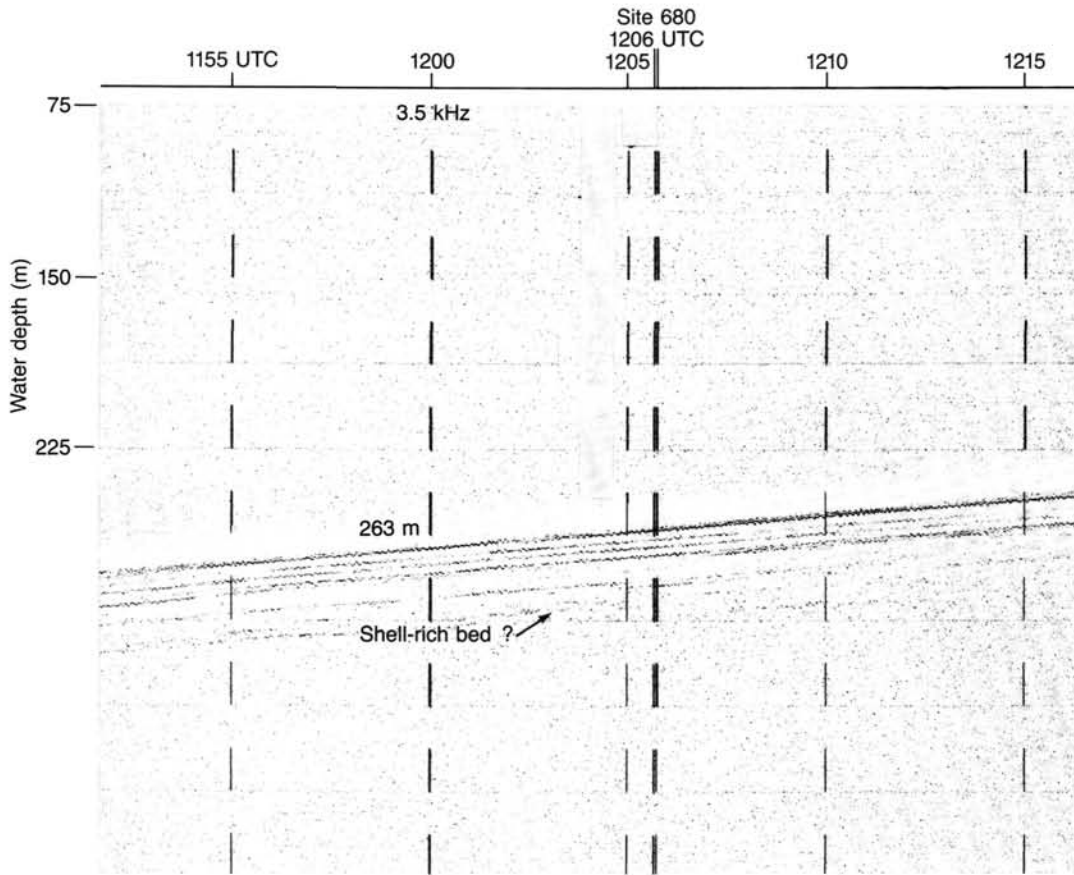


Figure 33. JOIDES Resolution 3.5-kHz record made during approach and beacon drop at Site 680.

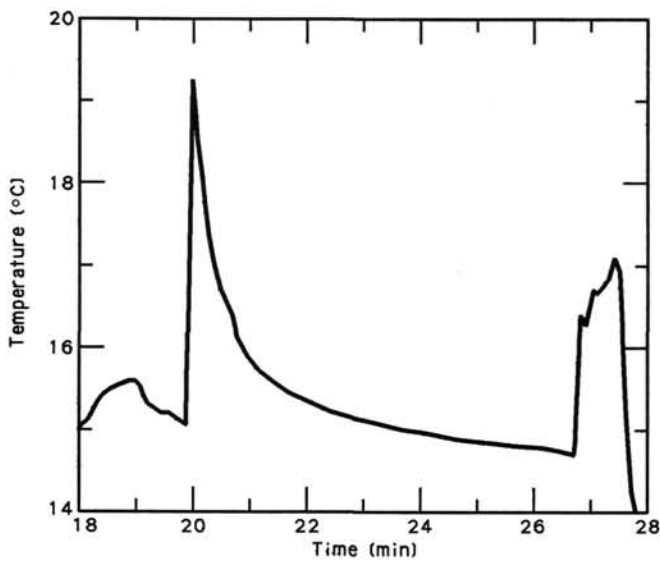


Figure 34. Temperature vs. time record obtained with the APC tool during recovery of Core 112-680B-4H at 34 mbsf.

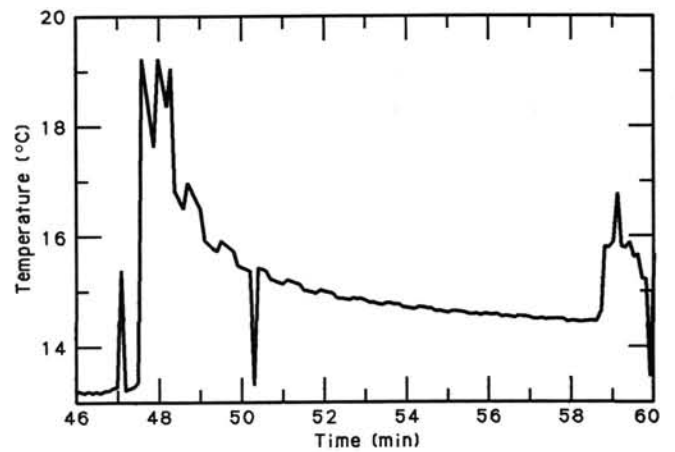
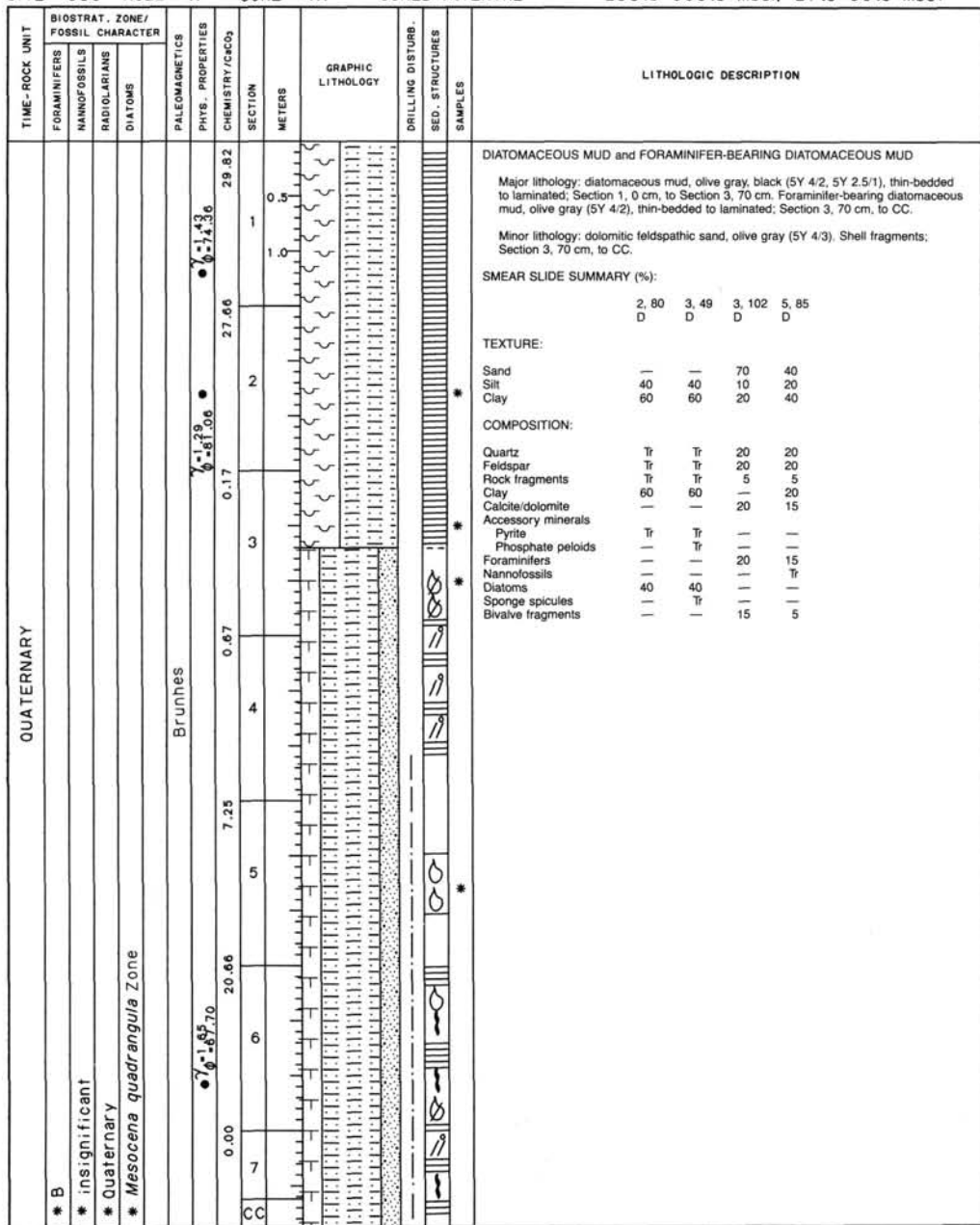
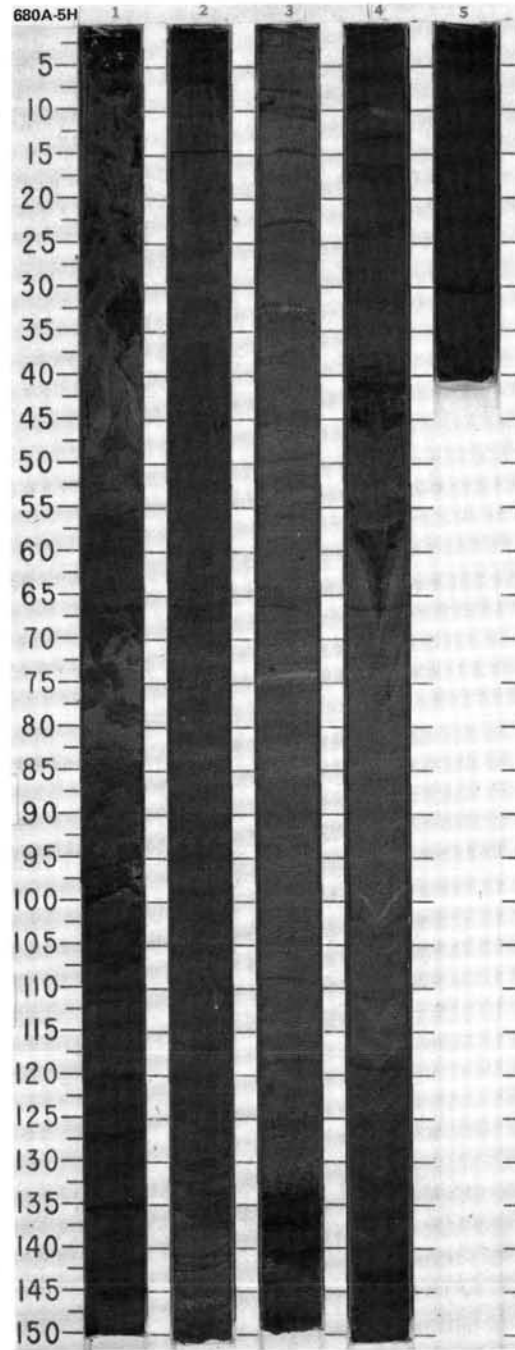


Figure 35. Temperature vs. time record obtained with the APC tool during recovery of Core 112-680C-3H at 24.8 mbsf.

SITE 680 HOLE A CORE 4H CORED INTERVAL 298.8-308.3 mbsl; 27.3-36.8 mbsf

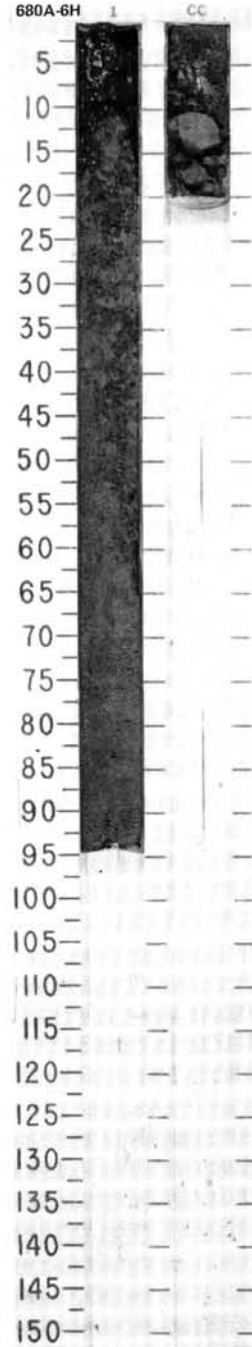


TIME-ROCK UNIT	BIOSTRAT. ZONE/ FOSSIL CHARACTER			PALEOMAGNETICS	PHYS. PROPERTIES	CHEMISTRY/CACO ₃	SECTION	METERS	GRAPHIC LITHOLOGY	DRILLING DISTURB.	BED. STRUCTURES	SAMPLES	LITHOLOGIC DESCRIPTION																																																																																																																														
	FORAMINIFERS	NANNOFOSSILS	RADIOLARIANS											DIATOMS																																																																																																																													
QUATERNARY	* N21 to N23												<p>DIATOMACEOUS MUD</p> <p>Major lithology: diatomaceous mud, dark olive gray, olive gray (5Y 3/2, 5Y 4/2). Thin-bedded to laminated.</p> <p>Minor lithology: foraminifer-bearing diatomaceous mud, black to olive gray (5Y 2.5/2, 5Y 4/2).</p> <p>SMEAR SLIDE SUMMARY (%):</p> <table border="1"> <tr> <td></td> <td>1, 51</td> <td>1, 61</td> <td>1, 98</td> <td>3, 136</td> <td>4, 42</td> </tr> <tr> <td></td> <td>D</td> <td>D</td> <td>M</td> <td>M</td> <td>D</td> </tr> </table> <p>TEXTURE:</p> <table border="1"> <tr> <td>Sand</td> <td>—</td> <td>—</td> <td>—</td> <td>95</td> <td>—</td> </tr> <tr> <td>Silt</td> <td>45</td> <td>40</td> <td>70</td> <td>5</td> <td>60</td> </tr> <tr> <td>Clay</td> <td>55</td> <td>60</td> <td>30</td> <td>—</td> <td>40</td> </tr> </table> <p>COMPOSITION:</p> <table border="1"> <tr> <td>Quartz</td> <td>5</td> <td>Tr</td> <td>Tr</td> <td>—</td> <td>—</td> </tr> <tr> <td>Feldspar</td> <td>5</td> <td>5</td> <td>Tr</td> <td>30</td> <td>5</td> </tr> <tr> <td>Rock fragments</td> <td>5</td> <td>—</td> <td>Tr</td> <td>25</td> <td>—</td> </tr> <tr> <td>Clay</td> <td>45</td> <td>50</td> <td>65</td> <td>—</td> <td>45</td> </tr> <tr> <td>Volcanic glass</td> <td>Tr</td> <td>—</td> <td>—</td> <td>—</td> <td>—</td> </tr> <tr> <td>Dolomite</td> <td>Tr</td> <td>—</td> <td>—</td> <td>Tr</td> <td>5</td> </tr> <tr> <td>Accessory minerals</td> <td></td> <td></td> <td></td> <td></td> <td></td> </tr> <tr> <td> Phosphate peloids</td> <td>5</td> <td>—</td> <td>Tr</td> <td>25</td> <td>—</td> </tr> <tr> <td> Pyrite</td> <td>—</td> <td>Tr</td> <td>Tr</td> <td>—</td> <td>Tr</td> </tr> <tr> <td>Foraminifers</td> <td>5</td> <td>15</td> <td>—</td> <td>—</td> <td>5</td> </tr> <tr> <td>Nannofossils</td> <td>—</td> <td>Tr</td> <td>—</td> <td>—</td> <td>—</td> </tr> <tr> <td>Diatoms</td> <td>30</td> <td>30</td> <td>35</td> <td>—</td> <td>40</td> </tr> <tr> <td>Sponge spicules</td> <td>Tr</td> <td>—</td> <td>Tr</td> <td>—</td> <td>—</td> </tr> <tr> <td>Silicoflagellates</td> <td>—</td> <td>—</td> <td>Tr</td> <td>—</td> <td>—</td> </tr> <tr> <td>Fish remains</td> <td>Tr</td> <td>—</td> <td>—</td> <td>15</td> <td>—</td> </tr> <tr> <td>Bioclasts</td> <td>—</td> <td>—</td> <td>—</td> <td>5</td> <td>—</td> </tr> </table>		1, 51	1, 61	1, 98	3, 136	4, 42		D	D	M	M	D	Sand	—	—	—	95	—	Silt	45	40	70	5	60	Clay	55	60	30	—	40	Quartz	5	Tr	Tr	—	—	Feldspar	5	5	Tr	30	5	Rock fragments	5	—	Tr	25	—	Clay	45	50	65	—	45	Volcanic glass	Tr	—	—	—	—	Dolomite	Tr	—	—	Tr	5	Accessory minerals						Phosphate peloids	5	—	Tr	25	—	Pyrite	—	Tr	Tr	—	Tr	Foraminifers	5	15	—	—	5	Nannofossils	—	Tr	—	—	—	Diatoms	30	30	35	—	40	Sponge spicules	Tr	—	Tr	—	—	Silicoflagellates	—	—	Tr	—	—	Fish remains	Tr	—	—	15	—	Bioclasts	—	—	—	5	—
		1, 51	1, 61	1, 98	3, 136	4, 42																																																																																																																																					
		D	D	M	M	D																																																																																																																																					
	Sand	—	—	—	95	—																																																																																																																																					
Silt	45	40	70	5	60																																																																																																																																						
Clay	55	60	30	—	40																																																																																																																																						
Quartz	5	Tr	Tr	—	—																																																																																																																																						
Feldspar	5	5	Tr	30	5																																																																																																																																						
Rock fragments	5	—	Tr	25	—																																																																																																																																						
Clay	45	50	65	—	45																																																																																																																																						
Volcanic glass	Tr	—	—	—	—																																																																																																																																						
Dolomite	Tr	—	—	Tr	5																																																																																																																																						
Accessory minerals																																																																																																																																											
Phosphate peloids	5	—	Tr	25	—																																																																																																																																						
Pyrite	—	Tr	Tr	—	Tr																																																																																																																																						
Foraminifers	5	15	—	—	5																																																																																																																																						
Nannofossils	—	Tr	—	—	—																																																																																																																																						
Diatoms	30	30	35	—	40																																																																																																																																						
Sponge spicules	Tr	—	Tr	—	—																																																																																																																																						
Silicoflagellates	—	—	Tr	—	—																																																																																																																																						
Fish remains	Tr	—	—	15	—																																																																																																																																						
Bioclasts	—	—	—	5	—																																																																																																																																						
	* insignificant	* NN19																																																																																																																																									
	* Quaternary																																																																																																																																										
	* <i>Mesocena quadrangula</i> Zone																																																																																																																																										
				Brunhes		4.85		0.5																																																																																																																																			
				Matuyama		2.50		1.0																																																																																																																																			
						0.17																																																																																																																																					
						0.92																																																																																																																																					
						7.35																																																																																																																																					
						2.17																																																																																																																																					

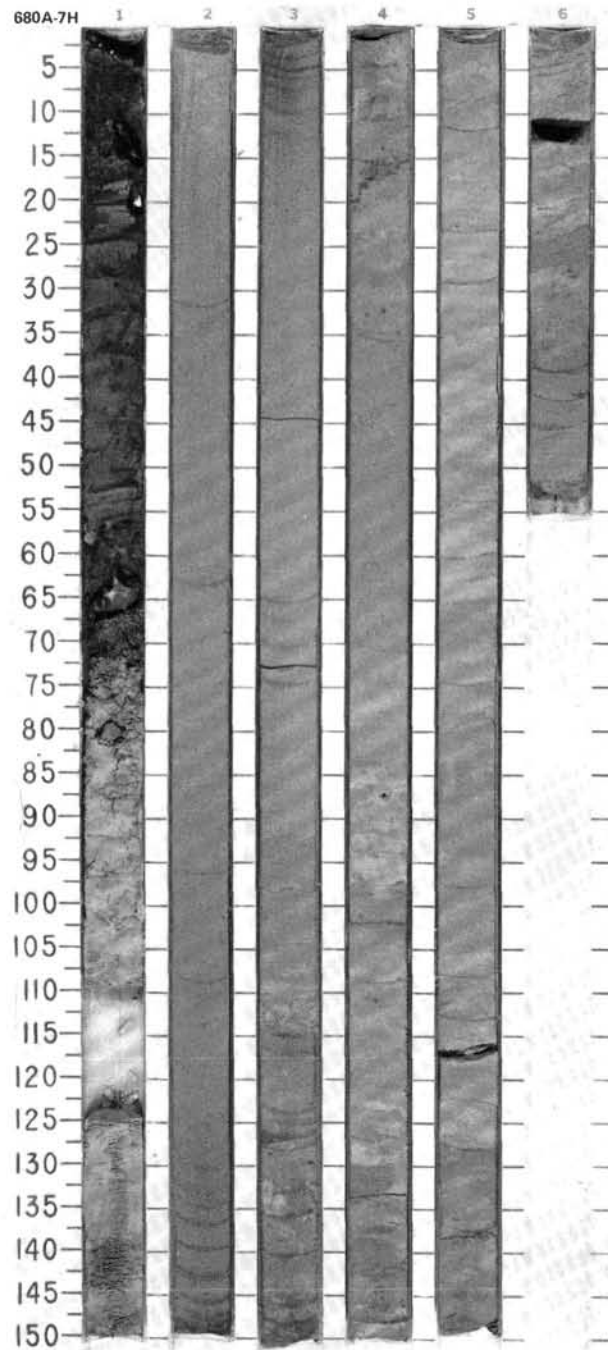


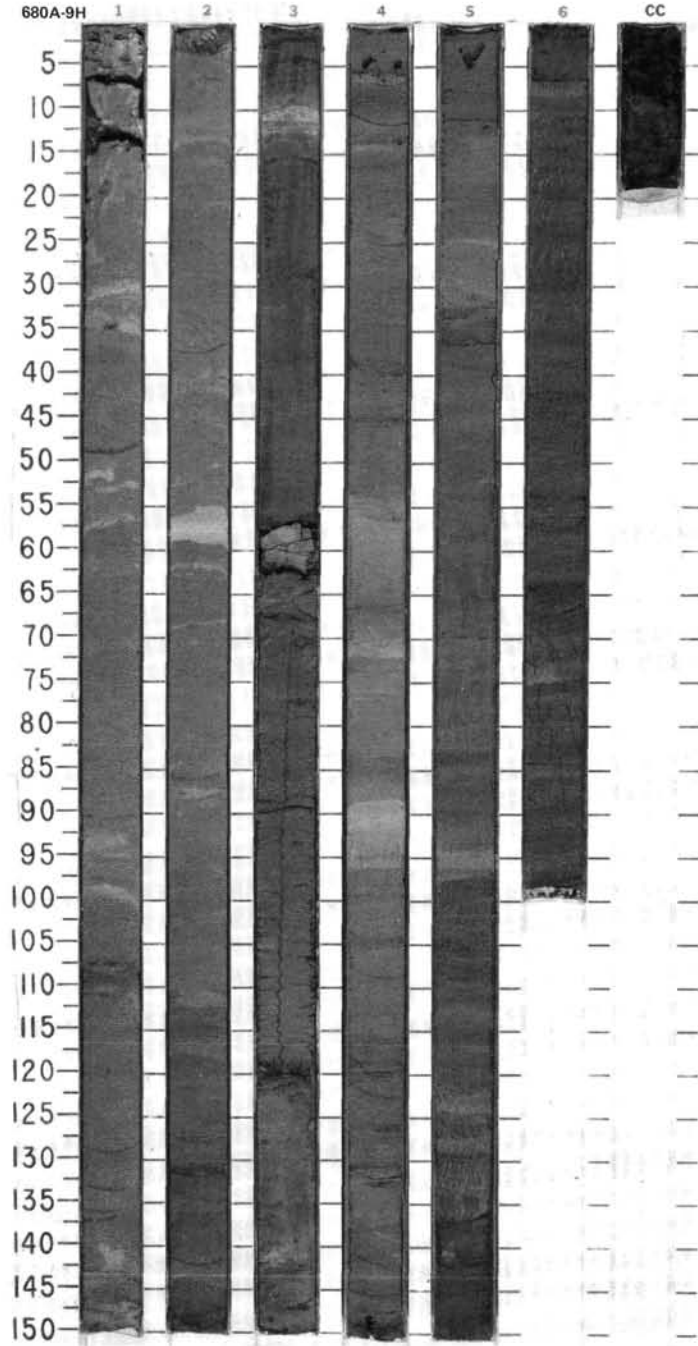
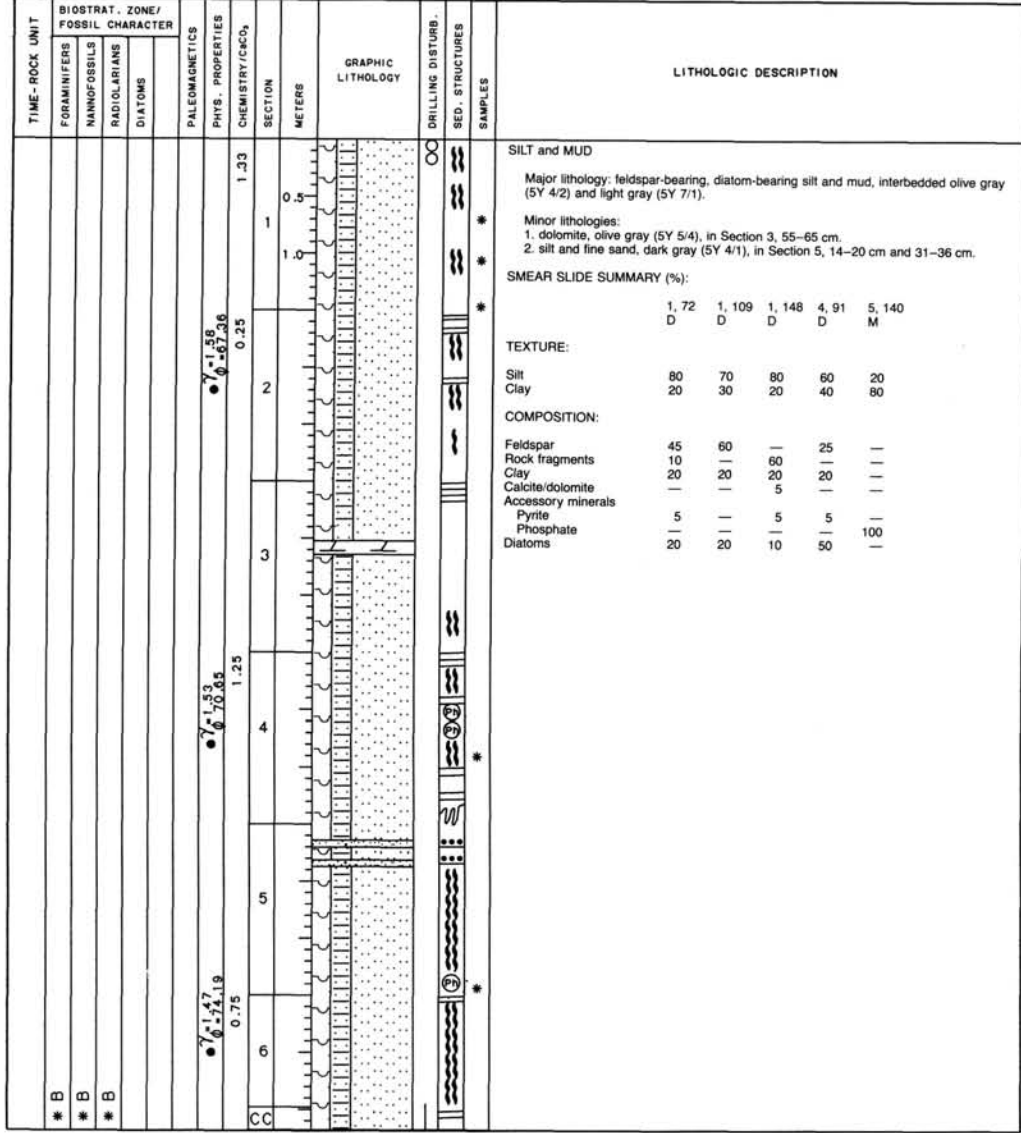
SITE 680 HOLE A CORE 6H CORED INTERVAL 317.8-327.3 mbsl; 46.3-55.8 mbsf

TIME-ROCK UNIT	BIOSTRAT. ZONE/ FOSSIL CHARACTER			PALEOMAGNETICS	PHYS. PROPERTIES	CHEMISTRY/CCODs	SECTION	METERS	GRAPHIC LITHOLOGY	DRILLING DISTURB.	SED. STRUCTURES	SAMPLES	LITHOLOGIC DESCRIPTION								
	FORAMINIFERS	NANNOFOSSILS	RADIOLARIANS																		
PLIOCENE	B *			Matuyama			1	0.5				*	DIATOMACEOUS MUD Major lithology: diatomaceous mud, olive gray (5Y 4/2). Minor lithology: dolomitic, olive (5Y 4/3). SMEAR SLIDE SUMMARY (%): <table style="margin-left: 20px;"> <tr> <td></td> <td>1.72</td> <td>CC, 15</td> <td>CC, 17</td> </tr> <tr> <td></td> <td>D</td> <td>M</td> <td>M</td> </tr> </table> TEXTURE: Silt 70 — — Clay 30 100 100 COMPOSITION: Quartz — — Tr Clay 20 — — Dolomite Tr 100 100 Diatoms 80 — —		1.72	CC, 15	CC, 17		D	M	M
		1.72	CC, 15		CC, 17																
	D	M	M																		
	B *	B *				CC	1.0					**									
	B *																				
		<i>Nitzschia reinholdi</i> Zone *																			

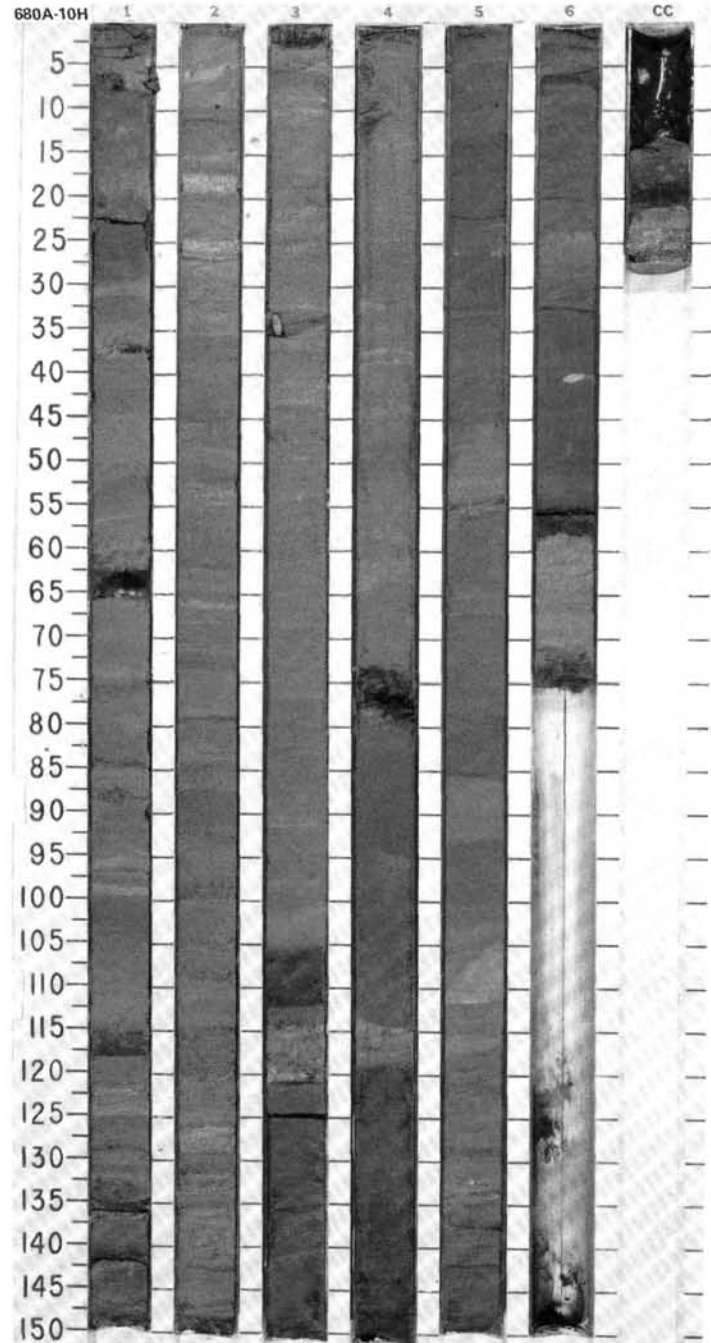
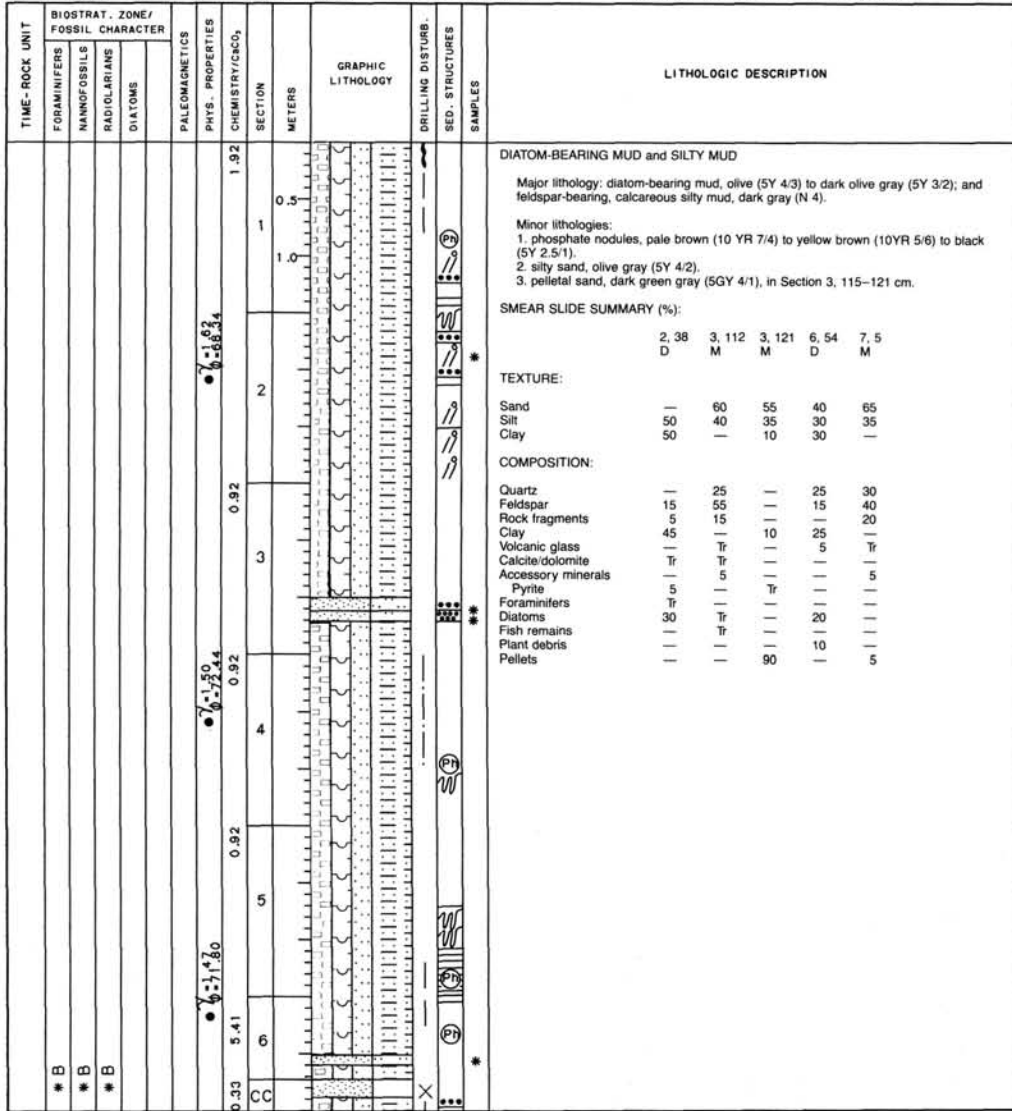


TIME-ROCK UNIT	BIOSTRAT. ZONE/ FOSSIL CHARACTER				PALEOMAGNETICS	PHYS. PROPERTIES	CHEMISTRY/C&C ₂	SECTION	METERS	GRAPHIC LITHOLOGY	DRILLING DISTURB.	SED. STRUCTURES	SAMPLES	LITHOLOGIC DESCRIPTION																																																																																															
	FORAMINIFERS	NANNOFOSSILS	RADIOLARIANS	DIATOMS																																																																																																									
PLIOCENE	* B							0-42						<p>DIATOMACEOUS MUD and FELDSPATHIC SILT</p> <p>Major lithology: diatomaceous mud, olive (5Y 4/4), in Section 1, 0 to 70 cm. Feldspathic silt, light gray, olive gray (5Y 6/1, 5Y 5/2). Laminated or bioturbated in Section 1, 70 cm, to Section 6, 53 cm.</p> <p>Minor lithology: black (5Y 2.5/1) phosphatic silt; Section 1, 0-70 cm.</p> <p>SMEAR SLIDE SUMMARY (%):</p> <table border="1"> <tr> <td></td> <td>1, 24</td> <td>1, 57</td> <td>2, 69</td> <td>3, 130</td> </tr> <tr> <td></td> <td>D</td> <td>M</td> <td>D</td> <td>D</td> </tr> </table> <p>TEXTURE:</p> <table border="1"> <tr> <td>Sand</td> <td>5</td> <td>90</td> <td>—</td> <td>5</td> </tr> <tr> <td>Silt</td> <td>40</td> <td>10</td> <td>65</td> <td>60</td> </tr> <tr> <td>Clay</td> <td>55</td> <td>—</td> <td>35</td> <td>35</td> </tr> </table> <p>COMPOSITION:</p> <table border="1"> <tr> <td>Quartz</td> <td>Tr</td> <td>20</td> <td>—</td> <td>—</td> </tr> <tr> <td>Feldspar</td> <td>Tr</td> <td>20</td> <td>65</td> <td>65</td> </tr> <tr> <td>Rock fragments</td> <td>5</td> <td>10</td> <td>—</td> <td>—</td> </tr> <tr> <td>Clay</td> <td>60</td> <td>—</td> <td>30</td> <td>25</td> </tr> <tr> <td>Volcanic glass</td> <td>—</td> <td>—</td> <td>5</td> <td>5</td> </tr> <tr> <td>Dolomite</td> <td>Tr</td> <td>—</td> <td>Tr</td> <td>Tr</td> </tr> <tr> <td>Accessory minerals</td> <td>—</td> <td>5</td> <td>—</td> <td>—</td> </tr> <tr> <td>Pyrite</td> <td>Tr</td> <td>—</td> <td>Tr</td> <td>—</td> </tr> <tr> <td>Phosphatic peloids</td> <td>—</td> <td>25</td> <td>—</td> <td>—</td> </tr> <tr> <td>Zeolites(?)</td> <td>—</td> <td>—</td> <td>—</td> <td>Tr</td> </tr> <tr> <td>Foraminifers</td> <td>—</td> <td>—</td> <td>—</td> <td>Tr</td> </tr> <tr> <td>Diatoms</td> <td>40</td> <td>10</td> <td>5</td> <td>5</td> </tr> <tr> <td>Sponge spicules</td> <td>—</td> <td>—</td> <td>Tr</td> <td>—</td> </tr> <tr> <td>Fish remains</td> <td>—</td> <td>10</td> <td>Tr</td> <td>—</td> </tr> </table>		1, 24	1, 57	2, 69	3, 130		D	M	D	D	Sand	5	90	—	5	Silt	40	10	65	60	Clay	55	—	35	35	Quartz	Tr	20	—	—	Feldspar	Tr	20	65	65	Rock fragments	5	10	—	—	Clay	60	—	30	25	Volcanic glass	—	—	5	5	Dolomite	Tr	—	Tr	Tr	Accessory minerals	—	5	—	—	Pyrite	Tr	—	Tr	—	Phosphatic peloids	—	25	—	—	Zeolites(?)	—	—	—	Tr	Foraminifers	—	—	—	Tr	Diatoms	40	10	5	5	Sponge spicules	—	—	Tr	—	Fish remains	—	10	Tr	—
		1, 24	1, 57	2, 69	3, 130																																																																																																								
		D	M	D	D																																																																																																								
	Sand	5	90	—	5																																																																																																								
	Silt	40	10	65	60																																																																																																								
	Clay	55	—	35	35																																																																																																								
Quartz	Tr	20	—	—																																																																																																									
Feldspar	Tr	20	65	65																																																																																																									
Rock fragments	5	10	—	—																																																																																																									
Clay	60	—	30	25																																																																																																									
Volcanic glass	—	—	5	5																																																																																																									
Dolomite	Tr	—	Tr	Tr																																																																																																									
Accessory minerals	—	5	—	—																																																																																																									
Pyrite	Tr	—	Tr	—																																																																																																									
Phosphatic peloids	—	25	—	—																																																																																																									
Zeolites(?)	—	—	—	Tr																																																																																																									
Foraminifers	—	—	—	Tr																																																																																																									
Diatoms	40	10	5	5																																																																																																									
Sponge spicules	—	—	Tr	—																																																																																																									
Fish remains	—	10	Tr	—																																																																																																									
	* B							1.84																																																																																																					
	* B							0.57, 7.0																																																																																																					
	* B							1.67																																																																																																					
	* <i>Nitzschia jouseae</i> Zone							2.55																																																																																																					
								3.76																																																																																																					
								1.72																																																																																																					
								0.1, 0.0																																																																																																					

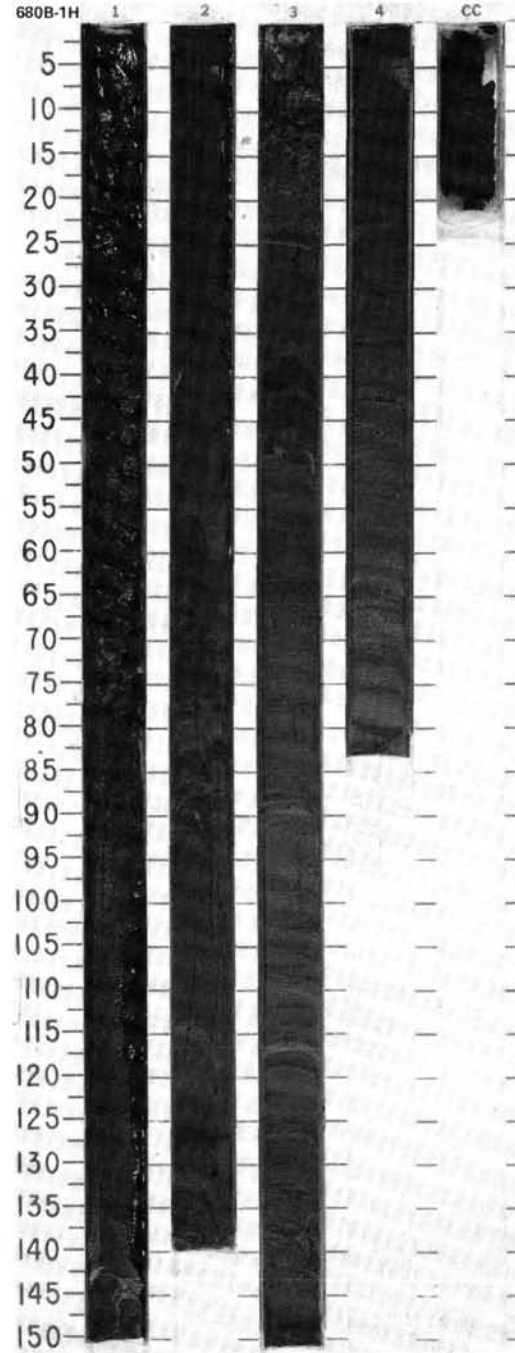


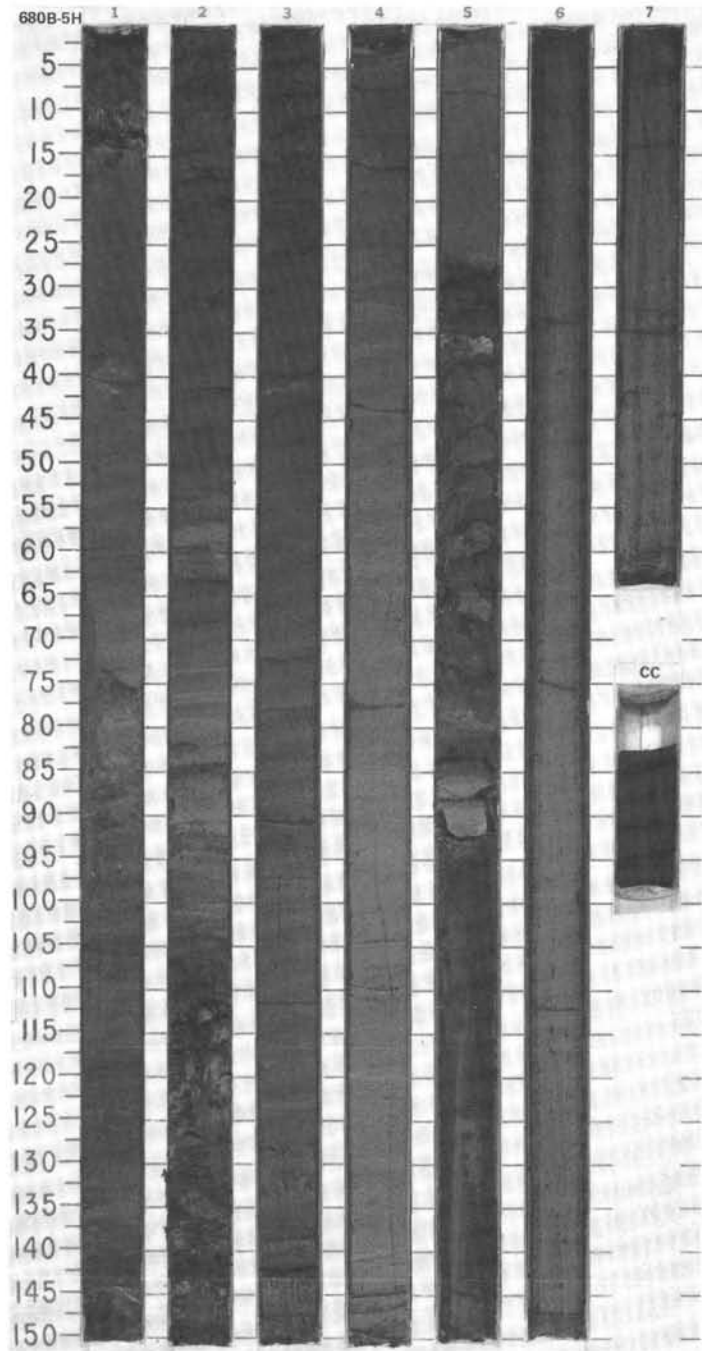
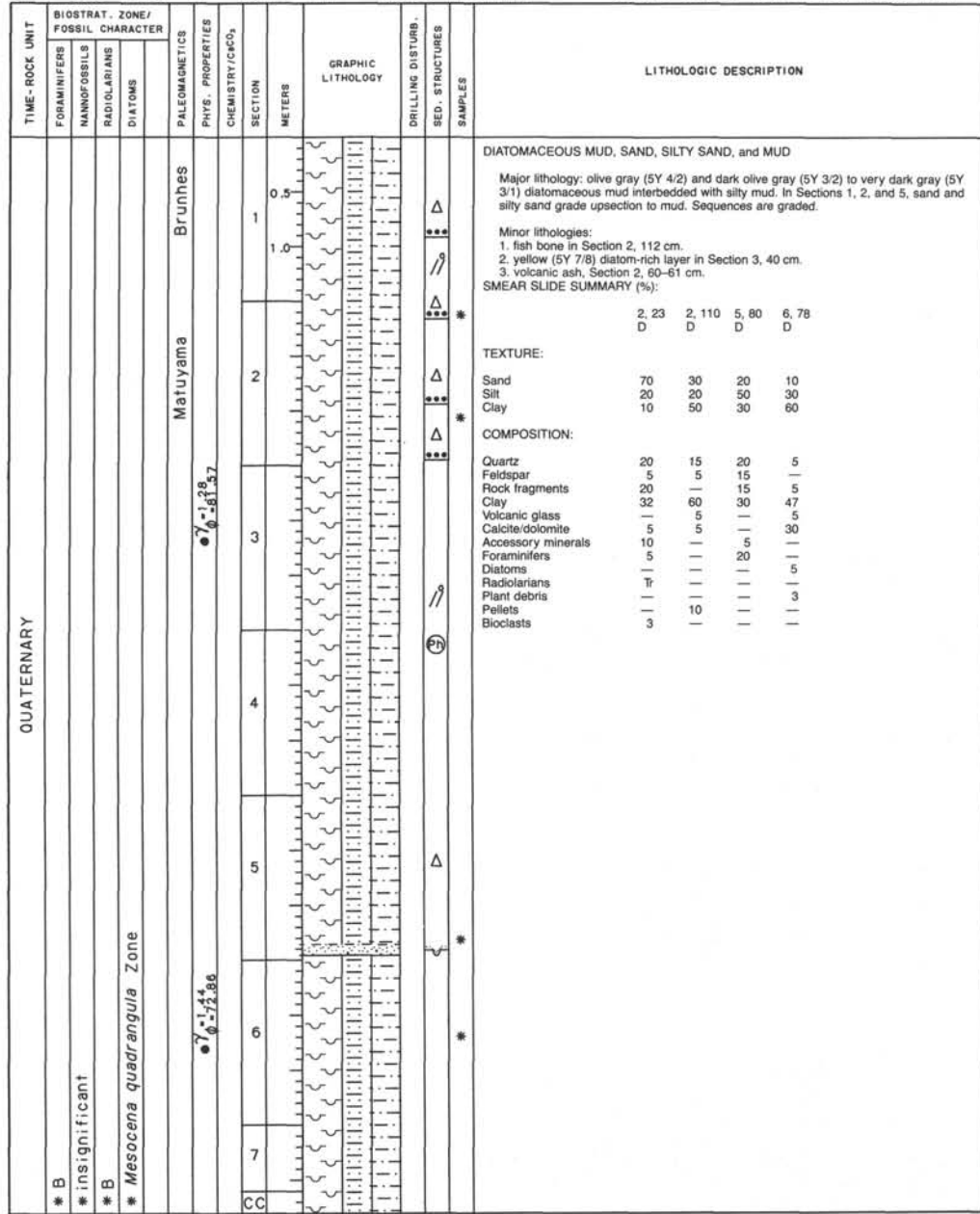


SITE 680 HOLE A CORE 10H CORED INTERVAL 355.8-365.3 mbsl; 84.3-93.8 mbsf

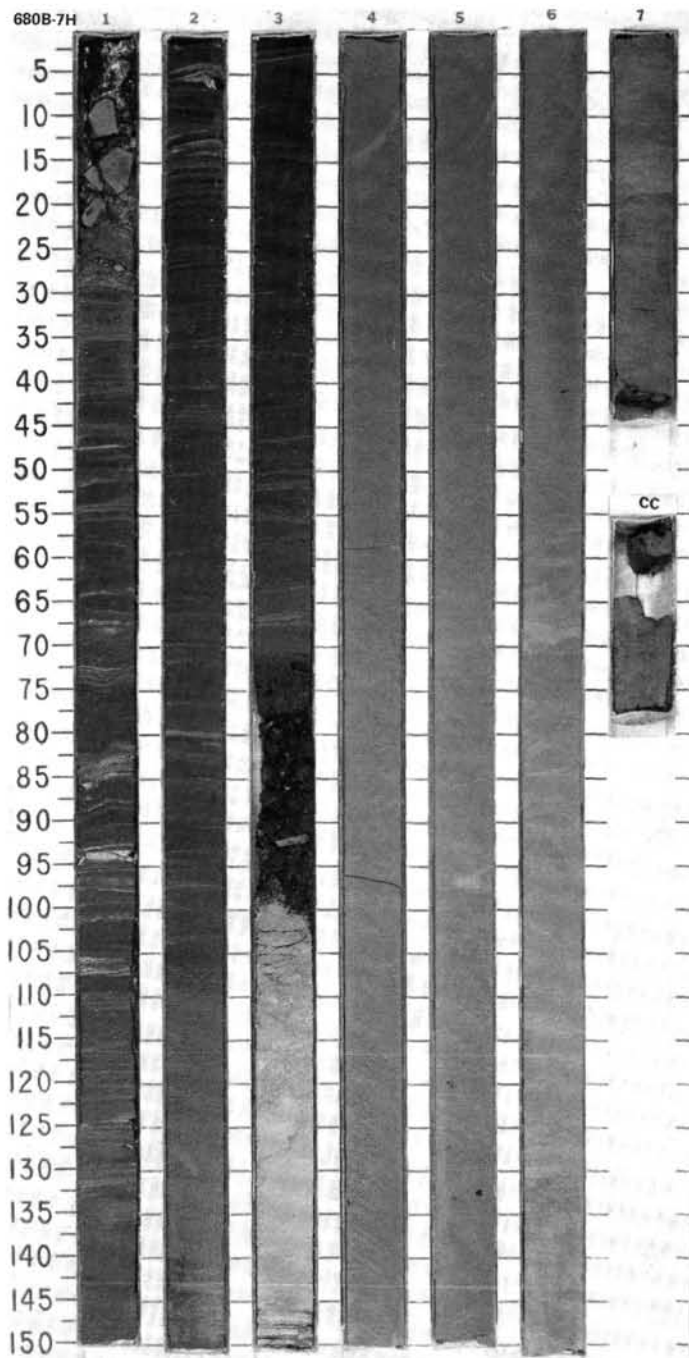
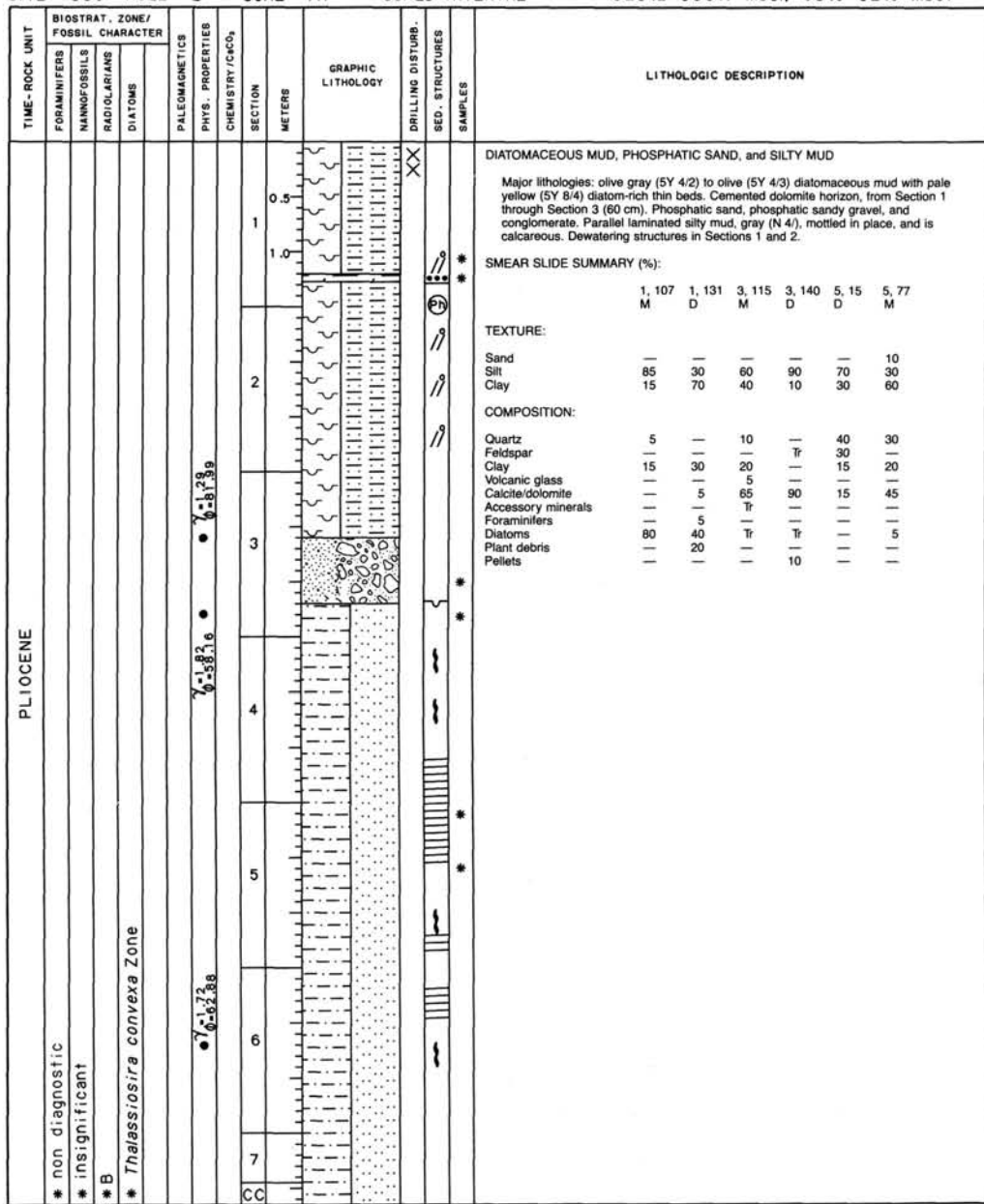


TIME-ROCK UNIT	BIOSTRAT. ZONE/ FOSSIL CHARACTER				PALEOMAGNETICS	PHYS. PROPERTIES CHEMISTRY/CaCO ₃	SECTION METERS	GRAPHIC LITHOLOGY	DRILLING DISTURB.	SED. STRUCTURES	SAMPLES	LITHOLOGIC DESCRIPTION																																					
	FORAMINIFERS	NANNOFOSSILS	RADIOLARIANS	DIATOMS																																													
QUATERNARY	* N21 - N23 * NN20 ? * Quaternary * <i>Pseudoebunotia doliolus</i> Zone				Brunhes ● 7.1, 3.4 ● 6.2, 6.3, 3.9	10.0, 1.4 0.15, 3.8	0.5 1.0					<p>* MUD</p> <p>Major lithology: diatom-bearing, foraminifer-bearing mud, dark olive gray (SY 4/4) and black (SY 2.5/2), thin bedded to laminated, silty sand as thin layers throughout.</p> <p>SMEAR SLIDE SUMMARY (%):</p> <table border="1"> <tr> <td>1, 18</td> <td>3, 63</td> </tr> <tr> <td>D</td> <td>D</td> </tr> </table> <p>TEXTURE:</p> <table border="1"> <tr> <td>Sand</td> <td>5</td> <td>—</td> </tr> <tr> <td>Silt</td> <td>45</td> <td>55</td> </tr> <tr> <td>Clay</td> <td>50</td> <td>45</td> </tr> </table> <p>COMPOSITION:</p> <table border="1"> <tr> <td>Quartz</td> <td>10</td> <td>5</td> </tr> <tr> <td>Feldspar</td> <td>10</td> <td>15</td> </tr> <tr> <td>Clay</td> <td>50</td> <td>35</td> </tr> <tr> <td>Volcanic glass</td> <td>—</td> <td>Tr</td> </tr> <tr> <td>Caliche/dolomite</td> <td>—</td> <td>Tr</td> </tr> <tr> <td>Foraminifers</td> <td>5</td> <td>5</td> </tr> <tr> <td>Nannofossils</td> <td>5</td> <td>—</td> </tr> <tr> <td>Diatoms</td> <td>20</td> <td>40</td> </tr> </table>	1, 18	3, 63	D	D	Sand	5	—	Silt	45	55	Clay	50	45	Quartz	10	5	Feldspar	10	15	Clay	50	35	Volcanic glass	—	Tr	Caliche/dolomite	—	Tr	Foraminifers	5	5	Nannofossils	5	—	Diatoms	20	40
1, 18	3, 63																																																
D	D																																																
Sand	5	—																																															
Silt	45	55																																															
Clay	50	45																																															
Quartz	10	5																																															
Feldspar	10	15																																															
Clay	50	35																																															
Volcanic glass	—	Tr																																															
Caliche/dolomite	—	Tr																																															
Foraminifers	5	5																																															
Nannofossils	5	—																																															
Diatoms	20	40																																															





SITE 680 HOLE B CORE 7H CORED INTERVAL 329.2-338.7 mbsl; 53.0-62.5 mbsf



SITE 680

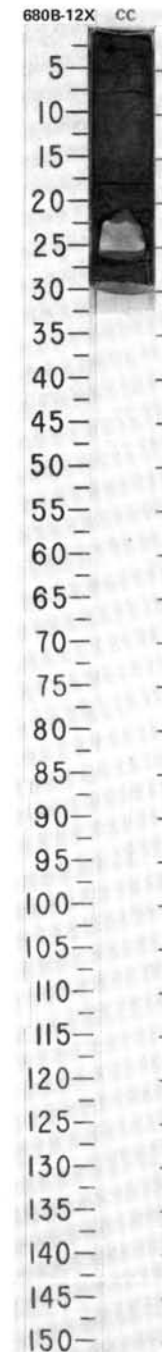
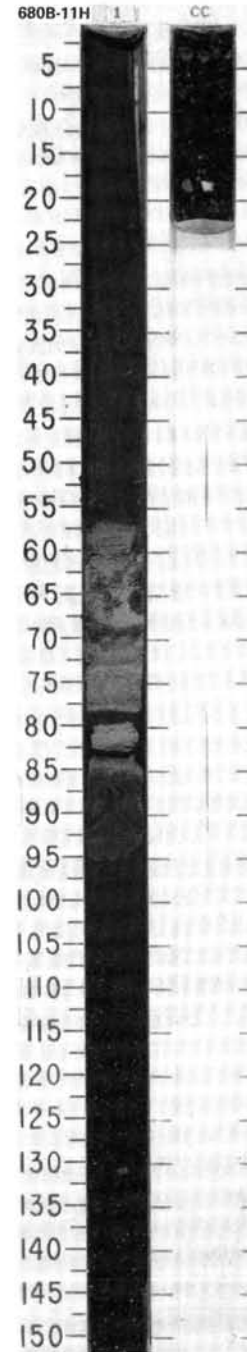
SITE 680 HOLE B CORE 11H CORED INTERVAL 367.2-368.2 mbsl; 91.0-92.0 mbsf

TIME-ROCK UNIT	BIOSTRAT. ZONE/ FOSSIL CHARACTER				PALEOMAGNETICS	PHYS. PROPERTIES	CHEMISTRY/cacO ₃	SECTION	METERS	GRAPHIC LITHOLOGY	DRILLING DISTURB. SED. STRUCTURES	SAMPLES	LITHOLOGIC DESCRIPTION																																																
	FORAMINIFERS	NANNOFOSSILS	RADIOLARIANS	DIATOMS																																																									
	* B							0.5 1.0					<p>SILTY SAND, SAND, and PHOSPHATIC PEBBLES</p> <p>Major lithology: black (5Y 2.5/1) feldspathic silty sand and sand, Dark gray (5Y 4/1) and dark olive gray (5Y 3/2) silt and fine sand, phosphatic sand, and black phosphatic pebbles.</p> <p>SMEAR SLIDE SUMMARY (%):</p> <table border="1"> <tr> <td></td> <td>1.42</td> <td>1.76</td> <td>1.97</td> </tr> <tr> <td>D</td> <td></td> <td></td> <td></td> </tr> </table> <p>TEXTURE:</p> <table border="1"> <tr> <td>Sand</td> <td>100</td> <td>15</td> <td>30</td> </tr> <tr> <td>Silt</td> <td>—</td> <td>65</td> <td>30</td> </tr> <tr> <td>Clay</td> <td>—</td> <td>20</td> <td>40</td> </tr> </table> <p>COMPOSITION:</p> <table border="1"> <tr> <td>Quartz</td> <td>20</td> <td>15</td> <td>15</td> </tr> <tr> <td>Feldspar</td> <td>45</td> <td>55</td> <td>20</td> </tr> <tr> <td>Rock fragments</td> <td>10</td> <td>5</td> <td>30</td> </tr> <tr> <td>Clay</td> <td>—</td> <td>20</td> <td>5</td> </tr> <tr> <td>Volcanic glass</td> <td>—</td> <td>5</td> <td>—</td> </tr> <tr> <td>Accessory minerals</td> <td>5</td> <td>—</td> <td>—</td> </tr> <tr> <td>Phosphate peloids</td> <td>20</td> <td>—</td> <td>20</td> </tr> </table>		1.42	1.76	1.97	D				Sand	100	15	30	Silt	—	65	30	Clay	—	20	40	Quartz	20	15	15	Feldspar	45	55	20	Rock fragments	10	5	30	Clay	—	20	5	Volcanic glass	—	5	—	Accessory minerals	5	—	—	Phosphate peloids	20	—	20
	1.42	1.76	1.97																																																										
D																																																													
Sand	100	15	30																																																										
Silt	—	65	30																																																										
Clay	—	20	40																																																										
Quartz	20	15	15																																																										
Feldspar	45	55	20																																																										
Rock fragments	10	5	30																																																										
Clay	—	20	5																																																										
Volcanic glass	—	5	—																																																										
Accessory minerals	5	—	—																																																										
Phosphate peloids	20	—	20																																																										

SITE 680 HOLE B CORE 12X CORED INTERVAL 368.2-376.7 mbsl; 92.0-100.5 mbsf;

TIME-ROCK UNIT	BIOSTRAT. ZONE/ FOSSIL CHARACTER				PALEOMAGNETICS	PHYS. PROPERTIES	CHEMISTRY/cacO ₃	SECTION	METERS	GRAPHIC LITHOLOGY	DRILLING DISTURB. SED. STRUCTURES	SAMPLES	LITHOLOGIC DESCRIPTION																																				
	FORAMINIFERS	NANNOFOSSILS	RADIOLARIANS	DIATOMS																																													
	* B	* B	* B					CC					<p>SILTY SAND and SILTSTONE</p> <p>Major lithology: dark gray (N 4) feldspathic silty sand, phosphatic, and very dark gray (5Y 3/1) siltstone, cemented.</p> <p>SMEAR SLIDE SUMMARY (%):</p> <table border="1"> <tr> <td></td> <td>CC, 6</td> <td>CC, 15</td> </tr> </table> <p>TEXTURE:</p> <table border="1"> <tr> <td>Sand</td> <td>80</td> <td>40</td> </tr> <tr> <td>Silt</td> <td>20</td> <td>30</td> </tr> <tr> <td>Clay</td> <td>—</td> <td>30</td> </tr> </table> <p>COMPOSITION:</p> <table border="1"> <tr> <td>Quartz</td> <td>10</td> <td>10</td> </tr> <tr> <td>Feldspar</td> <td>25</td> <td>20</td> </tr> <tr> <td>Rock fragments</td> <td>10</td> <td>37</td> </tr> <tr> <td>Clay</td> <td>—</td> <td>5</td> </tr> <tr> <td>Accessory minerals</td> <td></td> <td></td> </tr> <tr> <td>Phosphatic grains including gneiss and amphibole</td> <td>50</td> <td>20</td> </tr> <tr> <td>Hornblende</td> <td>5</td> <td>—</td> </tr> <tr> <td>Diatoms</td> <td>—</td> <td>3</td> </tr> </table>		CC, 6	CC, 15	Sand	80	40	Silt	20	30	Clay	—	30	Quartz	10	10	Feldspar	25	20	Rock fragments	10	37	Clay	—	5	Accessory minerals			Phosphatic grains including gneiss and amphibole	50	20	Hornblende	5	—	Diatoms	—	3
	CC, 6	CC, 15																																															
Sand	80	40																																															
Silt	20	30																																															
Clay	—	30																																															
Quartz	10	10																																															
Feldspar	25	20																																															
Rock fragments	10	37																																															
Clay	—	5																																															
Accessory minerals																																																	
Phosphatic grains including gneiss and amphibole	50	20																																															
Hornblende	5	—																																															
Diatoms	—	3																																															

CORE 112-680B-13X NO RECOVERY



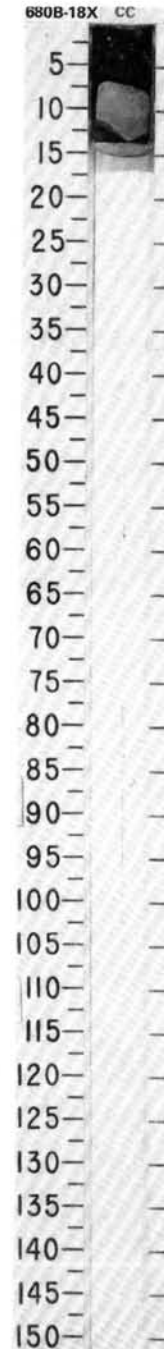
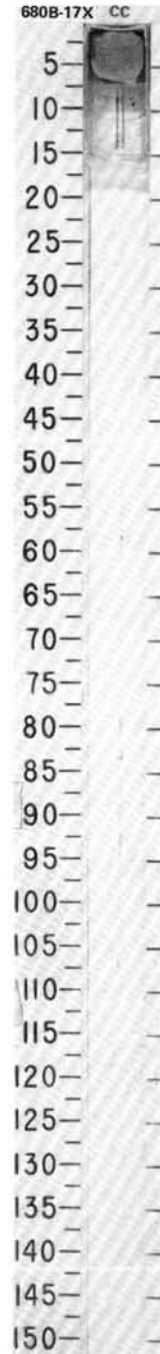
SITE 680

SITE 680 HOLE B CORE 17X CORED INTERVAL 414.7-425.5 mbsl; 138.5-148.0 mbsf

TIME-ROCK UNIT	BIOSTRAT. ZONE/ FOSSIL CHARACTER				PALEOMAGNETICS	PHYS. PROPERTIES	CHEMISTRY/CO ₂	SECTION	METERS	GRAPHIC LITHOLOGY	DRILLING DISTURB. SED. STRUCTURES	SAMPLES	LITHOLOGIC DESCRIPTION
	FORAMINIFERS	NANNOFOSSILS	RADIOLARIANS	DIATOMS									
													<p>SANDY SILTSTONE</p> <p>Major lithology: olive gray (5Y 4/2) sandy siltstone, feldspar and phosphite-rich, calcite cemented.</p>

SITE 680 HOLE B CORE 18X CORED INTERVAL 424.5-433.7 mbsl; 148.0-157.5 mbsf

TIME-ROCK UNIT	BIOSTRAT. ZONE/ FOSSIL CHARACTER				PALEOMAGNETICS	PHYS. PROPERTIES	CHEMISTRY/CO ₂	SECTION	METERS	GRAPHIC LITHOLOGY	DRILLING DISTURB. SED. STRUCTURES	SAMPLES	LITHOLOGIC DESCRIPTION
	FORAMINIFERS	NANNOFOSSILS	RADIOLARIANS	DIATOMS									
	*	*											<p>MUD and SANDSTONE</p> <p>Major lithology: olive gray (5Y 4/2) mud, phosphatic fragments, and cemented sandstone.</p> <p>SMEAR SLIDE SUMMARY (%):</p> <p style="padding-left: 40px;">CC, 3 D</p> <p>TEXTURE:</p> <p>Sand 10 Silt 45 Clay 45</p> <p>COMPOSITION:</p> <p>Quartz 10 Feldspar 15 Rock fragments 25 Clay 10 Accessory minerals Phosphatic peloids 15 Diatoms 25</p>



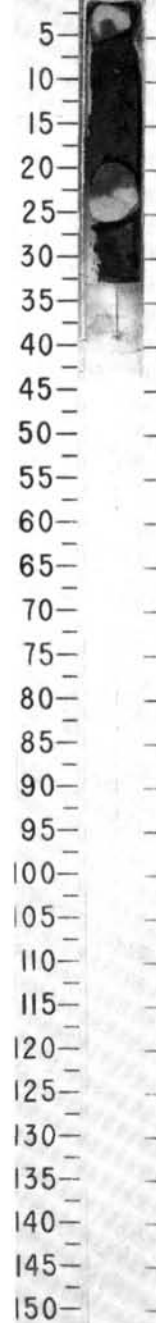
SITE 680 HOLE B CORE 19X CORED INTERVAL 433.7-443.2 mbsl; 157.5-167.0 mbsf

TIME-ROCK UNIT	BIOSTRAT. ZONE/ FOSSIL CHARACTER				PALEOMAGNETICS	PHYS. PROPERTIES	CHEMISTRY/CACO ₃	SECTION	METERS	GRAPHIC LITHOLOGY	DRILLING DISTURB. SED. STRUCTURES	SAMPLES	LITHOLOGIC DESCRIPTION
	FORAMINIFERS	NANNOFOSSILS	RADIOLARIANS	DIATOMS									
PLIOCENE / MIOCENE ?	B *	B *						CC				*	<p>MUD, SAND, and SANDSTONE</p> <p>Major lithology: olive gray (5Y 4/2) mud, phosphatic fragment, phosphatic sand, feldspar-rich, and cemented sandstone.</p> <p>SMEAR SLIDE SUMMARY (%):</p> <p style="text-align: right;">CC, 14 D</p> <p>TEXTURE:</p> <p>Sand 70 Silt 20 Clay 10</p> <p>COMPOSITION:</p> <p>Quartz 15 Feldspar 25 Rock fragments 15 Clay 10 Accessory minerals 5 Phosphatic grains 30</p>

SITE 680 HOLE B CORE 20X CORED INTERVAL 443.2-452.7 mbsl; 167.0-176.5 mbsf

TIME-ROCK UNIT	BIOSTRAT. ZONE/ FOSSIL CHARACTER				PALEOMAGNETICS	PHYS. PROPERTIES	CHEMISTRY/CACO ₃	SECTION	METERS	GRAPHIC LITHOLOGY	DRILLING DISTURB. SED. STRUCTURES	SAMPLES	LITHOLOGIC DESCRIPTION
	FORAMINIFERS	NANNOFOSSILS	RADIOLARIANS	DIATOMS									
	B *	B *						CC				*	<p>PHOSPHATIC SILTY SAND</p> <p>Major lithology: black (5Y 2.5/2) phosphatic silty sand, feldspar-rich.</p> <p>SMEAR SLIDE SUMMARY (%):</p> <p style="text-align: right;">CC, 16</p> <p>TEXTURE:</p> <p>Sand 20 Silt 35 Clay 45</p> <p>COMPOSITION:</p> <p>Quartz 5 Feldspar 20 Rock fragments 35 Clay 3 Accessory minerals Black, phosphatic 25 Hornblende 2 Diatoms 10</p>

680B-19X CC



680B-20X CC

